The morphology and surf conditions of Aramoana Beach, Otago: A surf break of national significance

A thesis

submitted in fulfilment

of the requirements for the degree

of

Masters of Science

in Earth Sciences

At

The University of Waikato

By

Jai Davies-Campbell

THE UNIVERSITY OF
WAIKATO
Te Whare Wānanga o Waikato

2018

Abstract

Aramoana Beach is a recognised surf break of regional and national significance and is protected under the New Zealand Coastal Policy Statement (2010). Until recently, little baseline data on the break had been collected. The objective of this thesis was to gain an understanding of how the morphological and surfing parameters vary and interact with each other and with the forcing wave climate. Ultimately, the baseline data gathered from this work will help inform and support the NZCPS (2010) in protecting Aramoana Beach and other surf breaks around New Zealand.

The state, morphology and in turn the surfing parameters of Aramoana Beach are correlated and are a function of the forcing wave climate present at any given time, which is observed to have seasonal and annual variations. The morphological parameters of interest are the sand-bar orientations and sand-bar lengths, whilst the surfing parameters of interest are the peel angles and the ride lengths. Two cameras were set up overlooking Aramoana Beach to record known favourable surfing locations. The two locations were separated by 300 m.

The results indicated that, at the camera one area of interest, El Niño phases as well as the forcing wave climate associated with autumn and winter, increased the sand-bar orientation, relative to true north (0°), to face north-east and decreased the sand-bar lengths, whilst the state of Aramoana Beach became more dissipative in nature. During El Niño phases, as well as autumn and winter, south-east swell waves were dominant, and the significant wave height increased. In contrast, La Niña phases, as well as the forcing wave climate associated with summer and spring, decreased the sand-bar orientations, relative to true north, to face north-north-east and increased the sand-bar lengths, whilst the state of Aramoana Beach became more reflective in nature. During La Niña phases, as well as spring and summer, north-east swell waves were dominant and the significant wave heights were smaller, relative to El Niño. The peel angles and ride lengths of the breaking waves were more favourable in El Niño years and during autumn and

winter compared to during La Niña years and during spring and summer at the camera one area of interest.

At the camera two area of interest, the El Niño phase decreased the sand-bar orientations, relative to true north to face north (opposite to the camera one area of interest) and decreased the sand-bar lengths. In contrast, the La Niña phase increased the sand-bar orientations, relative to true north to face north-north-east and increased sand-bar lengths. The seasonal trends at the camera two area of interest were likely inaccurate due to the paucity of data. Surfing conditions at the camera two area of interest were more favourable during La Niña phases compared to El Niño phases, which was opposite to the camera one area of interest.

The findings of this study add weight to the importance of protecting the swell corridors that contain the pre-conditioning features that are essential to producing the world-class surfing waves observed at Aramoana Beach.

Acknowledgements

First and foremost, I would like to thank my supervisor, Professor Karin Bryan, without whom this thesis would not be possible. I cannot thank you enough for the weekly meetings, constant encouragement and belief that I could learn 'Matlab'! It is an important skill I look forward to developing in the future. Your energy and passion for science is contagious and I can only hope that one day I will be half the scientist you are. Your mind is brilliant!

To Ed Atkin, Shaw Mead, Sam O'Neill and the team at eCoast Marine Consultancy and Research, your knowledge, willingness to help and time has been invaluable. I will never forget my first New Zealand Coastal Society Conference. What a time to be alive.

Thank you to Dean Sandwell for helping collect the ground control points with Ed Atkin. What a trooper! I hear the local seal population is quite friendly.

I would also like to thank Rebecca McGrouther and Port Otago Ltd, for providing the images, without which this thesis would not be possible. Also, thank you, George Payne, from the National Institute for Water and Atmospheric Research (NIWA) for providing the time-averaged images.

To the Ministry of Business, Innovation and Employment (MBIE) thank you for the funds in the second year of my MSc. The student life burden was significantly alleviated.

To my past and present University of Waikato alumni and colleagues, respectively, your knowledge, understanding natures and generosity with time will never be forgotten. To the alumni, thanks for the socialisation!

To Alexander Alan Williams, you really are the Wonderhorse. Thank you for all the mental support, ramen, coffee and cycling adventures. You have kept me level during this adventure.

Finally, to my gorgeous partner in crime Malesa McNearney. Your patience, love and support has been integral to my Hauora and getting this work done. I cannot wait to see what the future has install for us. Also, I would not be who I am and where I am without the unconditional love and support of my parents Andy Campbell and Patsi Davies and my brothers, especially Alexei, Ari, Marcus and Symonn. My success is your success! Arohanui!

Table of Contents

List of Tables

List of Figures

Chapter One

Introduction

1.1 Thesis Motivation

At the time of writing, there were an estimated 23 million surfers globally, 145,000 of which reside in New Zealand. The global growth rate is 12-16% per year in and generates in excess of 10 billion dollars per annum (Orams, 1999; Buckley, 2002; Scarfe et al., 2009a & b). In New Zealand, surfing is a popular sport, (Sport NZ, 2015) and it has positive impacts on local economies. Nelson (2007) reports that surfers significantly contribute to local economies, just as much, if not more than, regular beachgoers and surfers greatly extend the hours of tourism and expenditure within coastal communities. Yet, the surf breaks and surfers as coastal users, until very recently, have not been included in the decisions and designs of environmental coastal engineering projects. Mead (2003) and Scarfe et al. (2009a & b) contend that this situation has contributed to the loss of many high-quality surf breaks around the world. For example, Mundaka, Spain, was severely altered after dredging activities in 2005 (Peryman, 2011). In the last decade, however, there has been a global shift toward the protection of surf breaks. This has been accompanied by the introduction of multipurpose coastal constructions that incorporate surfing-related features in addition to coastal protection, habitat for marine organisms, recreational and commercial fishing, diving and swimming (Raybould & Mules, 1998; Mead, 2003; Scarfe et al., 2009a & b).

The shift in attitude toward protecting and creating surf breaks necessitated the development of coastal sciences to advance the understanding of how coastal processes and structures make high-quality surf breaks. Such a shift is significant because the sport of surfing requires a certain form of wave breaking, where the wave is required to have a steep enough gradient, which ensures a surfboard maintains a minimum speed but is not too steep that the wave breaks down (Button, 1991; Couriel et al., 1998; Mead & Black, 2001; Scarfe et al., 2009a & b).

For a surfer to successfully ride the unbroken face of a wave, the breaking part of the wave must 'peel', thus providing a continual section on which to ride laterally (Walker, 1974a, b; Hutt, 1997, Scarfe et al., 2009a & b). The steepness and peel of a breaking wave, however, is a function of the seabed morphology (Walker, 1974a, b; Peregrine, 1983; Hutt, 1997; Couriel et al., 1998; Scarfe et al., 2009a & b). Thus, the seabed morphology (reef shape) along with wave steepness (breaking intensity) and peel angle are the three most influential characteristics of world-class surfing waves (Mead & Black, 2001; Mead, 2003; Scarfe et al., 2009a & b).

The introduction of the New Zealand Coastal Policy Statement (NZCPS) in 2010, requires the protection of 17 surf breaks of national and regional significance. It was immediately evident, however, that little baseline data exists on the factors controlling the surf break and the potential current or future threats to their existence. As a result, it has been difficult for regional councils to follow the intention of the NZCPS and to put mechanisms in place to effectively protect these breaks.

In 2015, eCoast Marine Consultancy and Research and the University of Waikato received funding from the Ministry for Business, Innovation and Employment for a joint research project titled 'Remote Sensing, Classification and Management Guidelines for Surf Breaks of National and Regional Significance'. The project aims to develop guidelines and methodology for protecting surf breaks of national and regional significance. The breaks to be studied include Piha Beach near Auckland, Manu Bay in Raglan, 'The Bar' at Whangamata, 'Pines' at Gisborne's Wainui Beach, Lyall Bay in Wellington, and Aramoana and Whareakeake (also known as Murdering Bay) near Dunedin (see Figure 2.5B).

This thesis is set within the wider context of this overarching programme. It responds to the identified need to collect baseline data from surf breaks by specifically focussing on the surf break at Aramoana Beach, Otago Peninsula, New Zealand (Figure 2.5B). This surf break has been the subject of resource management hearings since 2011 (Otago Regional Council, 2010). There has been concern that the surf break and the beach could be affected by nearby Port Otago

Limited (POL) “Next Generation” dredge disposal activities (Otago Regional Council, 2010).

This thesis presents and interprets the baseline data gathered from the Aramoana surf break. Data collection was undertaken using remote camera imagery analysis, analysis of the forcing wave climate, and detailed information collected by the Port of Otago on the use of the break. Ultimately, the results of the study will help inform and support NZCPS in protecting the Aramoana surf break and other surf breaks throughout New Zealand.

1.2 Thesis Objective

The morphology of Aramoana Beach is a function of the local geology, antecedent beach state as well as local and far-field weather events. Thus, morphology is influenced spatially and temporally. In turn, the morphological parameters influence the local surfing parameters, which also vary over time and space. The objective of this work is to identify, relate and explain the observed morphology of the surfing parameters and how these parameters change over space and time. The geomorphic parameters of interest are the location, orientation and length of the sand-bars, whereas the surfing parameters of interest are the peel angles and length of rides.

The thesis objective will be achieved by answering the following sub-questions:

(1) *Can the morphological changes and changes to surfing parameters be successfully analysed from the time-averaged video imagery of Aramoana beach?*
(2) *Are surfing parameters correlated with changes in morphology?*
(3) *Are there predictable seasonal or interannual changes in morphology and surfing parameters?*
(4) *Can seasonal and interannual changes be linked to changes in the wave climate around the Otago coast?*

1.3 Thesis Structure

This thesis is organised into 5 subsequent chapters.

Chapter Two: Surf Science, Beach Morphology & Historical Background of Study Site

Chapter Two provides an insight into the key characteristics that form high-quality surfing waves at surfing breaks. Beach states and shoreline-sand-bar coupling are overviewed followed by a discussion about the video imagery techniques for identifying shorelines and sand-bars. It concludes with a detailed overview of the cultural history, geological setting, atmospheric and wave climate setting, the history of dredging and disposal near Aramoana Beach as well as the formation of the surf at Aramoana Beach.

Chapter Three: Methodology

Chapter Three introduces a detailed account of the methods used in this thesis to collect, process and analyse the data from two cameras overlooking Aramoana Beach and a brief explanation of the suite of computer algorithms used to extract the geomorphic parameters from time-averaged images and surfing parameters from snapshot images.

Chapter Four: Results

Chapter Four presents the analysed results from the datasets from the two cameras, the correlations and levels of statistical significance within and between the geomorphic parameters and surfing parameters. A brief overview of the forcing wave climate is discussed.

Chapter Five: General Discussion & Conclusions

Chapter Five discusses the results of the morphological and surfing parameters of interest with respect to the two camera areas of interest. It provides an explanation of the observed variation in the data from an annual and seasonal perspective. Comparisons are made between the two camera areas of interest. A brief summary of the thesis and concluding remarks on the discussed results is provided.

Chapter Six: Conclusions

Chapter Six contains a brief summary of the thesis and presents a number of implications arising the results and limitations of the study.

Chapter Two

Literature Review: Surf Science, Beach Morphology & Historical Background of Aramoana

2.1 Introduction

This literature review focusses firstly on the three aspects (peel angle, breaking intensity and reef shape/geomorphology), which are key to helping understand the quality of the surfing waves at Aramoana surf break, Otago Peninsular, New Zealand. Note, that Aramoana is actually located on the coast north of Dunedin Harbour, which is common usage, however, hereafter the coast north of Dunedin is referred to as the Otago Peninsular. Secondly, techniques on video imagery analysis are discussed with respect to the shoreline and sand-bar detection. Lastly, a detailed overview of the cultural history, geological setting, atmospheric and wave climate setting, history of dredging and disposal near Aramoana, history and formation of the surf at Aramoana Beach are all provided.

2.2 Surf Science

Surf science is critical to understanding the quality of surfing waves. The following discussion examines the main characteristics of surf science relevant to this thesis.

2.2.1 Peel Angle

The peel angle describes the speed at which a surfer must travel to succeed in traversing across the face of a wave. Mead (2003) defines the peel angle as “the angle between the trail of the broken white water and the crest of the unbroken part of the wave as it propagates shoreward”. Quality surfing waves peel laterally across the breaking region of a wave, which creates a continuous face to manoeuver on (Hutt, 1997; Mead, 2003). The speed that the breaking surface moves along the crest further defines the quality of a wave and is a function of the peel angle, whereby the smaller the peel angle, the faster the wave and the

greater the peel angle, the slower the wave. These peel angles range from 0° to 90°; however, different peel angles suit different forms of surfing. For example, short board surfing requires smaller peel angles with steeper faces, whereas long board surfing requires greater peel angles and shallower gradients (Mead, 2003).

Walker (1974) was one of the pioneers who developed techniques for measuring peel angles at surf breaks on Oahu's south coast, Hawaii. He developed a classification scheme that related peel angles to wave heights, which allowed particular waves to be grouped by the surfing abilities of surfers. Walker's classification scheme, however, did not incorporate the speed of the breaking peel angles, which is an important parameter to 'surfability'. For example, under his classification scheme, the Raglan point breaks were regarded as being at an intermediate level, when in fact they are regarded as ranging from beginner to expert depending on the surf conditions (Mead, 2003). Hutt et al. (2001) built on from Walker's (1974) scheme and developed a new classification scheme (shown in Table 2.1) of waves with a maximum height of 4.0 meters (m). The scheme defined 10 skill levels from "absolute beginner" to waves that were yet to be surfed by the world's best (Hutt et al., 2001; Mead, 2003). The classification scheme is split into three major groups: ratings from one to three represent beginner surfers; four to six represent intermediate surfers, and 7-9 represent expert surfers. With respect to peel angles and the skill level of surfers or 'surfability', peel angles ranging from 60° to 90° represent waves associated with beginners, peel angles of 40° to 59° are associated with intermediate surfers and peels angles of 27° to 39° are associated with expert surfers (Hutt et al., 2001).

Table 2-1. Rating of the skill level of surfers. Ratings are independent of the surf break quality or the degree of difficulty of waves (Hutt et al., 2001).

Rating	Descritption of Rating	Peel Angle Limits (degrees)	Min/Max Wave Height (m)
1	Beginner surfers not yet able to ride the face of a wave and simply moves forward as the wave advances.	90	0.7/1.00
2	Learner surfers able to successfully ride laterally along the crest of the wave.	70	0.65/1.50
3	Surfers that have successfully developed the skill to generate speed by 'pumping' on the face of the wave.	60	0.60/2.50
4	Surfers beginning to initiate and execute standard surfing manoeuvres on occasion.	55	0.55/4.00
5	Surfers able to execute standard manoeuvres consecutively on a single wave.	50	0.50/>4.00
6	Surfers able to execute standard manoeuvres consecutively. Executes advanced manoeuvres on occasion.	40	0.45/>4.00
7	Top amateur surfers able to consecutively execute advanced manoeuvres.	29	0.40/>4.00
8	Professional surfers able to consecutively execute advanced manoeuvres.	27	0.35/>4.00
9	Top 44 professional surfers able to consecutively execute advanced manoeuvres.	not reach	0.30/>4.00
10	Surfers in the future.	not reach	0.3/>4.00

2.2.2 Wave Steepness

Wave height and period, and wind strength and direction all influence wave steepness, otherwise known as breaking intensity (Wright & Short, 1984; Wright et al., 1985; Galloway et al., 1989; Button, 1991; Masselink & Hughes, 2003; Mead, 2003). As stated earlier, however, the most significant factor influencing wave steepness is the morphology of the underlying bathymetry (Peregrine, 1983; Sayce, 1997; Mead, 2003). Thus, it is the seabed gradient, which evidently controls the shape and steepness of a wave from a spilling through to a surging breaker. Spilling breakers and the more desired plunging breakers are essential for surfing. With increasing seabed gradients, breakers transition from spilling through to plunging. Plunging breakers provide steeper wave faces, which are essential for not only catching waves on shorter boards but also performing skilled manoeuvres. Furthermore, depending on the peel angle and bathymetry, surging breakers can offer the opportunity to ride within the tube (vortex), which is known commonly as “getting barreled or shacked” (Mead, 2003).

In the past, non-dimensional parameters such as the Irribarren number, surf scaling parameter, surf similarity parameter and the Dean’s parameter have been used to describe the wave breaking characteristics and in turn to define beach states (Gourlay & Meulen, 1968; Dean, 1973; Guza & Inman, 1975; Wright & Short, 1984; Mead, 2003). The output values of these respective parameters

differentiate between reflective, intermediate and dissipative beach states. These beach state defining parameters, however, do not necessarily discriminate well between breaker types (Button, 1991; Sayce, 1997; Couriel et al., 1998; Mead, 2003), since these values do not adequately explain the shape of the waves. These values are essential to defining the quality of a wave (Mead, 2003).

Sayce (1997) developed a method for predicting the shape of a plunging wave (cited by Mead, 2003), which involved using a computer programme to fit a cubic curve to the crest of parallel images of breaking waves. Sayce's (1997) programme calculated the vortex length (l) vortex width (w), vortex breaking angle (θ) and the wave height (H), as illustrated in Figure 2.1. This method, however, gave little information on the seabed gradients, thus it was hard to correlate seabed gradients and breaking intensities. Subsequently, Mead and Black (2001a) made an important breakthrough, when they found that wave intensity or steepness was correlated to the angle of the wave when travelling along relative to the seabed gradient, known as the 'orthogonal seabed gradient'. The orthogonal seabed gradient is important because waves must travel at an angle to the seabed gradient to produce the peel angle required for quality surfing waves (Hutt, 1997; Mead & Black, 2001a; Mead, 2003).

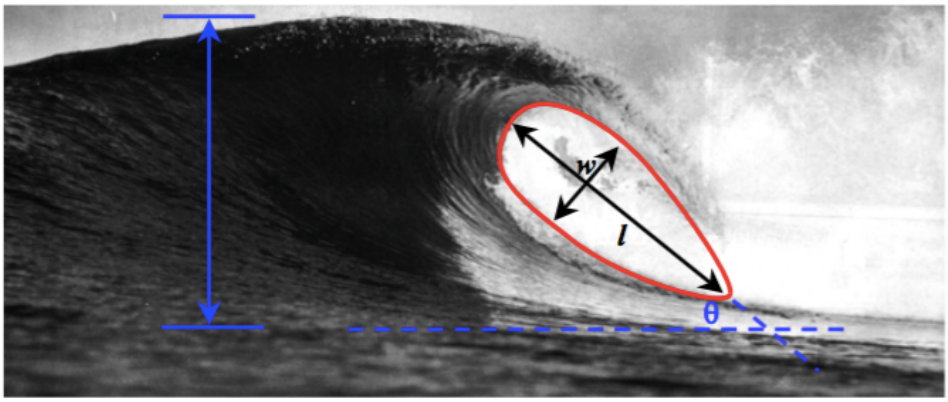

Figure 2-1 Curve fitting is applied to the face of a crest parallel to the wave image. This is used to calculate the vortex statistics described above (Sayce, 1997).

This relationship between the angle of the approaching wave relative to the seabed gradient and resulted breaking intensity is given by the linear equation:

$$Y = 0.065X + 0.821$$

where Y is the vortex ratio (tube length to width) and X is the orthogonal seabed gradient (Mead & Black, 2001a; Mead 2003). The range of surfing wave breaking intensities is illustrated in Table 2.2.

Table 2-2 Classification range of surfing breaking intensities (Mead & Black, 2001; Mead, 2003).

Intensity	Extreme	Very High	High	Medium/high	Medium
Vortex Ratio	1.6-1.9	1.91-2.2	2.21-2.5	2.51-2.8	2.81-3.1
Descriptive Terms	Square, spitting	Very hollow	Pitching, hollow.	Some tube sections	Steep faced, but rarely tubing
Example Break	Pipeline, Shark Island	Backdoor, Padang Padang	Kirra Point, Off-The-Wall	Bells Beach, Bingin	Manu Bay, Whangamata
Example Break Wave Profile					

Breaking intensity, however, can be affected by wave period and height. As the wave period increases, the breaking intensity also increases. In contrast, when wave height increases the breaking intensity decreases (Mead, 2003). Therefore, the breaking intensity of smaller waves is greater than the breaking intensity of larger waves on the same gradient structure. In general, smaller waves break closer to the shore (shallower water) compared to larger waves (deeper water). This suggests that wave breaking intensity is correlated with a critical wave height (i.e. a nearly linear relationship (Battjes 1974; Guza & Inman, 1975; Peregrine, 1983)). Mead (2003) suggest that this ratio is approximately 0.78 but ratios between 0.5 and 1.0 (wave height: water depth) can be observed. The breaking wave height to water depth relationship is critically important when protecting surf breaks of significance or producing 'artificial surf reefs' or 'ASRs' because the breaking intensity decreases with increasing wave height in areas producing larger waves. With regard to ASRs, Mead et al. (2003) suggest that rather than using a linear shape (wave height: wave depth), a convex reef shape structure is more

appropriate because it increases with depth towards the open ocean. Such a shape will reduce the undesirable reduction in breaking intensity associated with larger waves and is a shape characteristic of many significant surf breaks around the world.

2.2.3 Reef Shape

Of the important characteristics that influence the quality of a surfing break, seabed morphology is the most significant (Mead, 2003). The peel angles and the breaking wave intensity, which are the most important aspects of high-quality surfing waves, are dictated by the morphology of the seabed or reef shape (Mead & Black, 2001b). Early studies from Walker (1974) indicated that a 45° angle or V shapes produce the most desirable waves. Due to refraction, however, peel angles are significantly reduced in areas with these reef shapes, which means a faster and harder wave to ride (Black et al., 2001, cited in Mead, 2003). Black et al. (1998) and Mead and Black (2001b) found that world-class surfing breaks have very complex seabed morphologies. Their studies identified a commonality among mesoscale components from which all world class breaks are comprised (Mead, 2003). Mead and Black (2001b) classified these geomorphic components as a ramp, platform, wedge, ledge, focus, ridge and pinnacle, as shown in Figure 2.2 (a detailed description can be found in Mead and Black (2001b & c)). If the waves do not align with the favoured orthogonal direction, however, the waves that break will either peel too quickly or slowly, which would not be favoured for high-performance surfing (Mead & Black, 2001). This not only suggests that the reef shape is important but also that the swell direction is important relative to the reef shape or seabed morphology.

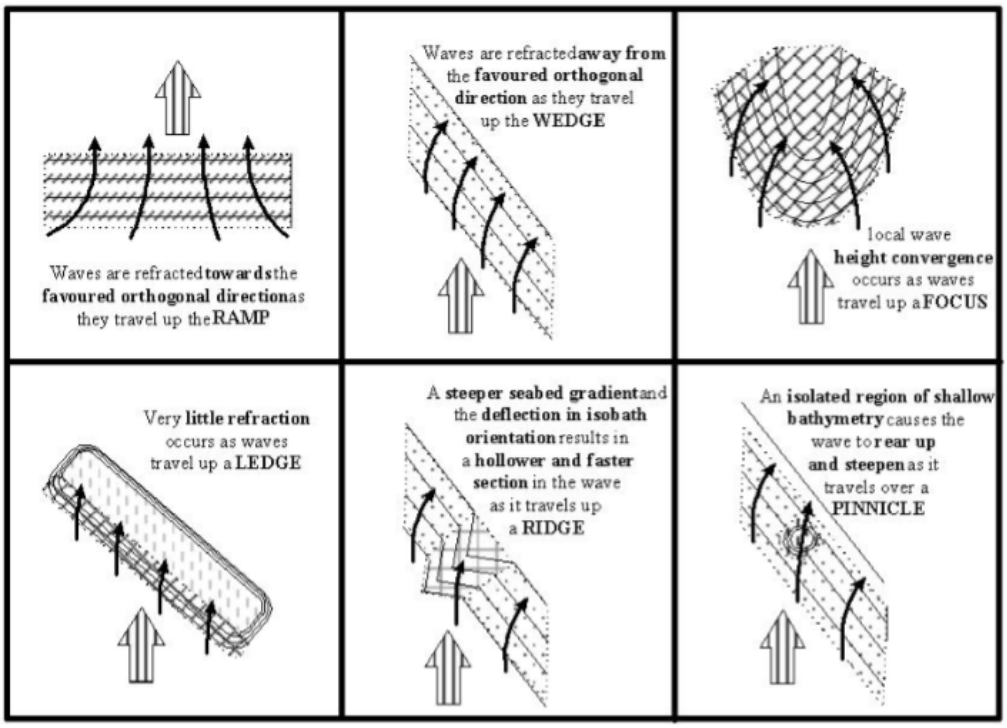

Figure 2-2 Illustrates the reef components that comprise the bathymetry of world class surf breaks. Isobaths become shallower in the direction of the wave propagation, which is up in this case. The large arrows represent the preferred orthogonal direction and the small arrows represent the wave refraction or actual wave orthogonal direction (Mead & Black, 2001b & c; Mead, 2003).

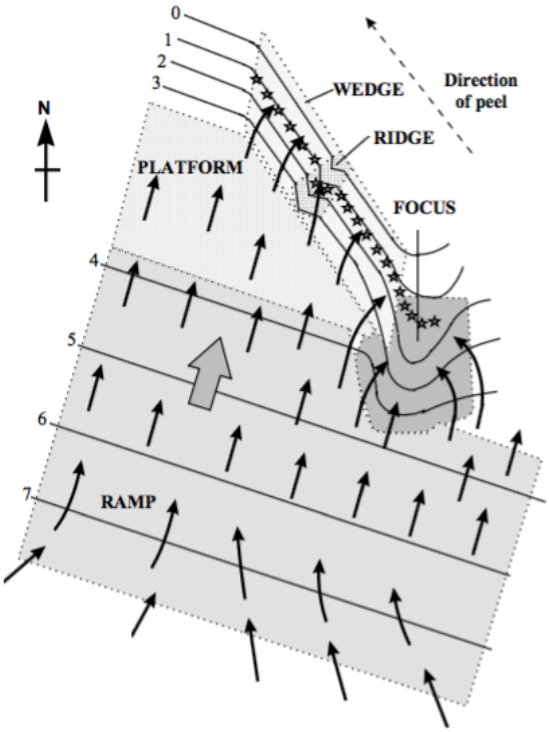

Figure 2-3 Illustrates the configuration of the many mesoscale components, which make up the world-class surf break that is Bingin Reef, Bali. The large arrows indicate the favoured orthogonal direction and the smaller arrows indicate the alignment of the wave orthogonal as they pass over the various components of the configuration (Mead, 2003).

Before wave breaking occurs, there is an element of wave conditioning, known as 'pre-conditioning', which occurs as a result of the components of the morphology offshore. The components can be separated into pre-conditioning components and breaking components, as illustrated in Table 2.3 (Mead and Black, 2001b). These components are all linked by refraction (Mead & Black, 2001c) because the peel angle and breaking intensity of waves are dependent on the level of refraction occurring (Mead, 2003). Wave refraction rotates wave crests to align with isobaths (observed in Figures 2.2 and 2.3) and is a result of friction between shallow water wave velocity and the seabed. Wave refraction can alter local wave heights via convergence and divergence of wave rays to preserve constant energy (Komar, 1998). The gradients in wave heights caused by refraction help promote and initiate wave breaking and peeling (Komar, 1998). Hence, the peel angle and breaking intensity are a function of the seabed morphology.

Table 2-3 Illustrates functions of surfing reef components (Mead & Black, 2001b).

Component	Function	Details
Ramp & Focus	1. Precondition waves	Precondition for other components
Platform		Convey waves without change
Wedge & Ledge	2. Break waves	Break waves for surfing
Ridge & Pinnacle		Modify breaking waves

2.3 Beach Geomorphology and States

Not all world class surfing breaks are reefs breaks. Beaches characteristic of sandy seabed morphology also produce world-class surfing waves. Therefore, understanding the seabed morphology and processes affecting this morphology is also important. The morphology, however, is highly susceptible to change from episodic and seasonal weather events (Wright & Short, 1984, Masselink & Hughes, 2003; van de Lageweg et al., 2013). Beach breaks work as a result of complex shoreline-sand-bar coupling, which is, in turn, a function of the antecedent or episodic wave climate (Wright & Short, 1984; van de Lageweg et al., 2013). This wave climate determines the amount of energy being dissipated onto a beach at any given time and as a result can be used to classify the morphodynamic states

of beaches (Wright and Short, 1984; Masselink & Short, 1993; Masselink & Hughes, 2003).

The term 'beach state' denotes the relationship between morphological features of a beach and hydrodynamic processes upon which the beach is subject. The morphology of a beach, at any one time, is a function of its sediment characteristics, the immediate and antecedent wave climate and tidal and wind conditions (Jackson et al., 2005). Over time, the most frequent or modal beach state will feature. The modal beach state is a direct result of the environmental conditions, in particular, the wave climate (Wright & Short, 1984) and also the geological setting, which comprises two dimensions: a) the framework of the beach, which limits the morphological evolution by limiting the shape and space to accommodate volume (McNinch, 2004); and b) the source and nature of the beach materials (Jackson et al., 2005).

Beach state models are often used to predict the morphology of beaches both spatially and temporally (Wright & Short, 1984). A number of methods and models have been used by authors in the past to predict beach states. These Include the surf scaling parameter (Guza & Inman, 1975); surf similarity parameter; and most commonly the Dean's parameter (1973) or dimensionless fall velocity parameter (Ω) given by:

$$\Omega = H_b / W_s T$$

where H_b is the breaking wave height, W_s is the sediment falling velocity and T is the wave period.

- Ω Values <1 = Reflective states
- Ω Values between 1 and 6 = Intermediate states
- Ω Values >6 = Dissipative states

The Ω, however, does not take into account the influence of the relative tides on the local wave regime. Therefore, Masselink & Short (1993) proposed an additional parameter of relative tidal range (RTR), developed from Gibbs et al.,

(1971), to take into account the tide-induced migration of the hydrodynamic processes. This is given by:

$$RTR = TR/H_b$$

Where TR is the tidal range. This parameter is important because the larger the tidal range the greater the potential influence of the wave forcing conditions, such as during storm surge (Sallenger, 2000; Jackson et al., 2005; Qi et al., 2010) and in turn influence on beach state and shoreline-sand-bar coupling. All of these factors influence the quality of the surfing waves at sandy beaches.

2.3.1 Beach States and Responses

According to the Wright & Short (1984) morphodynamic beach state concept, there are two extreme states one of which is dissipative and the other being reflective. Between the dissipative and reflective states, there are four intermediate states each with their own characteristics adopted from both the dissipative and reflective states. Below, the beach states and responses are defined and discussed, respectively (Wright & Short, 1984).

Qi et al. (2010) proposed that the storm intensity can be quantified using the mean profile change (MPC) on the foreshore, which is the absolute value of the average variation of a profile before and after a storm. The MPC is quantified via the change in beach profile gradient. Qi et al. (2010) proposed the beach gradient as the tangent value of the foreshore between the berm or dune and the lower intertidal zone. The starting point of the beach gradient after a storm is determined by the bottom of the scarp in front of a berm or dune after an erosional event. According to this method, dissipative beaches incurred the smallest gradient change, with moderate changes observed on reflective beaches and the greatest changes occurring on intermediate beaches.

2.3.1.1 Dissipative Beach States

Dissipative beach states are characterised as being high energy beaches with a wide surf zone (300-500 m) including two to three shore normal bars and troughs,

and a low-sloping and wide beach face consisting of fine sand (Wright & Short, 1984). Morphodynamic beaches of a dissipative nature typically exhibit a smooth and wide foreshore and a pronounced dune system on the backshore (Qi et al., 2010). During storm events, the beach profile flattens creating multiple breaker zones and in turn dissipation of storm energy (waves) occurs (Dean, 1991). As a result of this wave dissipation, the beach response to storms is typically weak and the beach is regarded as being very stable (Wright & Short, 1984; Qi et al., 2010). Typical erosional features include erosion to the dune toe and minor changes to the beach face gradient (MPC < 0.1 m). As the storm water level is controlled by both the storm surge and the astronomical tide, however, if storms were to coincide with spring tide cycles and high tides, this could result in exacerbated erosion to berms and the backshore dunes (Wright & Short, 1984; Qi et al., 2010).

2.3.1.2 Intermediate Beach States

There are four intermediate beach states (discussed below) and they usually develop in areas with strong tidal actions. These morphodynamic beach states typically reflect a steeper more reflective upper profile with a contrasting gentle, dissipative lower profile (Wright & Short, 1984; Qi et al., 2010). Significantly higher responses to storms are associated with intermediate states in comparison with dissipative states. Typically, the upper profile is significantly eroded and sediment deposited on the lower profile. This results in a markedly decreased beach face gradient (MPC >0.5 m) (Qi et al., 2010). Beaches that do not have berms platforms may erode, which may lead to the destruction of coastal structures.

2.3.1.2.1 Longshore Bar-Trough

This beach state is regarded as being the most energetic with the most dissipative qualities of all the intermediate states. 'Longshore bar and troughs' exhibit a steeper more reflective subaerial beach compared to dissipative beach states. This beach state typically also has a step, which is separated from a prominent 'high relief and locally dissipative bar by a deep trough'. The run-up is typically quite high on this beach compared to dissipative states. Beach cusps are often observed

on these beaches, which are generated by subharmonic edge waves operating near the subaerial beach (Wright & Short, 1984).

2.3.1.2.2 Rhythmic Bar and Beach

'Rhythmic bar and beach' states are similar to that of the 'longshore bar-trough' beach states, except rhythmic bar and beach states have crescentic bars and they have a megacusp type rhythmicity with the alongshore length scales, which can be in the order of 100 to 300 meters. Rip circulations are somewhat fixed and exhibit a moderate strength (Wright & Short, 1984).

2.3.1.2.3 Transverse Bar and Rip

Transverse bar and rip beach states are characterised by prominent longshore separated groups of dissipative and reflective areas with dissipative transverse bars or shoals alternating with deep reflective embayment's, between which very strong rips channels to occur. The transverse bars occur as the crescentic sand-bar horns weld to the beach (Wright & Short, 1984).

2.3.1.2.4 Ridge Runnel/Low Tide Terrace

This beach state is regarded as having the lowest energy of the intermediate states and sequentially speaking occurs just prior to the reflective state. Ridge runnel/ low tide terrace beach states are reflective at high tide and dissipative at low tide. Rip currents are common but small (Wright & Short, 1984).

2.3.1.3 Reflective Beach States

Reflective beaches are typically wave dominated by small tidal ranges and are sensitive to wave dynamics. Reflective beaches typically have a steep beach face with a step seaward. Beneath the step, lower gradients are observed. In contrast to dissipative beaches, reflective beaches have little subaqueous sand and are associated with beach cusps and subharmonic edge waves (Wright & Short, 1984). Reflective beach responses are more complex than other beach states and are more dependent on offshore and beach topography (Chen, 1995) and storm track

relative to location (Cai, Su, Xia, 2004). Significant modifications of beach profiles are induced as narrow surf zones are unable to dissipate wave energy (Qi et al., 2010).

During storm surges, reflective beaches are susceptible to over-wash where dunes are not present or where artificial embankments are not constructed on the backshore (Qi et al., 2010). Berm erosion, depletion of swash bar, seaward migration of subaqueous bars and greatly reduced beach face gradients (MPC =0.5) are typical responses of reflective beaches to storms. Furthermore, overwash can result in a landward loss of sediments from the beach face not just seaward (Qi et al*.,* 2010). Inundation is also prevalent on reflective beaches, especially during storm surges.

2.3.2 Shoreline and Sand-bar Coupling

Many studies have shown that the state of a beach and in turn shoreline-sand-bar coupling is a function of episodic storm events and antecedent wave climate (Gibbs, Mathews & Linke, 1971; Wright & Short, 1984; Masselink & Short, 1993; Masselink & Hughes, 2003; Jackson et al., 2005; van Enckevort & Ruessink, 2003; 2003b; van Enckevort, 2004; van de Lageweg et al., 2013). This highly dynamic beach state and shoreline-sand-bar relationship can be best illustrated by Sallenger's (2000) conceptual fair-weather and storm model, which illustrates the movement of beach sediments from the shoreface to the inner-shelf, not just to the surf-zone, where most beach profile studies occur (Wright et al., 1985).

During high energy events, such as episodic storms, suspended load transport associated with higher bed shear stresses play an important role, whereby particles are suspended into the water column without contact with the bed (Mil-Homens, 2016). During these periods of high energy, wave steepness increases, which results in greater turbulence when waves break and penetrate down to the sediment surface on beaches. As a result, large sediment volumes of various size classes are entrained into, and are suspended within, the water column and are unable to settle out. The cross-shore transport of sediment occurs as a result of

the offshore current, associated with the bed return flow, being stronger than the onshore current, associated with wave asymmetry. This results in a net flux of sediment moving offshore, which results in the shoreline retreating and sand-bars increasing in size and moving further offshore, as illustrated in Figure 2.4 (Wright, Short & Green, 1985; Sallenger, 2000; Masselink & Hughes, 2003; van de Lageweg et al., 2013).

In contrast, bedload transport, associated with low load bed shear stress, plays an important role in cross-shore transport during fair weather periods, whereby sediment rolls or moves in small jump like phases in small layers near the bed (Mil-Homens, 2016). During fair weather periods, wave steepness is reduced and this results in less turbulent energy and the inability to entrain sediments from the beach face into the water column. Thus, no suspended load transport. Moreover, the onshore current, associated with wave asymmetry is greater than the offshore current, associated with bed return flow, which results in a net transport of sediment shoreward. This shoreward flux of sediment results in shoreline accretion, the reduction in sand-bar size and the movement of sand-bars shoreward, as illustrated in Figure 2.4 (Wright, Short & Green, 1985; Sallenger, 2000; Masselink & Hughes, 2003; van de Lageweg et al., 2013).

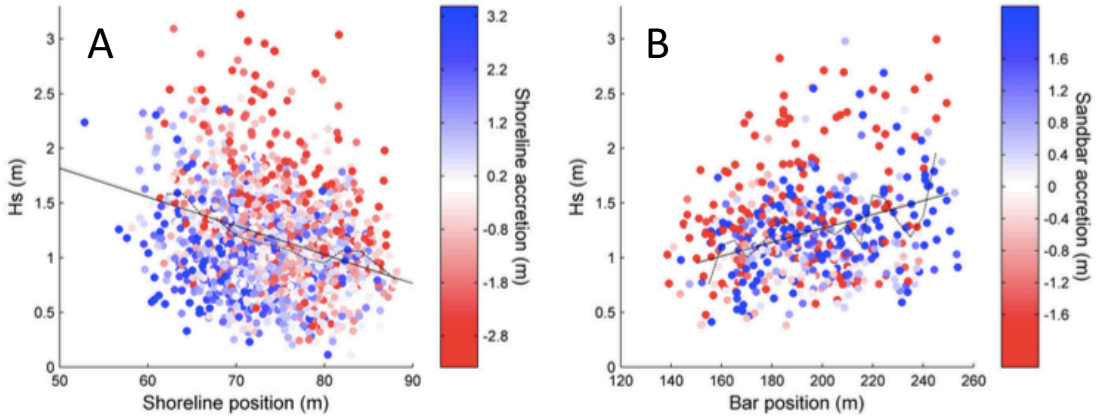

Figure 2-4 Illustrates the relationship between wave height (Hs) and shoreline accretion and location (panel A) and sand-bar accretion and location (panel B). Hs (m) is the mean wave height between measurements (van de Lageweg et al., 2013).

While cross-shore processes are crucial in creating the sand-bars during high energy events, it is the combination of the cross-shore and longshore processes, which play a crucial role in the rotation and positioning of the sand-bars to create the key components of the seabed morphology required for quality surfing waves, such as observed in Figure 2.2 (Mead and Black, 2001b; Mead, 2003; van de Lageweg et al., 2013). van de Lageweg et al. (2013) found that the orientation of the shoreline and sand-bars are generally in phase with the dominant direction of the alongshore component of the wave energy flux i.e. during periods when wave energy fluxes are dominant to the north, the northern ends of a beach would move seaward or rotate. Further, Masselink and Hughes (2003) observed longshore sediment transport and rotation to be a function of the combination of two conditions; longshore currents and wave-induced sediment suspension, as described earlier. Cross-shore gradients in the alongshore shear component of the radiation stress forces longshore currents (and rips). In turn, radiation stress is driven by incident breaking waves (Wright, Short & Green, 1985; Masselink & Hughes, 2003).

Both conditions, longshore currents and wave-induced sediment suspension, are required for significant longshore transport and manipulation of sand-bars to occur and generally both do to some extent as a result of breaking, wind generated, gravity waves (Masselink & Hughes, 2003). The longshore processes, however, which implicate the angle of wave incidence and in turn surf wave quality on a beach can be impacted by shadowing of geographical features such as headlands and engineered structures such as groins and breakwaters, which can cause longshore differences to the intensities of cross-shore processes (van de Lageweg et al., 2013). This shadowing effect may result in erosion immediately in the lee of headlands and artificial structures, which may directly implicate the shoreline-sand-bar coupling in those areas (van de Lageweg et al., 2013), thus affecting the surf wave quality (Mead, 2003).

2.4 Image Analysis Techniques for Extracting Geomorphic and Surfing Parameters from Video Imagery

2.4.1 Shoreline Detection

The knowledge of a shoreline and where it has been in the past is elemental in the prediction of where it will be in the future and thus is incredibly important to the work of coastal scientists, managers and engineers (Aarninkhof et al., 2003; Boak & Turner, 2005). Shoreline analysis is a fundamental component of coastal protection design, developing coastal hazard zones (Bellomo et al., 1999), the development of coastal policy and regulation and shoreline analysis is an integral part of coastal research and monitoring (Smith & Jackson, 1992). To that end, shoreline analysis is used to calibrate and verify models (Hanson et al., 1988). The term shoreline, however, is likely to remain as dynamic as the feature it defines (Boak & Turner, 2005), as different definitions are used for various applications. Therefore, identifying a shoreline can be site-specific and typically involves two stages. Stage one involves the selection and definition of a shoreline indicator that will act as a proxy for the land-water boundary. The second stage of identifying a shoreline involves the detection of a shoreline indicator within the available data source (Boak & Turner, 2005). Some studies (Stockdonf et al., 2002), however, indicate that both these techniques for identifying the shoreline location (shoreline detection) and the assumptions made during the selection of the shoreline indicator have the potential to introduce errors when estimating the shoreline location.

Over the years, many different shoreline indicator features have been used as proxies to delineate the land-water boundary. Moore et al. (1999) and Priest (1999) used the landward edge of cliff tops and the seaward edge of dunes as erosion indicators through manual aerial photograph analysis. These indicators, however, were typically case-specific and whilst indicated good erosion trends these indicators did not very clearly show accretion (time lag). The high-water line has been widely used as a common shoreline indicator feature, which also requires the manual analysis of aerial photographs. A variety of definitions of the high-water line (HWL), however, have been employed by various authors and

these have appeared to change over the years. For example, McCurdy (1950) defined the HWL as the seaward line of two lines of slight discolouration with the more landward line as the storm or debris line, whereas Stafford and Langfelder (1971) and many others (Anders & Byrnes, 1991; Leatherman, 1983; Leatherman & Anders, 1999; Zhang et al., 2002) defined the HWL as the change in colour or grey tone caused by differences in water content of the sand on either side of the HWL. Further, Byrnes et al. (1991) defined the HWL as the wet/dry boundary on a beach, recognised by an abrupt or subtle change in contrast. Those authors also recognised that this may be obscured by shell deposits, debris or vegetation. All of the above shoreline indicators, however, and many others that are similar (e.g. mean HWL) are flawed in the sense that they may not be clearly visible in the source data (e.g. aerial photographs) and they are all typically affected and do not take into account the atmospheric and in turn hydrodynamic conditions at the time of the data collection. Furthermore, these techniques are labour intensive and cost inefficient.

More recently, Aarninkhof et al. (2001) and others (Aarninkhof, 2003; Caljouw, 2000; Dronkers, 2001) through the analysis of Argus video time-exposure images (digital image analysis (DIG) have been able to detect the shorelines through pixel intensity clustering (PIC). PIC identifies shorelines by differentiating pixels based on the colour difference between the wet and the dry beach using Hue (H), Saturation (S) and Value (V). The wet and dry parts of the beach form well-separated clusters in the HS space, thus differentiation between wet and dry pixels in a photo. Furthermore, the vertical position of the shoreline is calculated based on recorded tide and wave information, hence accounts for the atmospheric and hydrodynamic issues that earlier methods did not. Further, this technique is beneficial, as an objective shoreline can be determined, it is repeatable and thus scientifically valid, and it is automated, which significantly increases turnaround times (Aarninkhof & Roelvink, 1999; Aarninkhof et al., 2003; Boak & Turner, 2005).

2.4.2 Sand-Bar and Peel Angle Detection

Similar to PIC, Artificial Neural Network (ANN) detection of sand-bars and shorelines is possible through DIA of Argus video time-averaged images. Pixels are differentiated based on the colour differences. Red, green and blue values of a pixel and are input to ANN, which outputs a binary classification of either water (0) or sand (1) (Aarninkhof & Roelvink, 1999; Aarninkhof et al., 2003; Boak & Turner, 2005). Holman et al. (1993) used the Argus coastal imaging system, which involved the setup of one or multiple cameras overlooking coastal locations of interest, to capture and process both time-averaged images as well as instantaneous images of coastal processes. One of the major benefits of the Argus system is that it is cost-effective, requires very little labour and the fact that the sensor is normally fixed at a location means that only the lens characteristics such as radial distortion and ground control points are required to geo-rectify an image for analysis (Boak & Turner, 2005). Furthermore, beach and surf zone morphology can rapidly change in storm events, thus the having cameras set up allows for sampling to occur at crucial time scales to collect valuable information, such as sand-bar movement during these storm events.

Using time-averaged images, Lippmann and Holman (1989) were first to prove the relationship between the bands of white in the images with the position of submerged sand-bars (cited in Gallop, 2009). The bubbles and foam that result from breaking waves produce patterns of light intensity on the time-averaged images. Lippmann and Holman (1989) made some assumptions regarding this observed pattern to fluid motions. It was hypothesized that the light intensity is recorded in the video images is proportional to the local incident wave energy dissipation (refer to Lippmann and Holman (1989) for equations relating to light intensity to local incident wave energy dissipation (Lippmann & Holman, 1989; as cited in Gallop, 2009)). The hypothesis is based on the premise that more waves break over the shallow areas than deeper areas. It must be said, however, that Lippmann and Holman's (1989) technique for locating submerged sand-bars provides a map of the submerged morphology and not the actual bathymetry (Gallop, 2009). Furthermore, the Lippmann and Holman's (1989) sand-bar finding technique is not without its limitations. During high wave energy events, it was

found that surface foam was persistent, which obscured the relationship between the image intensity to local dissipation. In contrast, during times of low energy, it was found that there were not enough breaking waves to determine to sand-bar locations. Generally speaking, however, during periods low energy, the surf-zone and/or sand-bar morphology does not rapidly change.

Gallop (2009) also found there to be limitation associated with Lippmann and Holman's (1989) sand-bar detection technique. Gallop (2009) found that some images were obscured due to "low amounts of sunlight, sun-glare, shadow, rain and/or condensation on the camera lens". The image issues led to a low degree of contrast between the sand-bars and the rip channels, between which Gallop (2009) was trying to distinguish. As a result, gaps in Gallop's (2009) data set were present, as there were no good quality images recorded during certain tidal cycles.

Atkin (2010) used Lippmann and Holman's (1989) sand-bar detecting technique for detecting peel angles of breaking waves. With the orientation of the white-waterline from the breaking waves known from Lippmann and Holman's (1989) sand-bar detection technique, the peel angle can be calculated when the orientation of the wave crest is known. Atkin (2010) recorded wave activity in 30-minute periods at Boscombe Beach, England, whereby still images could be extracted from the video. Images from the initial point of breaking through to the end of wave breaking were extracted. These still images were enlarged on Adobe Photoshop to accurately annotate the wave crest lines at the initial point of wave breaking, which Atkin (2010) defined as being the point at which white water was observed on the wave face and the white-water lines. Where Atkin (2010) observed a peel angle to change significantly over the course of a single wave (>10°) then a secondary wave crest and white-water line was recorded. In contrast, if variations were <10° then the first breaking section was used. Using the annotated white-water lines and wave crest lines, Atkin (2010) was able to calculate the peel angles of breaking waves through basic trigonometric calculations.

2.5 Study Area and Historical Background

2.5.1 Cultural Significance to Local Māori

Aramoana means “pathway of the sea” (Potiki, 2011 & 2016) and is a place of historical significance to the local iwi. The manawhenua (territorial rights) over the Aramoana is held by Te Rūnaka o Otākou. This responsibility, however, is shared with close hapū including Kāti Huirapa and the wider Kai Tahu iwi. Until the 1900s, a small village existed at Aramoana, which forms the northern shore of the Otago Harbour (Potiki, 2011 & 2016). The highly populated settlement of Otākau was located on the southern shore of the Otago Harbour, the area of which now bears the Otākau Marae. The marae now stands as a cornerstone for the tangata whenua of the region and has a rich history of holding various events of significance.

The Otago Harbour is a site of great importance for Otākau Māori and for the Kai Tahu iwi. Otago Harbour is of great value to the tangata whenua, because it has been an important source of kai moana, it has been used as a major highway, it has provided a sheltering location for human settlement, a place of burial, and finally, it is a symbol of ancestral, spiritual and religious practices of Kai Tahu (Potiki, 2011 & 2016). Like many of the other local bay areas, Aramoana was and is an important mahika kai area (source of food) for local Māori. Between Waitati and Aramoana, the Kaumatua (elders) in 1880 counted 41 mahika kai sites. The mahika kai provided tui, pigeons, fern root, tuna, paua, grouper, mullet, flounder, seals, pipi, cockles and flax (Potiki, 2011 & 2016).

The environmental health of the area is looked after by the local organisation Kāi Tahu ki Otago Ltd (KTKO). KTKO represent all of the surrounding Rūnaka of Otago including Te Rūnanga o Moeraki, Kāti Huirapa Rūnaka ki Puketeraki, Te Rūnanga o Ōtākou and Hokonui Rūnanga. KTKO Ltd works closely alongside Port Otago Ltd with respect to all environmental issues, including the dredging of Otago Harbour with Rūnaka on each of the port dredging boards. Subject to various conditions, the Rūnaka is supportive of the dredging and sees economic and employment opportunities for their people arising from such projects (Potiki, 2011 & 2016).

2.5.2 Regional and Local Geology

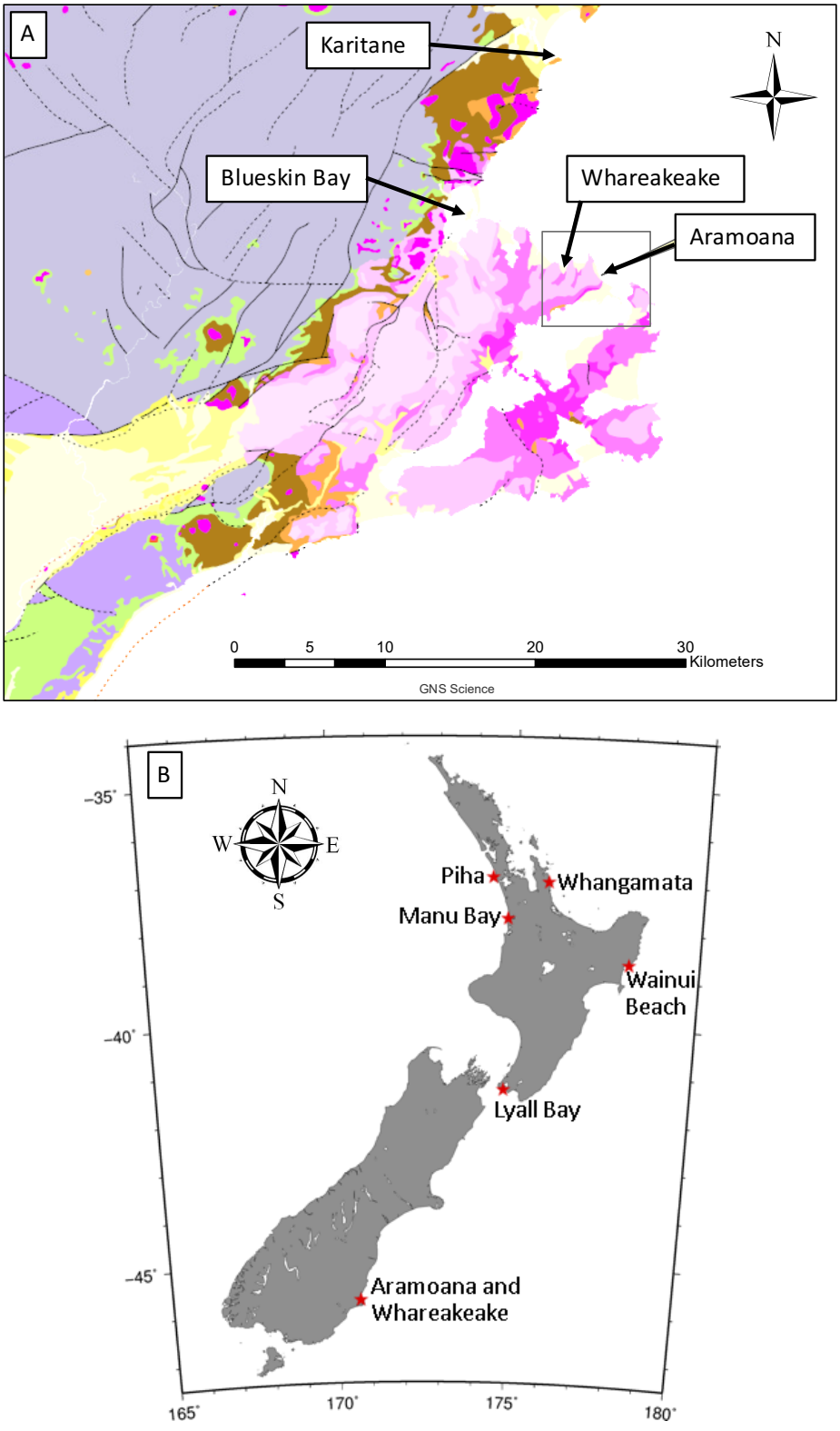

Figure 2-5 Illustrates the geological location plan of Aramoana and Whareakeake surf breaks and the wider Dunedin area (A) and Image (B) depicts the location of all the surf breaks within New Zealand to be studied as part of the 'Remote Sensing, Classification and Management Guidelines for Surf Breaks of National and Regional Significance (GNS, 2014).

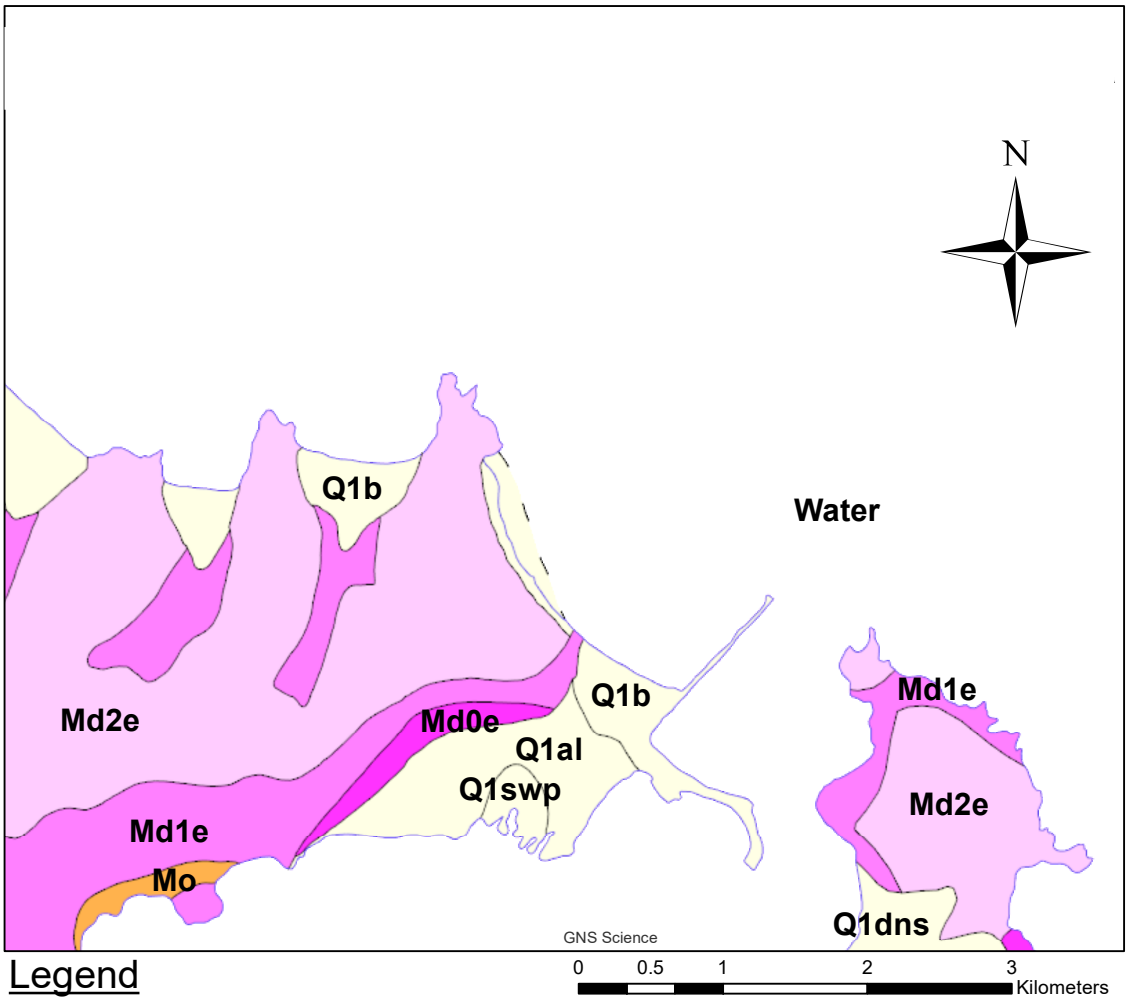

Legend

Mo	Undifferentiated Otakou Group Sandstone - Sandstone - 13 to 22 m/y. Calcareous sandstone, sandy limestone and minor tuff.
Md0e	Dunedin Volcanic Group - Trachyte - 13 to 13.5 m/y. Initial phase extrusives. Trachytic flows and tuffs.
Md1e	Dunedin Volcanic Group - Basalt - 12 to 13 m/y. First main phase extrusives. Extensive flows consisting of olivine basalt, plagioclase basalt, basanite Kaiwekite and trachyandersite.
Md2e	Dunedin Volcanic Group - Basalt - 11.3 to 12.2 m/y. Second main phase extrusives. Extensive flows of trachybasalt, olivine dolerite and basalt phonolite.
Q1b	Holocene Ocean Beach Deposits 0 to 0.007 m/y Loose, well sorted, sand deposited predominantly by marine and lesser aeolian processes with minor gravel and silt.
Q1al	Holocene Shoreline Deposits - Sand - 0.0 to 0.007 m/y. Loose well sorted sandstone, schist and volcanic derived gravel and sand, often quartzose, minor mud and peat.
Q1dns	Holocene Wind Blown Deposits - 0 to 0.007 m/y Loose, well sorted sand and silt deposited mainly by aeolian processes, may show dune forms.
Q1swp	Holocene Swamp Deposits - 0 to 0.014 m/y Poorly consolidated to firm interbedded mud and peat with minor sand, inland peats lack sand.

Figure 2-6 Geological site plan of Aramoana and Whareakeake surf breaks. Note: the legend letters correspond to the letter within the above image (GNS, 2014).

The local geology of Aramoana and the surrounding area is important because the sediment characteristics of Aramoana Beach are a direct function of the local and further field geology (Nicholson, 1979; Hicks, 1985; Griggs, 1987; Single et al., 2010). The erosion rates of the geology and littoral transport up the east coast of the Otago Peninsular determine the sediment budgets of the beach cells up the coastline. Understanding the sediment characteristics of Aramoana Beach is incredibly important when undertaking nourishment or dredge disposal projects. The sediment used in such projects must be similar to the naturally occurring beach sediment or severe erosion can occur directly on the subject beach if the grain size is too small or further up the coastline if the grain size is too big. Erosion of subject beaches (nourishment or disposal of spoil) occurs as the energy acting on the beach is above the grain size entrainment threshold. In contrast, erosion of beach cells down drift can occur when the energy acting on the beach is below the grains size entrainment threshold (Nicholson, 1979; Hicks, 1985; Griggs, 1987; Single et al., 2010).

In general, the geological setting of Dunedin and the Otago Coast represent four main stages of geological history. The first comprises the basement rock, which is formed from Tertiary schist (Figure 2.5A); the second comprises two Tertiary sedimentary sequences (Figure 2.6); the third comprises three late Tertiary eruption phases of the Dunedin Volcano (Figure 2.6) and the fourth comprises the glacial and inter-glacial deposits which were laid down 15,000 to 10,000 years ago (Figure 2.6) (Nicholson, 1979; Single et al., 2010). The Otago Harbour and Otago Peninsular are believed to be located on what is thought to be the center of the Dunedin Volcano. The shorelines of the Otago Peninsular and Blueskin Bay are dominated by the Dunedin Volcanic Complex and modern alluvial deposits. The geology of northern coastline between Blueskin Bay to Karitane is characterised by Tertiary sediments and remnants of volcanic flows. These flows form the currently exposed cliffs that are observed along the sea. About 1.8 million years ago, during the Quaternary period, alluvium deposits were laid down over the volcanic deposits. Lying on the alluvium, loess deposits are observed, and the source is thought to be derived from the seabed. These would have been

deposited during the glacial periods when the sea level was significantly lower (Nicholson, 1979; Single et al., 2010).

The morphology of the Otago Shelf and the sedimentary deposits on the shores are a product of the glacial and interglacial periods that featured during the Late Quaternary through to the Holocene period. The sand deposits observed at the shores are somewhat young (>6,500 years) (Nicholson, 1979; Single et al., 2010). The mineral composition of the nearshore sediments comprise quartz, sodic plagioclase, chlorite, epidote, zoisite, garnet, biotite and wollastonite many of which are signature minerals of the Haast Schist derived from the Clutha River (Andrews, 1973, 1976; Bardsley, 1977; Williams, 1979). These younger sediments are mainly derived from the Clutha River (~3 M m^3/year), Teieri River (~0.6 M m^3/year) and the Southland Shelf (~0.4 M m^3 /year) (Carter, 1986). These sandy sediments are characterised as typically very well sorted, fine to medium sands, which typically have a diameter of between 0.125 mm and 0.14 mm. The sorting is a function wave energy acting upon the shoreline between Karitane and Taiaroa Head. There are of course localised areas where the sediments are not well sorted, however (Nicholson, 1979; Single et al., 2010). Interestingly, Single et al. (2010) suggest that despite all the dredge spoil disposal that has occurred for many decades at Aramoana, Heyward Point and Shelly Beach from Port Otago Ltd operations, the textural nature of the sediments on the beaches and within the nearshore zone of the coastal system between Taiaroa Head and Heyward Point has not changed significantly.

2.5.3 Atmospheric and Wave Climate

The Southern Annual Mode (SAM) plays the most crucial role in the wave direction climate around New Zealand (Godoi et al., 2016). An increase in the SAM causes the waves to rotate clockwise to the south of New Zealand and anticlockwise along and adjacent to the north and west coasts. The SAM is responsible for alternating shifts in windiness and storm events between the middle latitudes, where New Zealand is located (40 to 50 degrees south). During positive phases of the SAM, strong westerlies winds over the southern oceans can be expected, whilst light

winds and more settled weather can be expected over New Zealand. In contrast, during negative phases of SAM, westerly winds and unsettled weather are expected to increase over New Zealand, whilst storm activity and windiness ease over the southern oceans (Renwick & Thompson, 2006).

Another atmospheric oscillation mode that affects the south Pacific weather and/ or ocean is the El Niño-Southern Oscillation (ENSO). ENSO is characterised by sea surface temperature anomalies (Zhang et al., 1997) over the equatorial region of the Pacific Ocean with interannual cycles that range between two and seven years (Trenberth & Hurrel, 1994; Godoi et al*.,* 2016). ENSO is measured by the Southern Oscillation Index (SOI), which gives an indication of the development and intensity of El Niño and La Niña events in the Pacific Ocean and is calculated using the pressure difference between Tahiti and Darwin (Trenberth & Hurrel, 1994; Godoi et al*.,* 2016). Although ENSO only accounts for approximately 25 percent of the year to year seasonal variance in temperature and rainfall, ENSO can have significant implications for New Zealand's climate. Persistent negative values of lower than -7 are indicative of El Niño phase, whereas persistent positive values higher than 7 are associated with La Niña phases (Trenberth & Hurrel, 1994; Godoi et al*.,* 2016).

ENSO has three distinct phases: neutral, El Niño and La Niña. During the El Niño phase (negative ENSO phase), south-westerlies increase around New Zealand (Gordon, 1986; Laing, 2000; Godoi et al., 2016), which results in larger waves propagating from the south and south-west with longer associated wave periods. In contrast, during the La Niña phase (positive ENSO phase), north-easterlies increase around New Zealand, which results in larger waves with small wave periods propagating from the north and north-east (Gordon, 1986; Gorman et al., 2003; Godoi et al., 2016). In 2017-2018, New Zealand was in a positive ENSO phase or La Niña phase, which had been present since early 2016. Prior to 2016, New Zealand experienced a strong El Niño phase, which occurred from early 2014 and peaked in late 2015. Before this, New Zealand was subject to a La Niña phase which began in early 2013 (NIWA, 2017) (refer to Figure A4.1 in Appendix 4).

A 40-year (1961-2001) hindcast study carried out by Sanford South Island Ltd (2001), which assessed sea state conditions at Taiaroa Head concluded that the dominant swell waves were from the north-east followed by southerly swell waves. The study also revealed that the more locally generated north-easterly swell waves were smaller than the waves generated from the south. In contrast, seasonal trends were recognised with larger wave energy events, heights greater than five meters, observed throughout autumn and winter. These were typically propagated from the south and south-east (Single et al*.,* 2010). A more recent study carried out by NIWA (Oldman et al., 2008), using a 20-year WAM hindcast model for an area located three nautical miles east of Taiaroa Head, revealed that the mean significant wave height (Hs) was 1.1 meters, whilst the mean wave approach direction was from 125 degrees (south-east) (as cited by Single et al., 2010).

The Otago Peninsular is exposed to a range of oceanographic forces that act at a local and regional scale. The south-east coast of New Zealand is subject to frequent energetic southerly swells, as well as north-east swells generated from local and far-field events to the north-east. The Otago Peninsular acts to somewhat shelter the northern beaches of Otago from the southerly swells, however, these beaches remain exposed to the north and northeasterly swells. As a result, typical wave heights are around 1.0 m at Aramoana Beach (Single & Benn, 2007; Single et al., 2010).

The Southland Current also plays a role in the hydrodynamics of the region. The Southland Current is a northward flow of water along the south-east coast of New Zealand. The northern littoral drift of sediments along the south-eastern coast of Otago is a function of the combination of the southerly swells and the Southland Current. The northward drifting sediment tends to deposit in the Blueskin Bay area. This deposition is a result of the reduced wave energy within the region and the fact that Blueskin Bay is set back from the Otago Shelf (Single & Benn, 2007; Single et al., 2010).

A portion of the of the northward drifting sediment enters the Otago Harbour on the flood tide. Whilst some of this sediment is transported back out of the Otago Harbour on the ebb tide the majority is retained. Once within the harbour cell, the sediment is transported further up into the harbour where is it deposited in areas of low current strength, such as in wide sections of the channel and on bends. During periods of heavy rainfall, fine silts also enter the Otago Harbour through the Leith River, small creeks and stormwater drains (Single & Benn, 2007; Single et al., 2010). Thus, to allow for safe navigation within Otago Harbour, the Harbour is dredged by Port Otago Ltd.

2.5.4 Dredging History of the Otago Harbour and Disposal at Aramoana & Whareakeake

The Otago Harbour shipping channel is separated into two parts. The stretch from Dunedin to Port Chalmers is known as the Victoria Channel (VC), whilst the stretch from Port Chalmers to the harbour entrance is known as the Lower Harbour Channel (LHC). Construction of the main shipping channel, the LHC, took place from 1877 to 1881, during which time around 3 M m^3 of sediment was excavated. The majority of this excavated material was believed to be used in reclamation projects or was else disposed of at Heyward Point. In the late 1880s, the channel was extended from Port Chalmers to Dunedin. Between the years of 1882 and 1886, the sand-bar at the harbour entrance was dredged. The last of the channel developments within the 19th century occurred in 1898 when the VC was deepened to 7.0 m. Approximately 1 M m^3 of sediment was excavated. In 1976 the LHC was again developed and deepened to 12.0 m to accommodate greater navigational opportunities. This produced an estimated 3 M m^3 of sediments dredged, however, little of these sediments were used in reclamation projects. The various disposal locations and respective percentages disposed at these locations, through the years between 1914 and 1984, can be observed in Figure 2.7 (Lusseau, 1999).

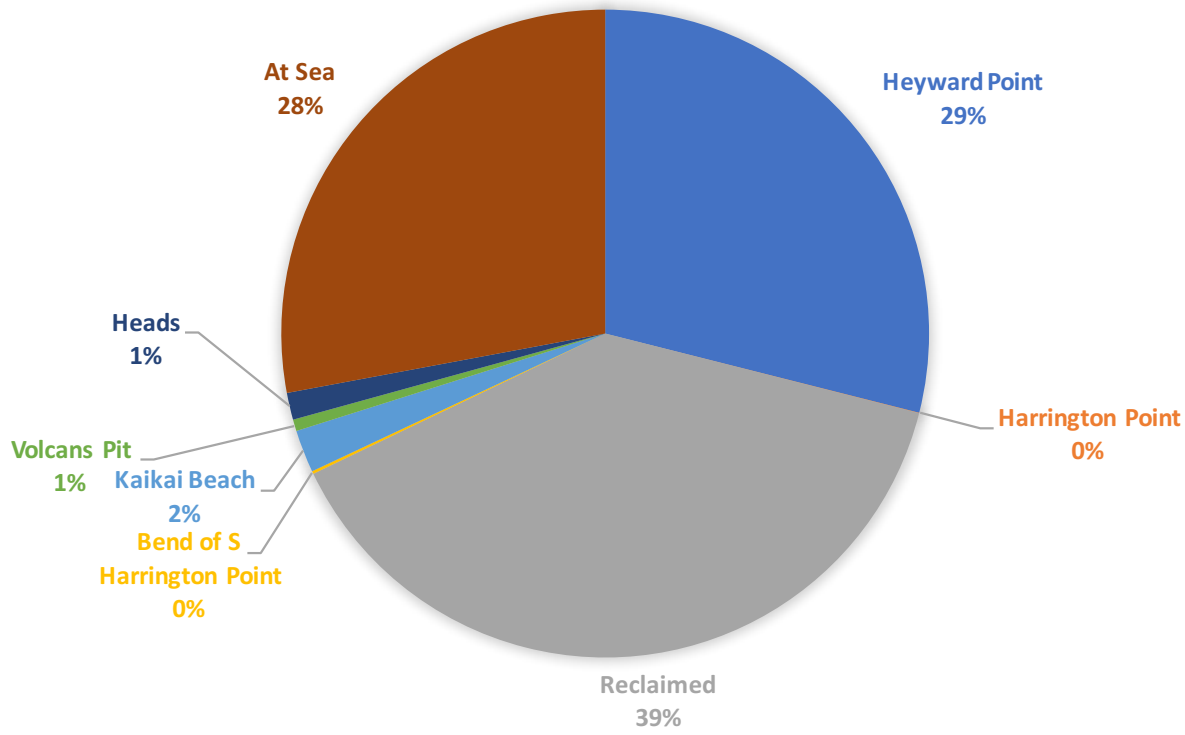

Figure 2-7 Indicates dredge spoil disposal locations and percentages of material disposed at these locations during the years between 1914 and 1984. Note: no records before 1914 exist and that the "at sea" disposal location most likely represents the Heyward Point location (Lusseau, 1999).

As illustrated in Figure 2.7, the majority of the material was disposed at Heyward Point; however, that disposal location is not entirely the same as the one used (at the time of writing). Lusseau (1999) discovered that after the last development, in 1976, a secondary disposal site at Heyward Point, only a few hundred meters away from the original site, was opened to help dissipate the large quantity of spoil that had been excavated during that capital dredging period. With the opening of new disposal sites, the "Spit" in 1985 and the "South Spit Beach" in 1987, the Heyward Point site became less utilized and was no longer the primary disposal site, as illustrated in Figure 2.8.

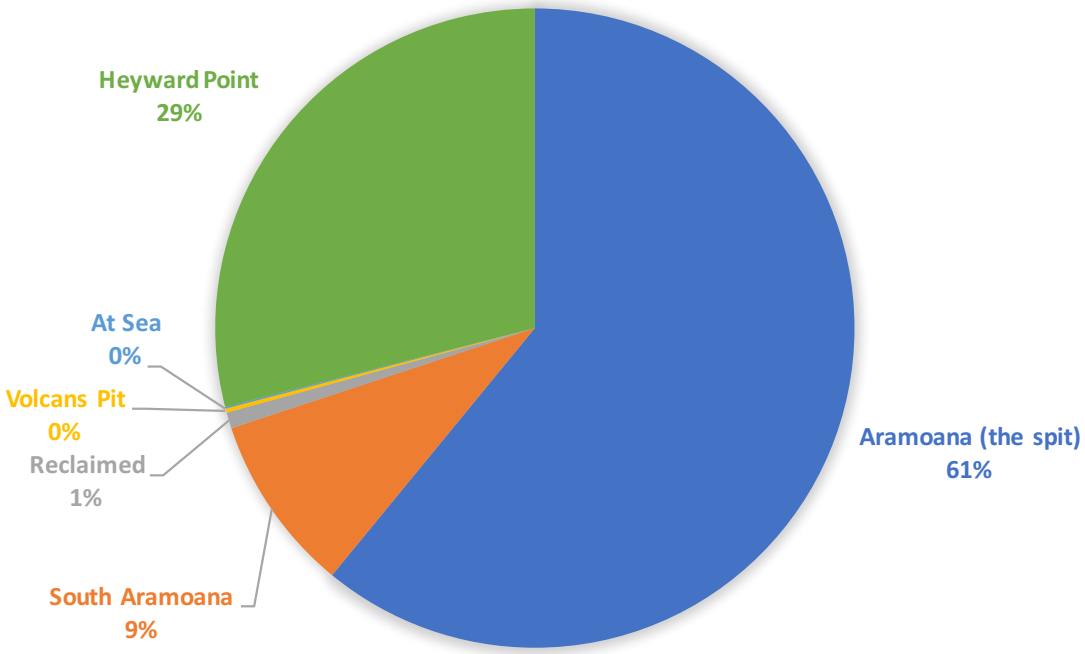

Figure 2-8 Indicates dredge spoil disposal locations and percentages of material disposed at these locations during the years between 1985 through to 1987. Note: That the "at sea" disposal location most likely represents the Heyward Point location (Lusseau, 1999).

From 1985 through to 2005, there was an overall decline in dredge spoil disposal across all three major disposal sites at sea; Heyward Point, the Spit (Aramoana) and Shelly Beach, as observed in Figure 2.9 (Port Otago Ltd, 2013). The reduction in disposal is related to the reduction in maintenance dredging over time because the slopes of the lower channel began to stabilise (Weppe et al., 2015). Records indicate a consistent decline in dredge disposal activity at sea, with the previous 10-year average from 2003 to 2013 of only 140,796 m^3 compared a previous 29-year average from 1985 to 2013 of 207, 891 m^3. Figure 2.9, however, also indicates that from approximately 2008 onwards, the major disposal site changed once again from the Spit back to Heyward Point (Port Otago Ltd, 2013). More recent records provided by Port Otago Ltd, indicate that the previous five-year dredge disposal average, from 2010 to 2014, at the Spit was only 14,120 m^3 per year, whereas at Heyward Point the previous five-year average was 143,992 m^3, which is just over ten times greater than dredge disposal at the Spit (Weppe et al., 2015). In fact, disposal at Shelley Beach was on average higher per year over the previous six-year period than the Spit, with 18,577 m^3 per year (Port Otago Ltd, 2013). The

three main disposal sites; Heyward Point, Aramoana (the spit) and Shelly Beach, that were used up to 2014 are illustrated in Figure 1.6.

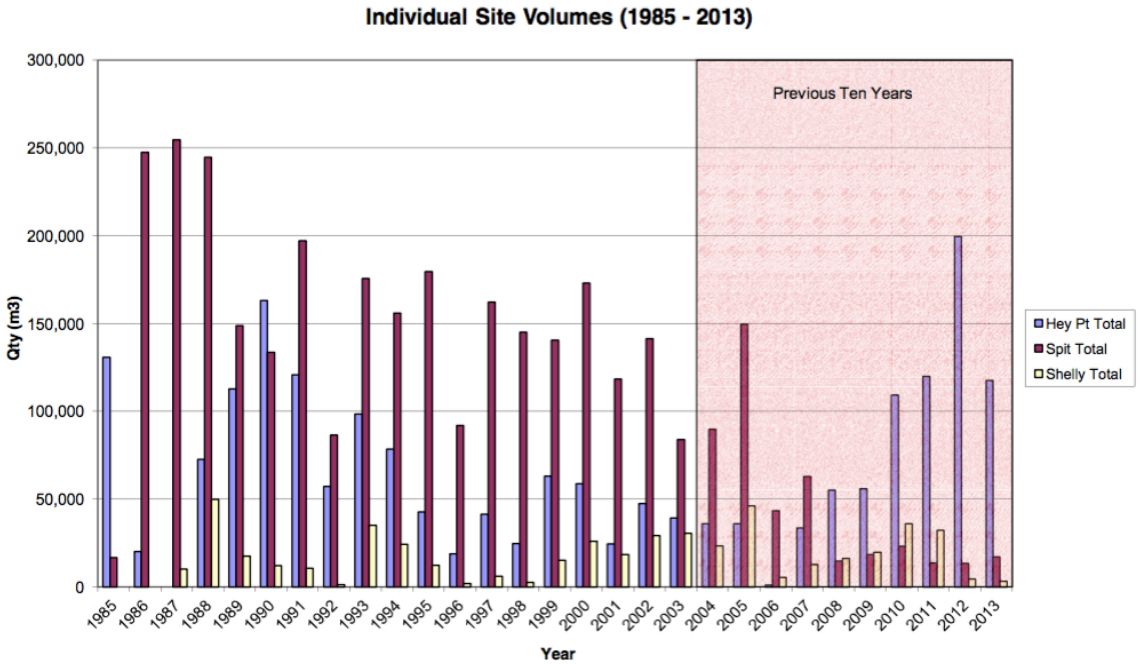

Figure 2-9 Individual disposal volumes (m^3) per year at Heyward Point (blue bars), the Spit (red) and Shelly Beach (yellow) from 1985 to 2013 (Port Otago Ltd, 2013).

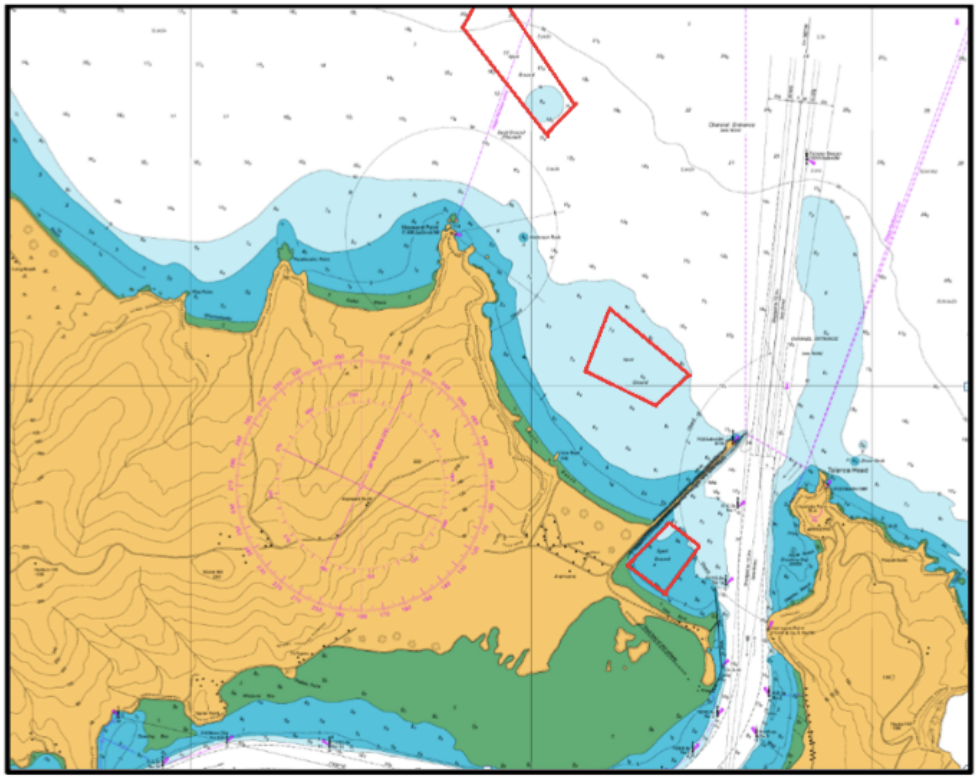

Figure 2-10 Nautical chart illustrating the three-main dredge spoil deposal grounds that were used up until 2014, as indicated by the red polygons. Top polygon represents the Heyward Point ground, the middle polygon represents the Aramoana ground and the bottom polygon represents the Shelly Beach ground (Weppe et al., 2015).

2.5.5 Next Generation Project (Next Gen)

On the 7 June 2017, Port Otago Ltd (POL) obtained a new 25-year consent from the Otago Regional Council to deepen and widen the LHC including the entrance region. Studies indicated that up 7.2 M m^3 of sediment would be dredged initially as part of the capital dredging campaign (Weppe et al., 2015), which will affect the hydrodynamics and the sediment within the Otago Harbour and at the entrance (Bell et al., 2009). The dredging consent (Otago Regional Council 2010) allows for disposal across three sites; Shelly Beach, Aramoana and Heyward Point (see Figure 1.6). The conditions of the consent allow for a maximum disposal quantity of 450,000 m^3 across all three sites. The total volume deposited across the Heyward point and Aramoana disposal grounds shall not exceed an average of 300,000 m^3 per year, calculated over a five-year period. Notwithstanding the previous condition, the total volume deposited at Aramoana should not exceed an average of 100,000 m^3 per year, calculated over any five-year period and no more than 50,000 m^3 per year shall be deposited of on an annual basis at Shelly Beach. It is the intention of the consent that the normal annual deposition of 100,000 m^3 at Aramoana and up to 200,000 m^3 at Heyward Point is carried out.

Currently, at the time of writing, on average, 60,000 m^3 of sediment are dredged each year as part of entrance channel maintenance, which ensures the prevention of channel infilling, which in turn ensures safe navigation (Weppe et al., 2015). Weppe et al. (2015) indicate that with the additional deepening and widening of the LHC this annual maintenance dredging will have to increase by about 60% to 100,000 m^3. This a direct result of the northern and westward flux of sediment travelling up the coast from the strong southerly swells and the Southland Current (Heath, 1972).

As these sediments drift up and around the coastline, larger quantities will become trapped within the proposed deeper channel with additional sediment trapped on the eastern side of the submerged ebb tidal delta (Weppe et al., 2015). These sediments would otherwise drift past the channel and nourish Aramoana Beach. Thus, a significant deficit within the Aramoana sediment budget will likely occur if dredge disposal within the Aramoana compartment does not occur.

Moreover, the sediment depletion will affect the beaches further up (north) the Otago Peninsular, such as Kaikai Beach, Whareakeake Beach, Long Beach as well as affecting the natural infilling processes at Purakanui Bay and Blueskin Bay (see Figure 2.11) (Elliot, 1958). Furthermore, studies indicate that annual storm activities can move anywhere between 50-100,000 m^3 per year of sediment around Heyward Point from the Aramoana cell (Weppe et al., 2015), further highlighting the need for nourishment.

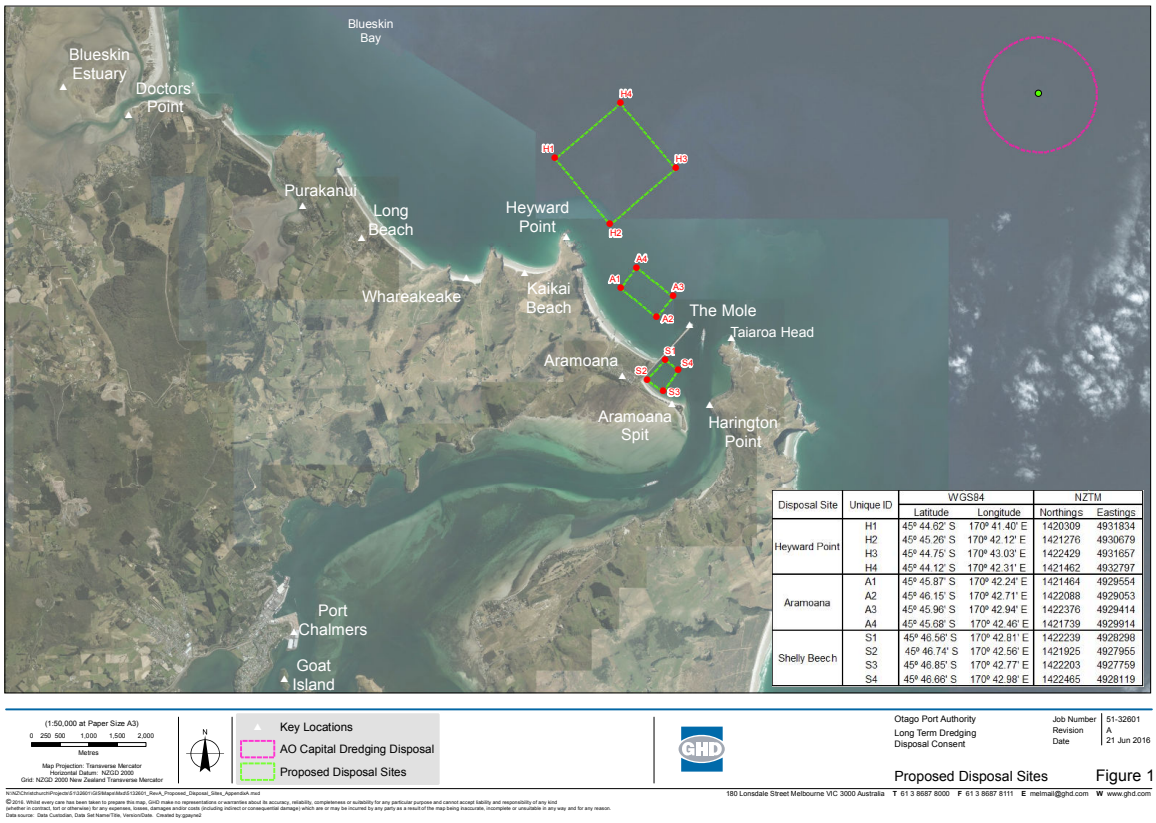

Disposal Site	Unique ID	WGS84 Latitude	WGS84 Longitude	NZTM Northings	NZTM Eastings
Heyward Point	H1	45º 44.62' S	170º 41.40' E	1420309	4931834
	H2	45º 45.26' S	170º 42.12' E	1421276	4930679
	H3	45º 44.75' S	170º 43.03' E	1422429	4931657
	H4	45º 44.12' S	170º 42.31' E	1421462	4932797
Aramoana	A1	45º 45.87' S	170º 42.24' E	1421464	4929554
	A2	45º 46.15' S	170º 42.71' E	1422088	4929053
	A3	45º 45.96' S	170º 42.94' E	1422376	4929414
	A4	45º 45.68' S	170º 42.46' E	1421739	4929914
Shelly Beech	S1	45º 46.56' S	170º 42.81' E	1422239	4928298
	S2	45º 46.74' S	170º 42.56' E	1421925	4927955
	S3	45º 46.85' S	170º 42.77' E	1422203	4927759
	S4	45º 46.66' S	170º 42.98' E	1422465	4928119

Figure 2-11. Illustrates the new Heyward Point Spoil Ground (HPSG), which overlaps the original HPSG, comprising 100 150 m^2 cells, the new Aramoana Spoil Ground (ASG) and new Shelly Beach Spoil Ground, as confirmed in the approved Port Otago Ltd Next Generation Consent (Otago Regional Council, 2017; Port Otago Ltd, 2018).

The construction of "the mole" at the Otago Harbour entrance and the nourishment of Shelly and Aramoana Beaches are of great importance to maintaining the sandy character and the beach states of these two beaches (Bunting et al., 2003; Kilpatrick, 2005; Scarfe et al., 2009a &b). With respect to Aramoana Beach, however, it is not clear how these effects change the beach character. Up until recently (2008), dredge spoil from the channel was primarily

deposited at the nearshore Aramoana spoil ground, as depicted in Figure 2.10, which resulted in beach accretion. The spoil disposal nourished Aramoana Beach, conserving its volume. This deposition, however, also resulted in the choking of the beach, because too much sediment drifted shoreward and welded to the shoreline. During this time, a reduction in bifurcation (splitting) of the wave crests in lee of the existing spoil mound was observed, which is a fundamental component in creating the world-class quality surfing waves Aramoana Beach is known for (Bunting et al., 2003; Kilpatrick, 2005; Scarfe et al., 2009a & b; Weppe et al., 2015). In turn, surfers observed a reduction in surfing quality during the period leading up to 2008 (personal communication from eCoast stakeholder meeting in Dunedin on the 14th May 2016).

After 2008, POL changed the primary disposal ground back to the Heyward Point ground. Through the years between 2015 to 2016, POL all but ceased disposal at the Aramoana spoil ground. Since then, surfers have observed a slight return in surfing quality over time (personal communication from eCoast stakeholder meeting in Dunedin on the 14th May 2016). The observed return in surfing quality is arguably the result of a combination two variables 1) the reduction in shoreward movement of sediment from the Aramoana spoil ground, (i.e. less welding of sediment onto the shoreline) and greater bifurcation (splitting) in lee of the existing Aramoana spoil mound and 2) the loss of sediment from the Aramoana Beach cell around Heyward Point due to normal littoral drift, which may have been enhanced by winter storms. Evidence suggests, however, that if disposal of an optimal beach nourishment quantity is not resumed, Aramoana Beach will erode, which may deteriorate the surfing quality once again (Bunting et al., 2003; Kilpatrick, 2005; Scarfe et al., 2009a & b; Weppe et al., 2015). Thus, targeted sediment disposal at the Aramoana spoil ground (ASG) is essential to ensuring the appropriate surfing components are not compromised and to ensure Aramoana Beach is appropriately nourished.

Research by Weppe and McComb (2016b) suggests that beach nourishment in the order of ~70 to 90,000 m^3 per year may be required to compensate the additional sediment budget deficit within the Aramoana compartment from Project NextGen

dredging activities. This is broken down into two components. The first being ~35,000 m^3 as the best estimate of the optimal annual volume needed to maintain a sediment equilibrium on Aramoana Beach and the remaining 35 to 55,000 m^3 is needed to compensate for the sediment volumes lost around Heyward Point due to strong westerlies developed by storms.

2.5.6 Formation of Surf at Aramoana and Whareakeake

Studies by Kilpatrick (2005) and Scarfe et al. (2009a & b*)* indicate that the world-class surfing waves observed at Aramoana and Whareakeake are almost purely a function of the offshore preconditioning over the offshore features. A hydrographic survey carried out by Kilpatrick (2005) and a wave refraction model undertaken by Scarfe et al. (2009a & b) indicate that the surfing waves form due to the extreme wave focusing over the Otago Harbour ebb tidal delta (OHETD) and the Aramoana spoil mound (ASM) and Heyward Point spoil mound (HPSM), which further improve the observed surfing conditions at Aramoana. The same wave focusing mechanism causes improvements to occur in the Whareakeake surf breaks also, but to a lesser extent. Kilpatrick (2005) was able to create a before and after bathymetry dataset, which enabled Kilpatrick to make a direct assessment of wave transformations that occurred before and after the spoil mounds presents.

The model results indicated distinctly, that the waves converge and focus over the OHETD and that this enhances the wave energy in the lee of the OHETD, which is in turn further enhanced by additional converging and focusing over the ASM. The converging and wave focusing in lee of the OHETD and ASM improve the surfing by creating a gradient in height along the wave crest, which promotes wave peeling, because the higher areas of the wave (created by the focusing) initiate breaking first followed by the areas along the crest of the wave with smaller heights (Kilpatrick, 2005; Scarfe et al., 2009a & b), an effect which has also been illustrated in many other studies (Battalio, 1994; Beamsley & Black, 2003; Mead, 2003; Mead & Black, 2001; Mead et al., 2003). The OHETD and ASM also act to enhance the surf quality by slightly rotating the wave by refraction, which reduces

the angle between the wave orthogonal and the ideal surf contours. The wave focusing, and rotational effects can be observed in Figure 2.12.

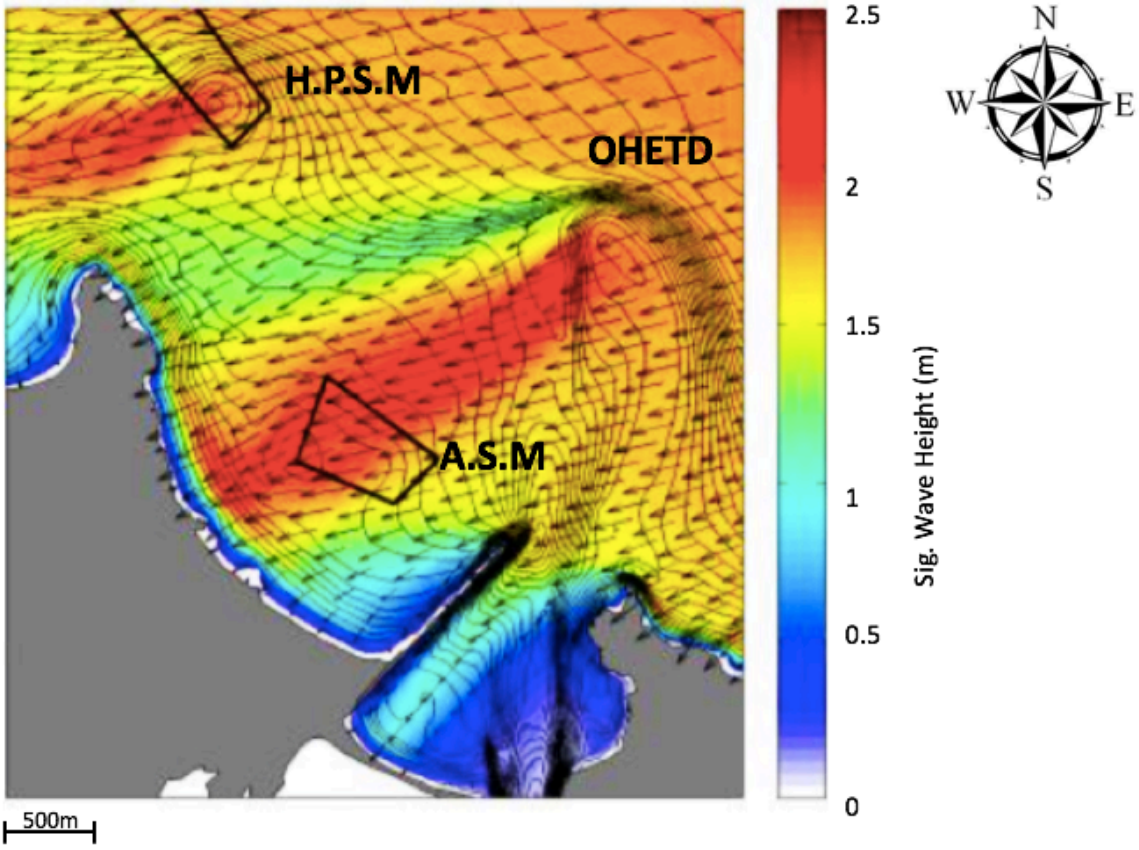

Figure 2-12 MIKE 21 nearshore wind-wave model indicating extreme wave focusing over the Otago Harbour ebb-tidal delta, which is further enhanced by the Aramoana spoil mound just offshore of the surfing break (McComb, 2016).

2.5.7 Surfing History – The Local Perspective

POL carried out multiple surveys with local surfers to gain a better understanding of the public opinion of surfing quality at Whareakeake and Aramoana. In general, Aramoana was found to be a far more popular break, as the surf is more consistent with the quality of wave observed compared to Whareakeake. Aramoana Beach is broken down into three main areas; north, mid and south end. Mid is regarded as the most popular area to surf, which is possibly a result of the preconditioning of the waves. The preconditioning aligns the waves perfectly with the middle section of Aramoana Beach. When the long-range swell waves arrive at Aramoana Beach, the largest most desirable surfing waves are observed in the middle section. This is followed by the north end. It was found that the south end is not surfed very often because ideal surfing waves are not often observed there. Furthermore, the

south end is often regarded as the "kiddie corner" by local surfers. One possible explanation for this is that the mole shadows the south end and any incoming waves deflect off the mole. Hence, the waves do not reach the south end as often as the mid and north end. Conditions in the south, however, depend on the incoming swell direction. The most desirable waves are observed at low tides across all surf areas with an offshore wind (McKenzie, 2015).

Whareakeake surf break had the most observed "barrels" (plunging waves) along with the mid location at Aramoana Beach. Such waves, however, are uncommon at Whareakeake. This is because the ideal swell direction is from the north, which does not often produce many high energy swell events (McKenzie, 2015).

2.6 Chapter Summary

There are three key components which influence and control world class surfing waves around the world: the peel angle; wave steepness; and reef shape or beach morphology. The peel angle describes the speed at which a surfer must travel along a wave to succeed in traversing across the face of a wave and is defined as the angle between the trail of the broken white water and the crest of the unbroken part of the wave as it propagates shoreward. The ability of a surfer is a direct function of the peel angle; the smaller the peel angle the better the surfer must be. The wave steepness or breaking intensity is a function of the orthogonal seabed gradient. This relationship between the angle of the approaching wave relative to the seabed gradient determines the breaking intensity of a wave. Further, breaking intensity is a function of wave period and wave height. As wave period increases, the breaking intensity increases, whereas as when wave height increases the breaking intensity decreases. The morphology of the seabed is the most important factor controlling the quality of surfing waves, as the peel angle and breaking intensity are a direct function of the seabed morphology.

The morphology of the seabed preconditions incoming swell waves to align with the isobaths by wave refraction. The preconditioning acts to promote convergence and divergence, which alters local wave heights to preserve constant energy,

which in turn promotes and initiates wave breaking and peeling. Sandy beach breaks are susceptible to rapid changes in morphology because they lack a reef type structure. Beach breaks work as a result of complex shoreline-sand-bar coupling, which in turn is a function of the antecedent or episodic wave climate. The wave climate determines the amount of energy being dissipated onto a beach at any given time and as a result, can be used to classify the morphodynamic state of a beach. Beach state denotes the relationship between morphological features of a beach and hydrodynamic processes upon which the beach is subject. Beach states range from dissipative at one extreme to reflective at the other extreme with four intermediate states in between and can be determined by the Dean's Parameter (1973). During fair-weather periods, beaches typically exhibit a more reflective state, whereas, during storm-weather periods, beaches typically exhibit a more dissipative state.

Sand-bar orientations, lengths and positions on a beach at any given time are a direct function of the beach state, which in turn is a function of the forcing wave climate. In turn, the geomorphic and surfing parameters extracted, using techniques such as ANN (Aarninkhof & Roelvink, 1999), Lippmann and Holman's (1989) sand-bar detection technique and Atkin's (2010) use of the sand-bar detection technique to determine the peel angle, are a direct function of the beach state and forcing wave climate.

The study site of Aramoana is of singular site importance to Otākau Māori and for the Kai Tahu iwi. Otago Harbour is of great value to the tangata whenua, because it has been an important source of kai moana, it has been used as a major highway, it has provided a sheltering location for human settlement, a place of burial, and finally, it is a symbol of ancestral, spiritual and religious practices of the people of Kai Tahu.

The sediment characteristics of Aramoana Beach are a direct function of the local and further field geology. The erosion rates of the geology and littoral transport up the east coast of the Otago Peninsular determine the sediment characteristics and budgets of the beach cells up the coastline. The SAM and ENSO play significant

roles in the New Zealand climate. ENSO specifically has a significant effect. During El Niño phases, strong westerlies, unsettled weather and increased wave heights propagating from the south-west (refract to south-east) are common, whereas, during La Niña phases, north-easterlies, settled weather and increased waves (to a lesser extent than El Niño) propagating from the north-east are common. At Aramoana, seasonal trends indicate dominant swell waves from the south-east during autumn and winter and from the north-east during spring and summer.

The LHC has been dredged since 1877 with many capital dredging projects since then. The majority of the at sea spoil has been disposed of at three sites; Hayward Point, Aramoana Beach and Shelly Beach. Project Next Generation could cause damage to the Aramoana surf break if dredge spoil disposal is not carried out appropriately. Surfing waves at Aramoana Beach are purely a function of the offshore precondition over the offshore features. Surfing waves form due to the extreme wave focusing over the OHETD and the ASM. The waves converge and focus over the OHETD and this enhances the wave energy in the lee of the OHETD, which is in turn further enhanced by additional converging and focusing over the ASM. The converging creates gradients in wave heights, which in turn promotes and initiates wave breaking and peeling. The OHETD and ASM also refract the waves to align with the ideal surf contours. Surfing is reportedly most popular in the middle region of Aramoana Beach, known as ‘the mid'. ‘The mid' reportedly has the biggest and most consistent waves along the beach.

Chapter Three

Methodology

3.1 Introduction

This chapter discusses the methodology used to collect and process the data, the techniques on image capture and the detailed processes of image rectification. Computer algorithms used to process the data are also critically discussed while highlighting unsuccessful methodologies for the benefit of future learning. Extrinsic calibration is the process of ensuring data can be used from cameras without any errors. With the extrinsic matrix, the orientation between the camera and an object in an image is calculated, where the object can be confirmed in many images. As previously mentioned, Aramoana Beach is the surf break of interest; however, the methodology for image capture and processing at Whareakeake surf break was nearly identical to that used for Aramoana. The research of Whareakeake surf break for the purpose of this thesis was ended after the image processing stage, as the algorithms created for finding the sand-bar and trough locations were not successful. The methodology for rectifying the Whareakeake camera is found in Appendix 2.

3.2 Extrinsic Calibration

3.2.1 Remote Imagery Acquisition

Remote cameras were set up above Aramoana Beach by Port Otago Limited (POL) to monitor for the change in surf quality over time with respect to dredging spoil disposal. Two cameras were set up on the cliffs above Aramoana surf break to capture a wider scope of the break (cameras one and two). The position of these cameras is indicated on the Figure 3.1A. Camera one and two are located at 45 46' 22.30''S 170 42' 00.05''E. These cameras were programmed to record a snapshot of the surf breaks every five minutes. Snapshot images have been recorded since

September 2013 from camera one and April 2015 from camera two to present and will continue into the future. An example of the images recorded from each the respective cameras is illustrated in the Figure 3.1B and C. Images are stored on a hard drive at the remote camera locations. POL regularly downloads these images and stores them in their database. These images have been made available by POL to the University of Waikato and eCoast for surf break analysis.

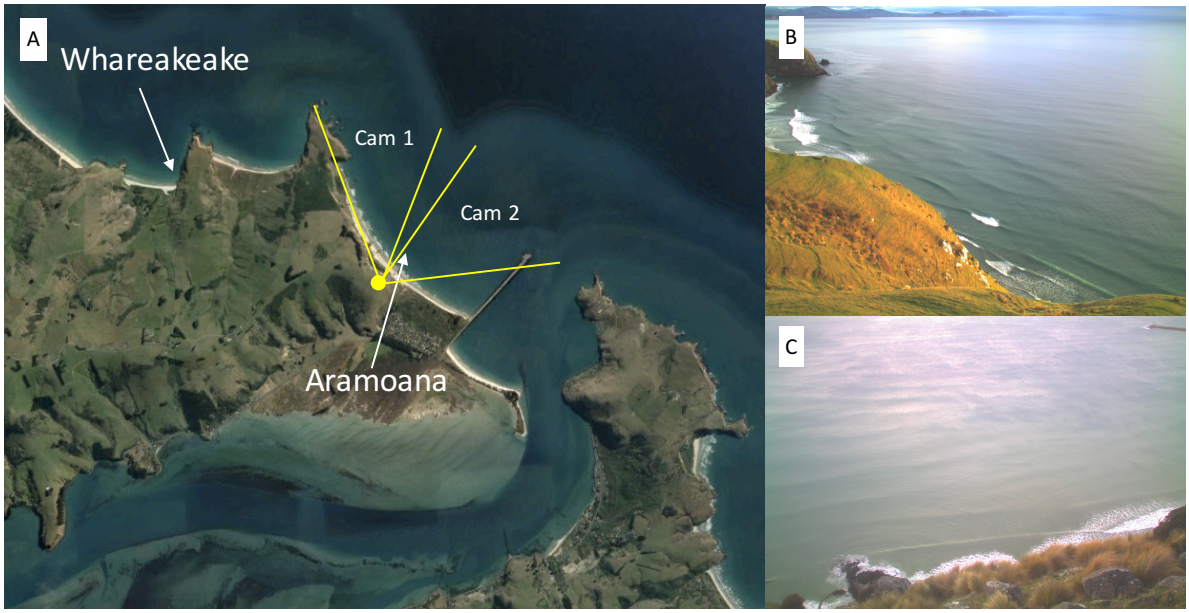

Figure 3-1 Indicates the Aramoana Surf Break location as well as the camera locations and angle (A). Note: Cam 1 represents Camera 1 and Cam 2 represents Camera 2 (Google Earth, 2017). The right-hand panel depicts images from camera 1 (B) and camera 2 (C).

3.2.2 Rectification of Images

Once the images were received from POL, the process of rectifying the images could begin. Image rectification is the process of converting images to a standard map co-ordinates system. This is typically achieved by matching ground control points (GCPs) in the mapping system to points or coordinates from the images (Ranasinghe et al., 2004; Toutin, 2004). The GCPs were collected by staff from POL. A survey boat was navigated up and down Aramoana Beach while stopping at various non-specific locations that covered a wide range of proximities to the Aramoana coastline. Once stationed at these sites, a Global Positioning System (GPS), which was positioned on the back on the boat (near the motor), was turned on, and recorded the exact time (UTC), date, easting and northing coordinates of

the respective GCPs and the water level relative to ellipsoid (m). These non-specific sites were also given a location name. As the cameras were programmed to take a snapshot at five-minute intervals, it was essential that the boat be stationed at the sites during the times the images were periodically taken. Examples of the GCP collecting process can be observed in Figure 3.2.

The time-stamped GCP data was then synchronised with the time-stamped images to create a chronological match. The images were then loaded into Matlab to an algorithm called *'Findpos_Stoyanov_jai'*. This script used information on the properties of lenses of each camera to correct the images for any distortions. The properties of the lenses were measured in the laboratory by the National Institute for Water and Atmospheric Research, by taking images of black and white grids from a number of different positions. These were used by a computer algorithm to find the optimum values of the focal length, image center, aspect ratio and radial and tangential distortion coefficients (the intrinsic parameters of the camera). Image coordinate points (ICPs) could be ascertained from locating the boat positions within a reference image from each camera (Figure 3.2). The locations of the ICPs (associated with each of the GCPs) along Aramoana Beach can be observed in Figures 3.3 and 3.4. The saved GCP and ICP data were then reloaded back into the '*Findpos_Stoyanov_Jai'* script so that the discrepancies between the actual GCPs and ICPs calculated by the software could be compared. Through error identification, the discrepancies between the actual and calculated GCPs and ICPs, within the plots (Figures 3.5A, 3.5B, 3.5C and 3.6A, 3.6B, 3.6C), were removed, which produced a rectified image (birds-eye-view) from the respective cameras. Figures 3.5A and 3.6A depict an example of a rectified image from camera one (Figure 3.5A) and camera two (Figure 3.6A).

Figure 3-2 Image depicts GCPs being collected along Aramoana Beach on the 11th March 2015 by a POL boat The left panel is an image snapped by Camera 1 at Aramoana and the right panel is an image snapped by Camera 2 at Aramoana. Note: the red boxes indicate the position of the survey boat.

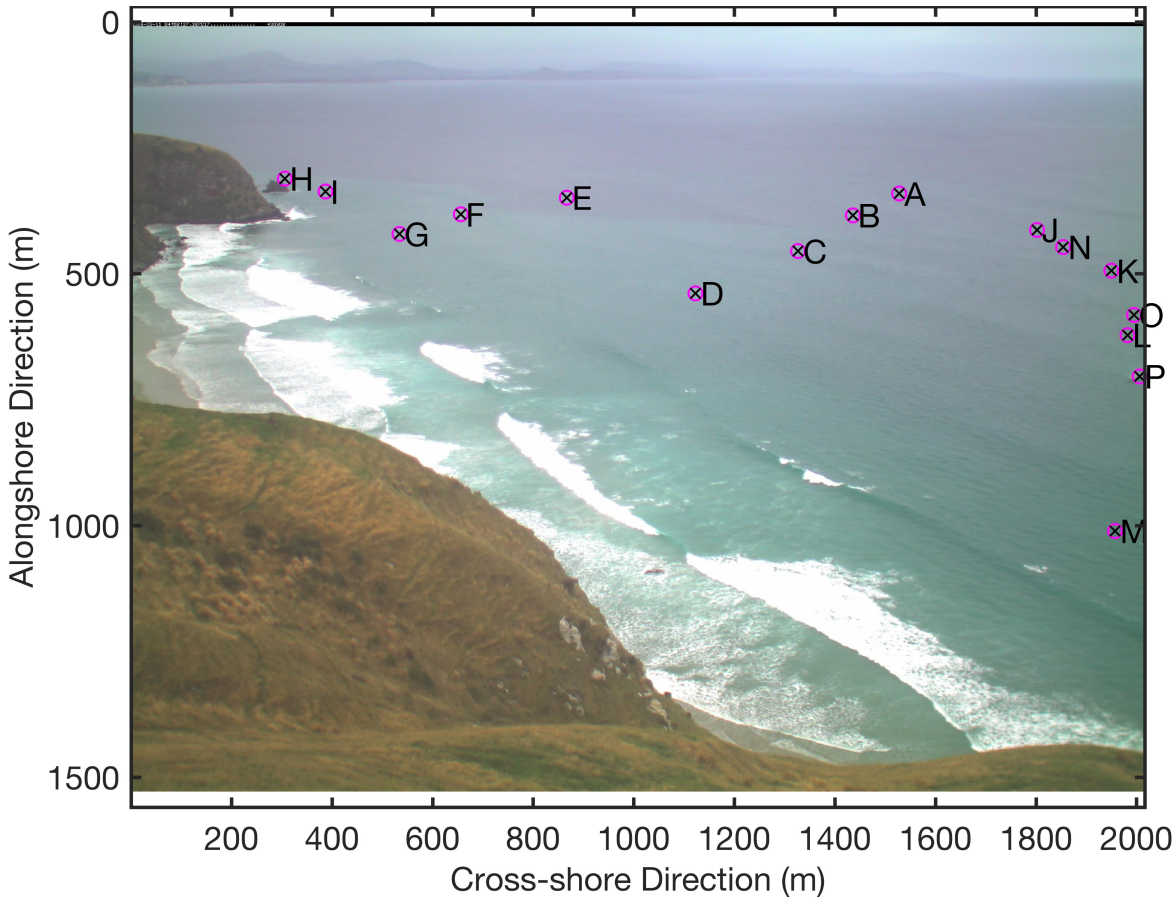

Figure 3-3 Depicts the easting and northing (m) image coordinates of the GCPs from Camera 1 on Aramoana Beach. Each letter corresponds to a GCP. This image was recorded on the 11th March 2015 at 17.06.54pm. Note: the letters do not correspond to Camera 2 and 3 letters.

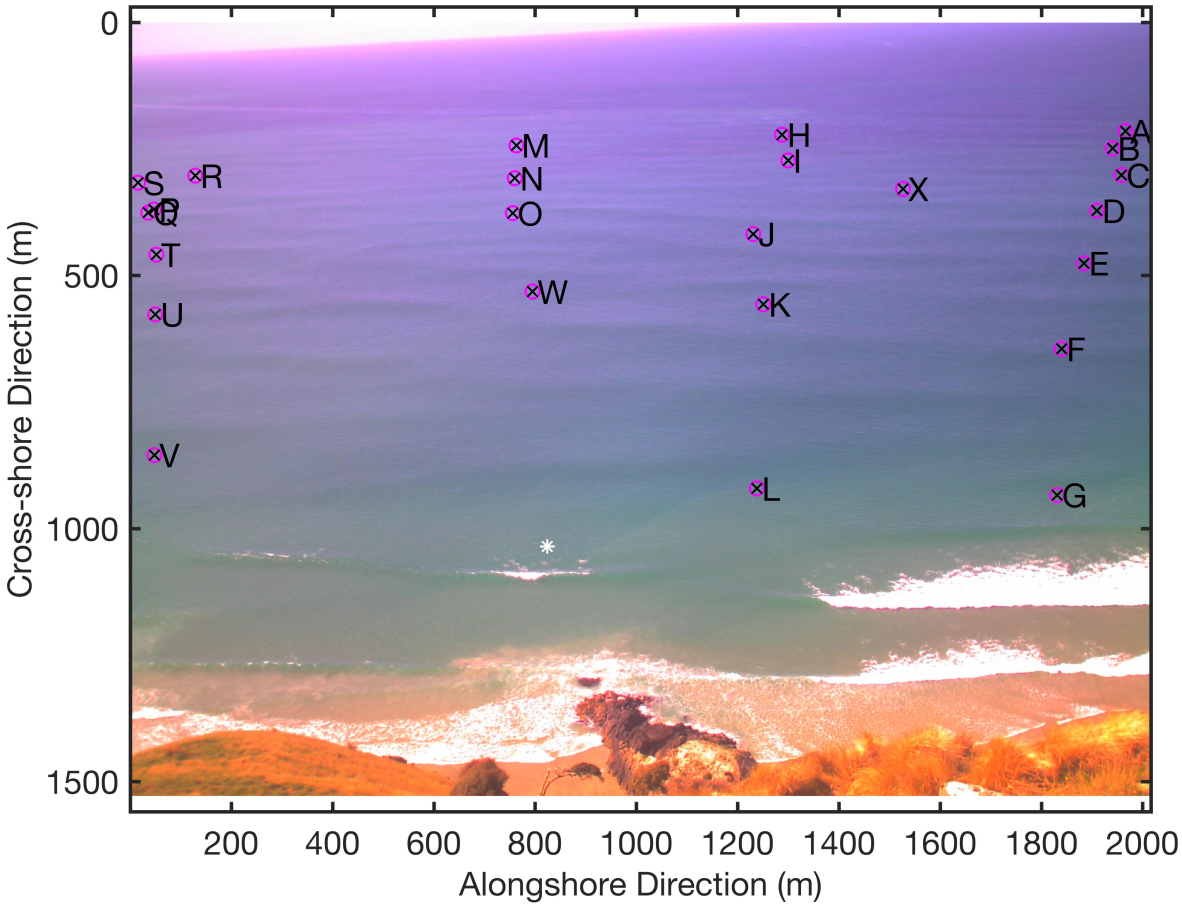

Figure 3-4 Depicts the easting and northing (m) image coordinates of the GCPs from Camera 2 on Aramoana Beach. Each letter corresponds to a GCP. This image was taken on the 11th March 2015 at 14:22:53pm. Note: the letters do not correspond to Camera 1 and 3 letters.

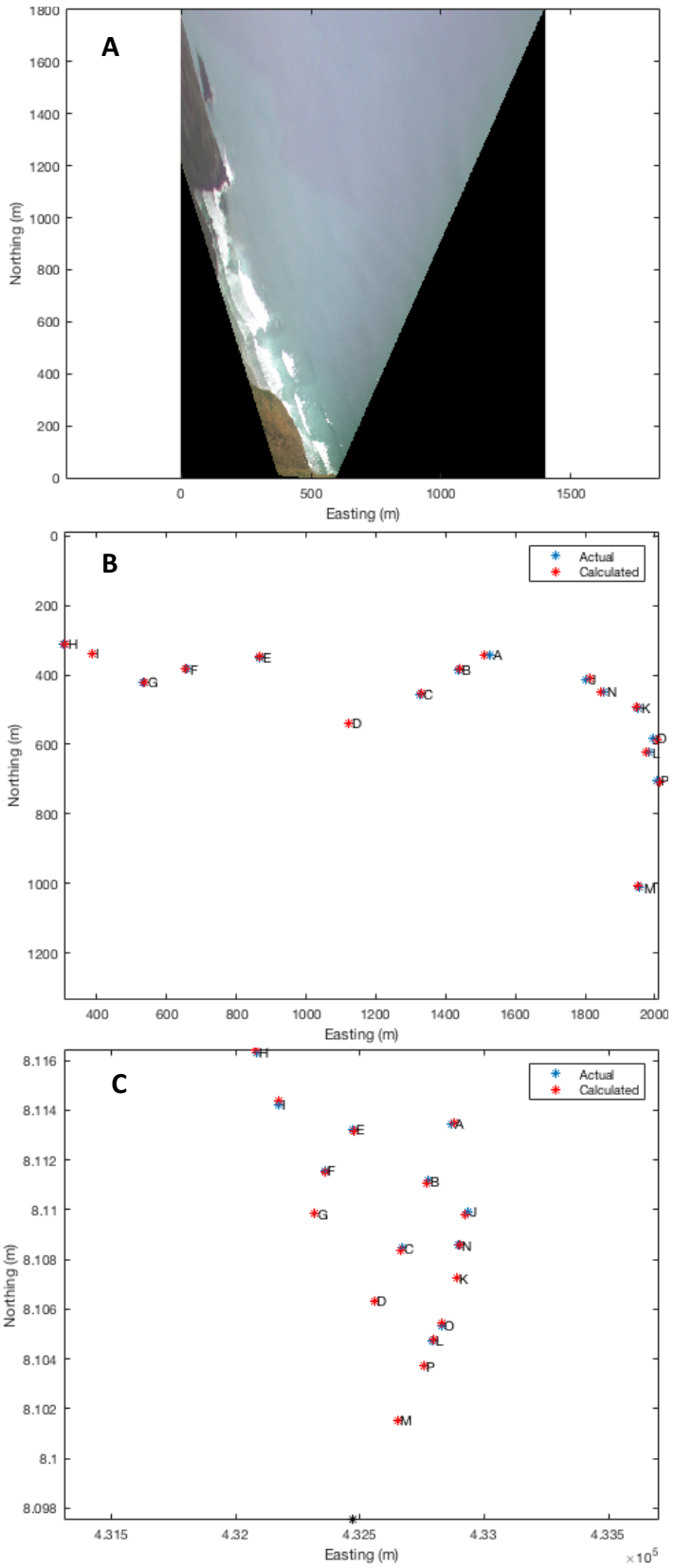

Figure 3-5 Depicts the rectified images for camera one (A), the actual ICPs plotted against calculated ICPs for camera 1(B), and the actual GCPs plotted against the calculated GCPs for camera 1 (C). Note: the axes vary in length (m). The GCPs are a function of GPS coordinates (easting and northing (m)) and the ICPs are a function of image coordinate triangulation (easting and northing (m)).

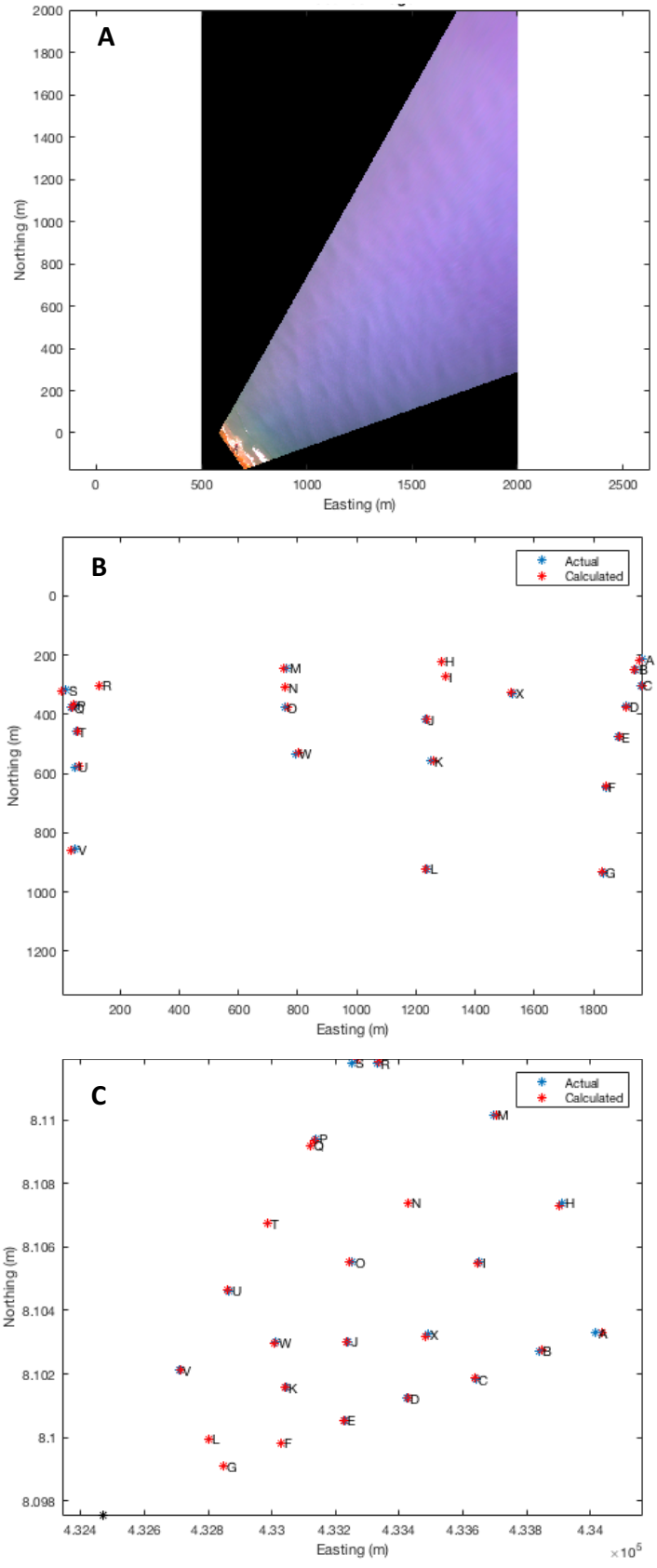

Figure 3-6 Depicts the rectified images for camera two (A), the actual ICPs plotted against calculated ICPs for camera 1(B), and the actual GCPs plotted against the calculated GCPs for camera 1 (C). Note: the axes vary in length (m). The GCPs are a function of GPS coordinates (easting and northing (m)) and the ICPs are a function of image coordinate triangulation (easting and northing (m)).

Tidal data from 1st January 2014 through to 14th January 2017 of the Otago Harbour Entrance were extracted from the NIWA tidal model to represent the tidal heights at both Aramoana and Whareakeake surf breaks. The tidal data were loaded into T-Tide to extract the tidal constituents, which were subsequently made into tidal predictions for each image in the *'Findpos_Stoyanov_jai'* script, allowing the images to be rectified to the correct vertical level. Rectifying to a lower level makes objects appear larger than they should be and vice versa. The result of this process was a position file containing the orientation and position of the camera (the extrinsic camera parameters). This position file is needed, along with a vertical datum, to rectify any camera image.

The reference images from camera one and two were then digitised in the *'Rectify_all'* script to provided reference points which were used as a means to check if any of the cameras had moved over time. Each image was individually cross-referenced against the reference image reference points to see if the cameras had moved. If an image had moved, the reference points were used to correct the change in camera position, at which point a new camera position file for that particular image was saved. An example of this can be observed below in Figure 3.7, which depicts how camera two (Aramoana) has moved from its original position (A) to a position now where 'the mole' can be observable (B). Because the camera had moved, the time lapsed image (B) was then digitised to match the reference points from the reference image.

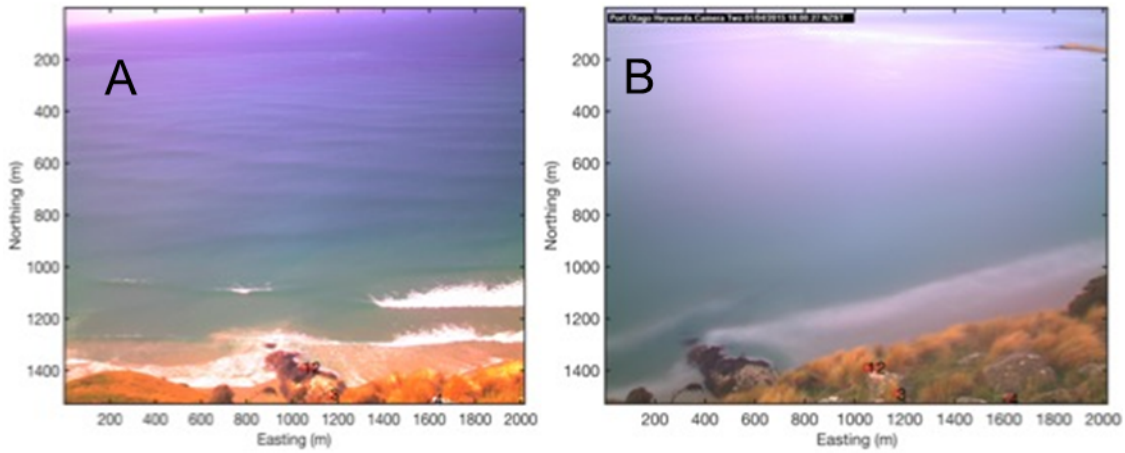

Figure 3-7 Depicts the reference image (A) and associated reference points one to six (represented by small red circles and numbers) and the time lapsed images (B) with the reference points, not in the same position as the reference image, which indicates that camera two has moved from its original position. The x-axis represents the easting (m) and the y-axis represents the northing (m).

With the newly saved image position files (camera position files) from the Aramoana Beach cameras, it was then possible to batch rectify the images in the *'Rectify_all'* script. The time-averaged images, which were provided by NIWA, and the associated individual snapshot images, provided by POL, were then rectified. Not all images, however, were rectified. To prevent the unnecessary and time-consuming analyses of thousands of images, only images situated around low tide were rectified and even then, there was a selection process. A script called *'Find_low_Tide'* was created, which as the name suggests, found the low tide for each day using T-Tide (mentioned above), and found the associated images situated around these low tide times for each day. From here, the images around the low tide times were individually checked to see if the images were of a high enough calibre. Only these images were saved to a final image folder. With respect to the snapshot images, however, only images identified as having breaking waves and that were of a high caliber were saved. These saved images were then batch rectified in the *'Rectify_all'* script.

Identifying images of a high caliber and with breaking waves observed was not as simple as it seemed. Many of the images during autumn and winter with breaking waves observed were not quality images, as these images were in one way or

another distorted or ruined. Low-quality images resulted from rainy days, low cloud and or fog, smudges or drops on the camera lens, sun glare reflecting off the ocean surface, stormy conditions creating messy wave environments and multiple swell directions interrupting wave identification processes. Thus, there is a paucity of data collated during autumn and winter (refer to Chapter Four).

3.3 Extracting Geomorphic Parameters from Time-Averaged Images

3.3.1 Shoreline Detection

An algorithm called "Shoreline_Finder" was created to detect shorelines within the rectified time-averaged images (RTAI). This algorithm worked by detecting gradients in colour intensity within the images and is based on the shoreline detection algorithm developed by Smith and Bryan (2007) and explored and utilised by Salmon (2008) and Gallop (2009). Within the computer programme, Matlab, the images collected were stored as three matrices (801x551x3) representing the colours red, green and blue. Values between 0 and 256 within each of the matrices indicate the intensity of each colour in an image. The algorithm delineates the shoreline based on the ratio of red light of the beach to blue light of the water. This is based on the idea that the beach would contain shell content, the colour of red, and thus have a higher portion of red light compared to the water, which would have a high portion of blue light because of the fact that the water appears blue. The whitish area within the images near the shoreline is a result of breaking waves, which contain similar levels of red, blue and green light. Thus, the algorithm used in this thesis was written to find the shoreline location via the sharp shift in the ratio between red and blue light, as per the Smith and Bryan (2007) algorithm.

Similar to Gallop (2009), however, it was observed that the colour intensities from image to image changed significantly due to factors such as weather and solar radiation penetration inefficiencies which created differences in the observed conditions between various times of the day and throughout the seasons. As a result, a threshold which delineated between the beach and water colours red and

blue, respectively, was found by manually digitizing two boxes, one on the beach and one within the ocean. The two boxes created two mean values, which could be divided by the total number of means to create a mean threshold value. This mean threshold value representative of the shoreline location was then cross-referenced (looped) across the entire image to create a line depicting the shoreline location. In cases where the shoreline was not a continuous feature because of camera obstructions, such as observed in Aramoana camera one images, two identical shoreline location thresholds were created for different sections of the beach in the alongshore direction. The identical shoreline thresholds allowed for one continuous shoreline to be fitted to an image by interpolating the threshold between two locations.

Where the shoreline location within an image was erroneous (i.e. not where it should be based upon visual inspection the RTAI), manual corrections were made. The errors could be caused by a person or object on the beach, either of which confuse the shoreline detection algorithm. The corrections were achieved by digitising and interpolating a polynomial spline within the erroneous areas, which although subjective, was deemed necessary and produced a reasonable position of the shoreline location.

The *'Shoreline_Finder'* algorithm was applied to all of the images produced from cameras one and two. Due to the angle of the cameras and the obvious obstructions hindering the full view of the beach faces within the images, however, the shoreline locations that were produced from the algorithm were not visible enough or of a high enough quality to be of further use to this thesis. Therefore, the avenue of collecting shoreline locations was discontinued.

3.3.2 Sand-Bar and Trough Detection

An algorithm called *'Barline_Finder'* was written to detect the location of sand-bars within the RTAI database. This algorithm worked by searching for local light intensity maxima associated with the whitish colours from the foam of breaking

waves. This technique was based on work from Lippmann and Holman (1989). Prior to the algorithm being utilised, however, the RTAI were visually inspected to ensure that breaking waves were actually observed within the images and only those images were analysed. The importance of visually inspecting the images for breaking waves is that the nature of breaking waves is a direct function of a critical wave height to water depth ratio, which Mead (2003) suggests that is roughly around 0.78 (however, ratios of between 0.5 and 1.0 meters can be observed). Thus, if waves are of an insufficient height within the nearshore zone the waves will not break, and the algorithm will not be able to detect the sand-bar and trough locations.

The *'Barline_Finder'* algorithm was based on the Lippmann and Holman (1989) remote sensing technique that allowed 'visualisation and subsequent quantification of nearshore morphology based on patterns of incident waves breaking'. The technique works on the premise that more waves break over the shallow nature of sand-bars than other areas within the nearshore zone. Further, Lippmann and Holman (1989) used long-term exposure images (time-averaged images), which averaged out 'fluctuations due to incident wave modulations', in turn, giving a statistically stable image of a wave breaking pattern.

For the purpose of this thesis, only images that had distinct breaking waves were run through the algorithm. The algorithm worked by searching along transects in the cross and alongshore directions for local light intensity maxima and minima, which corresponded to the potential location of sand-bars and troughs, respectively. Originally, the algorithm was designed to start detecting the sand-bar and trough locations from the shoreline locations obtained from *'Shoreline_Finder'*. As the obtained shoreline locations were not visible enough (refer to Section 3.2.1), however, a line representing an approximate shoreline location, referred to as q_lower, was digitised to give a starting point for the algorithm to work from. Further, a maximum cross-shore limit, referred to as q_upper, was also digitised just seaward of the observed surf-zone breakers (Figure 3.8A). This allowed the algorithm to work within the desired area

containing the parameters of interest. Furthermore, by restricting the work of the algorithm to within this area, this removed unwanted detection of light intensity maxima and minima, such as sun glare, further seaward and shoreward.

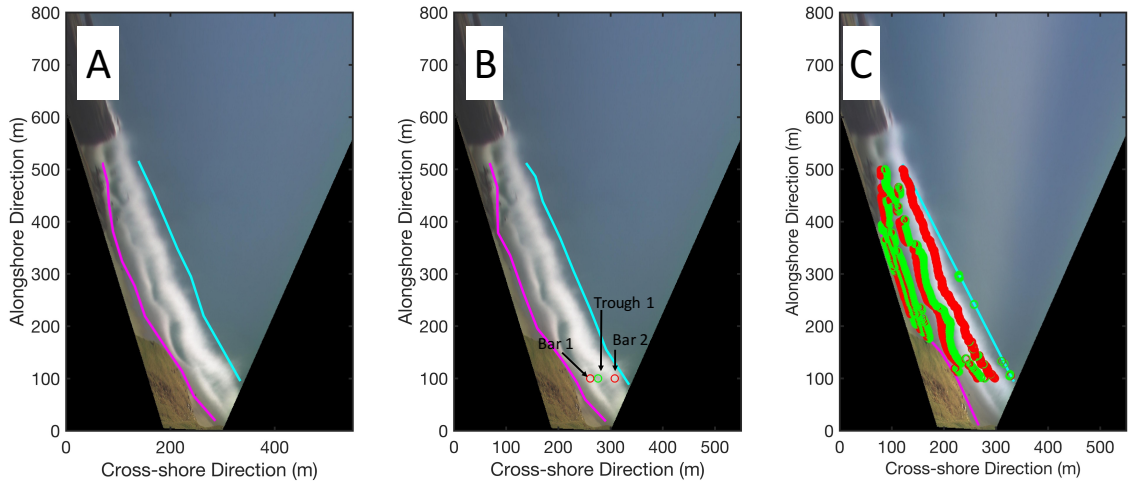

Figure 3-8 An example image illustrating the area within which the 'Barline_Finder' algorithm worked to detect the sand-bar and trough locations (A). Note the magenta line represents the approximate shoreline location (q_lower) and the cyan line represents the cross-shore maximum limit. Both the magenta and cyan lines were manually digitised and interpolated based on visual inspection of the image. B) Illustrates the search of the "Barline_Finder" algorithm for light intensity maxima and minima in the cross-shore direction. The red circles represent the sand-bar locations and the green circles represent the trough locations. C) Illustrates the completion of the search of the "Barline_Finder" algorithm for light intensity maxima and minima in the cross-shore direction.

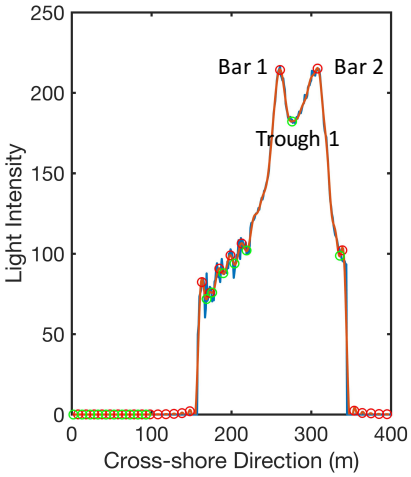

Figure 3-9 Illustrates the light intensity maxima and minima in the cross-shore direction at the alongshore location, as observed in Figure 3.8, which detects the sand-bar and trough locations, respectively. The blue line represents the raw light intensity and the red line represents the polynomial of light intensity. The red circles represent the sand-bar locations and the green circles represent the trough locations. Note the circles below the light intensity value of 150 are representative of noise, such as shoreline breakers (left-hand side around the value of 100). Bar 1, Bar 2 and Trough 1 correspond to Figure 3.8.

Once the defined areas were digitised in the alongshore direction the *'Barline_Finder'* algorithm then started the cross-shore search for light intensity maxima and minima. The algorithm worked from the bottom to the top of the area in the alongshore direction, as illustrated in Figure 3.8B. This section of the *'Barline_Finder'* algorithm located the light intensity maxima and minima according to the mean light intensity values of the image colours (i.e. the mean light intensity value of red, green and blue). Further, a low pass filter routine within the algorithm was created to ensure the small variability in the intensity did not confuse the algorithm.

The result created a raw light intensity line per cross-shore transect (blue line in Figure 3.9) from which a polynomial spline was fitted (red line in Figure 3.9). The spline was fitted to remove the small-scale variation in light intensity, which may have created confusion regarding what is and is not a sand-bar or trough. Position files of the final sand-bar and trough locations (Figure 3.8C) were saved.

3.3.2.1 Erroneous Sand-bar Removal

Once the light intensity maxima and minima routine had located the corresponding sand-bar and trough locations along the cross-shore transects (Figure 3.8C) of the desired beach area of interest, the process of eliminating the erroneous sand-bars could begin. The saved position files of the sand-bar locations were then loaded into a new algorithm called *'Clean_Bar'* (Figure 3.10A). First, the algorithm checked each identified sand-bar to determine whether the sand-bar was too small and if it was, it was removed. This checking and removal process was achieved by creating a routine that searched for individual cells that had been identified as sand-bars. If the sand-bars were less than 10 cells long (an arbitrary threshold), then the algorithm removed these "sand-bar cells" (observed removal between Figures 3.10A, 3.10B and 3.11C).

Erroneous sand-bars were then visually identified and confirmed by a routine constructed in the *'Clean_Bar'* algorithm, which allowed for visual inspection of

the sand-bar locations relative to the associated breaking wave features within the rectified snapshot images and RTAIs. In general, the erroneous sand-bars were mainly associated with the breaking of waves directly near the shoreline location, thus not breaking over sand-bars and were eligible for removal. The secondary removal process involved manually digitising spot coordinates of the offending sand-bars, at which point the algorithm could search the dataset for them and delete them. A routine was created to ensure that if any offending sand-bars were missed in the first pass process of elimination then options of a secondary and if needed tertiary pass was made available.

3.3.2.2 Breaking of Sand-bar Segments

To gain detailed knowledge of specific areas of the beaches of interest, the long sand-bar segments were broken down into smaller segments based on segment orientation. This was achieved by visually inspecting the long sand-bar segments in the '*Clean_Bar*' script and identifying where the change in orientation along the sand-bar segment occurred. The sand-bars were then broken into those sections by digitizing the location where the break should occur, finding the bar in the database, then dividing the bar into two separate bars (Figure 3.10D). This allowed the orientation and position of individual sand-bar segments to be obtained in specific areas for the purpose of analysing whether these were associated with the identified peel angles from the observed breaking waves in those specific areas. The mean sand-bar positions collected within the area of interest for camera one and two can be observed in Figures 3.11 and 3.12 (refer to Section 3.3.1 for the cropped areas of interest). Not all the sand-bar locations were used, however, since the area of most interest to surfers was a focus of this thesis. The location of bars where the peel angles were quantified is represented by the black dots in Figures 3.12 and 3.13.

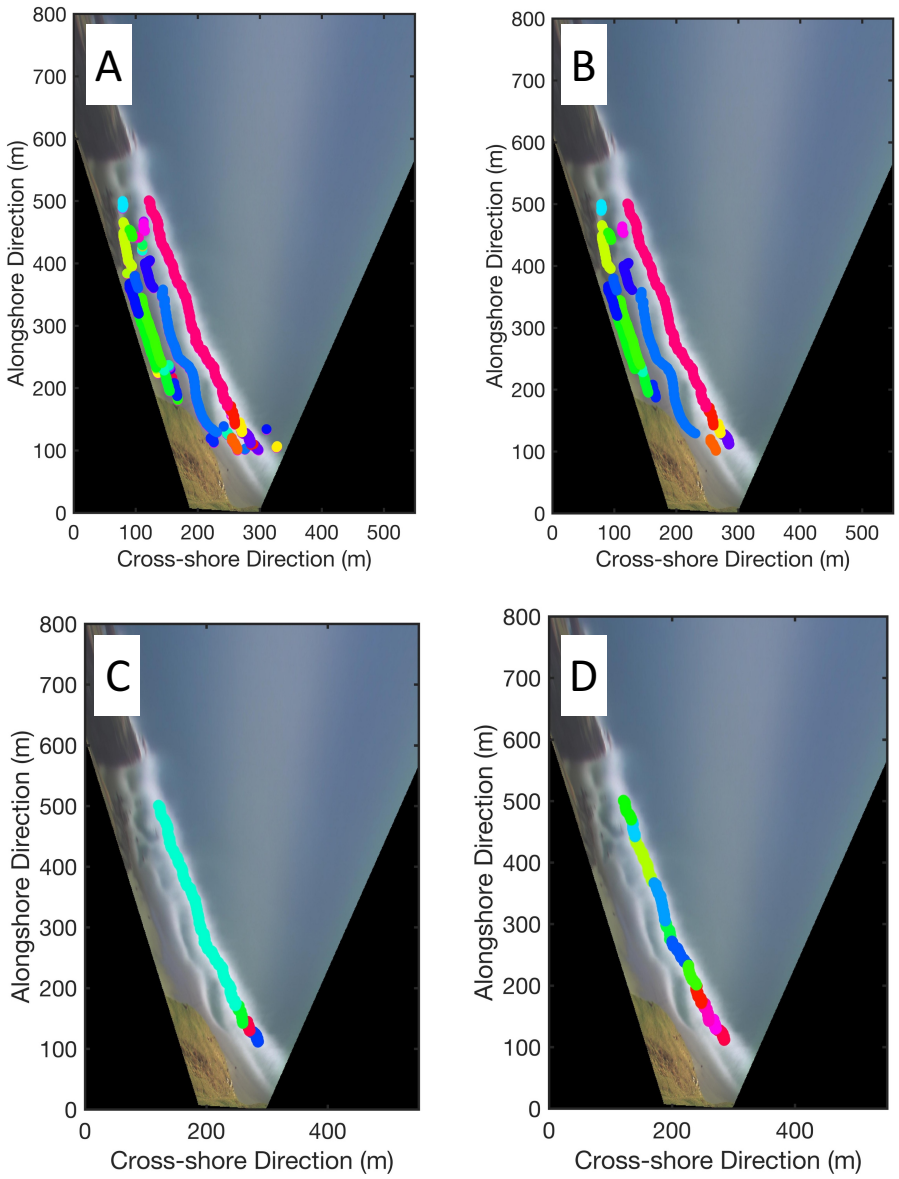

Figure 3-10 Illustrates an example of the loaded position file data of the detected sand-bar locations to the algorithm 'Clean_Bar' saved from the 'Barline_Finder' algorithm (A). The area of interest in the alongshore direction is between 100 and 500 m. Each different colour represents an individual identified sand-bar. B) Depicts the initial removal of identified sand-bar cells that are below 10 cells in length. C) Depicts the observed remaining sand-bars after the digitised removal of identified offending sand-bars. D) Depicts the segmented sand-bar after the breaking process via digitising has occurred. Each colour represents an individual segment of the initial much larger sand-bar. Note data is from an image taken on the 27th September 2015 at 9 am from Aramoana camera one.

3.4 Extracting Surfing Parameters from Snap Images

With the knowledge of which images contained the individual sand-bar segments, a subset of snapshot images collected on the exact same day could be collated. Approximately, six snapshot images, three either side of the time of the RTAI, were rectified using the same method as discussed above. The rectified snapshot images (RSSI) were then cropped to allow targeted analysis of identified areas of interest along the beach segments. The cropping further enabled more precise peel angle and length of ride detection.

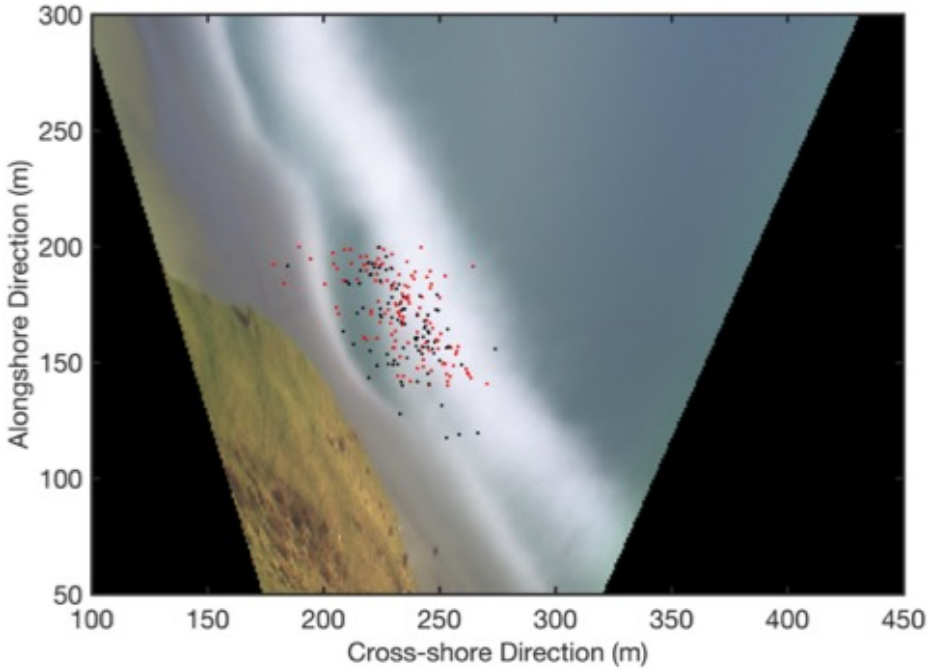

Figure 3-11 Illustrates the mean sand-bar positions located within the area of interest for camera one, Aramoana (2013 to 2017). Note: the red and black dots indicate the mean sand-bar positions not used and used, respectively, for data analysis. This is a RTAI from the 27 September 2015.

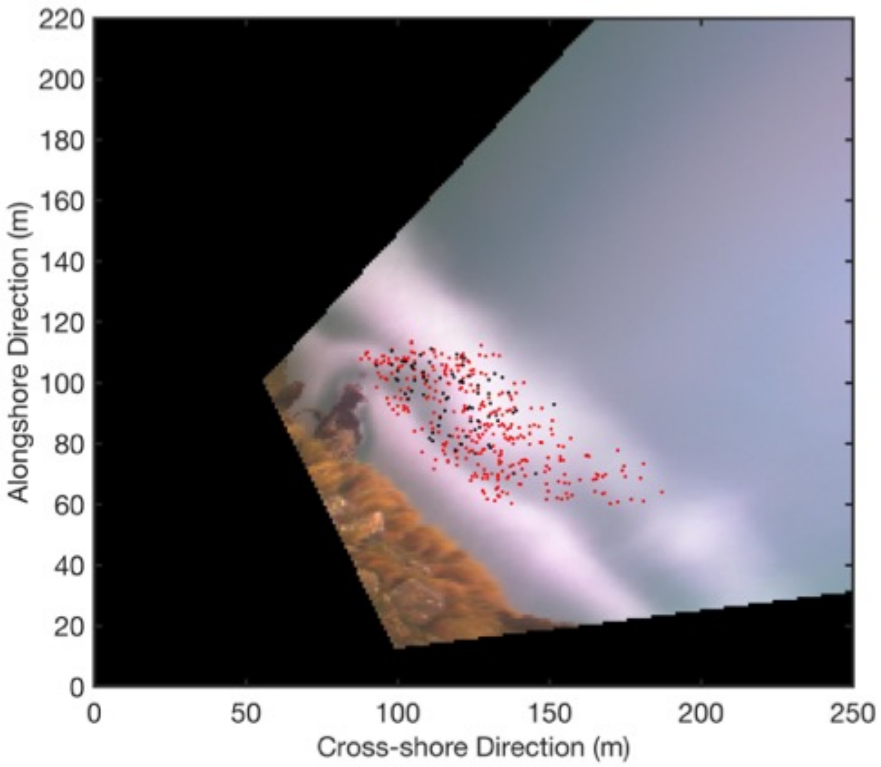

Figure 3- Illustrates the mean sand-bar positions located within the area of interest for camera two, Aramoana (2015 to 2016). Note: the red and black dots indicate the mean sand-bar positions not used and used, respectively, for data analysis. This is a RTAI from the 3rd April 2016.

3.4.1 Cropped Area of Interest

The cropped areas of interest were selected based on the POL surfing surveys carried out between 2014 and 2016. The most surfed location along Aramoana is known as 'the mid', which is the middle section of the beach. Thus, it made sense to crop the images closest to the middle of Aramoana Beach because these areas, referred to as the areas of interest, are likely to experience higher volumes of quality surfing waves compared to other locations along Aramoana. In turn, one would assume it makes sense to look at the geomorphic parameters and surfing parameters of interest within these areas of interest. Figure 3.13B indicates the area of interest with respect to camera one and Figure 3.14B indicates the area of interest with respect to camera two. The camera one area of interest lies approximately 300 m north of the camera two area of interest. The camera one area of interest is characterised by a sandy beach, whereas, the camera two area of interest lies directly in front of a small rocky outcrop.

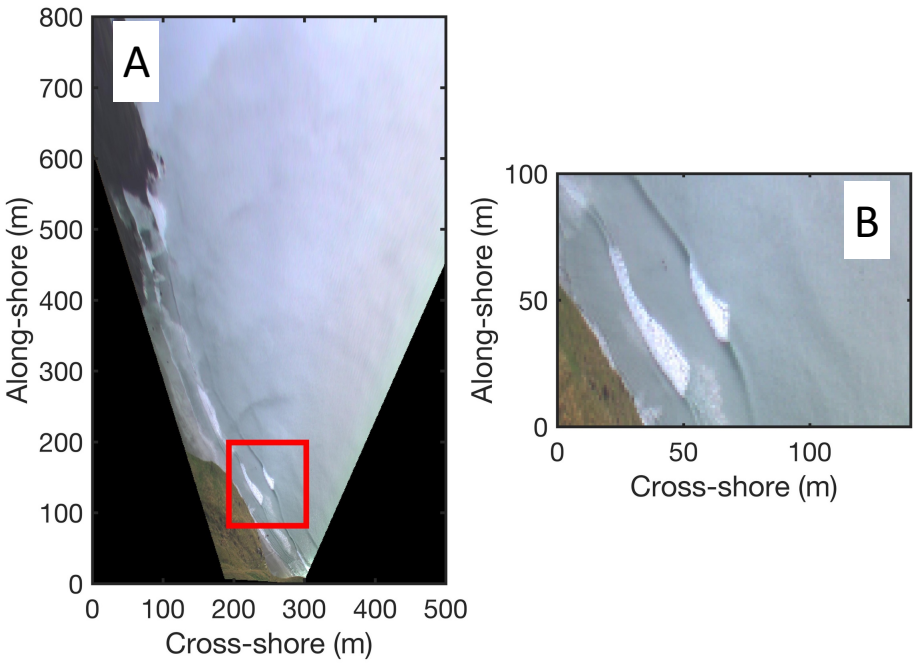

Figure 3-12 Indicates the original RSSI (A) for camera one and cropped RSSI area of interest (B) for camera one. The red box on the original RSSI is indicative of the cropped area of interest.

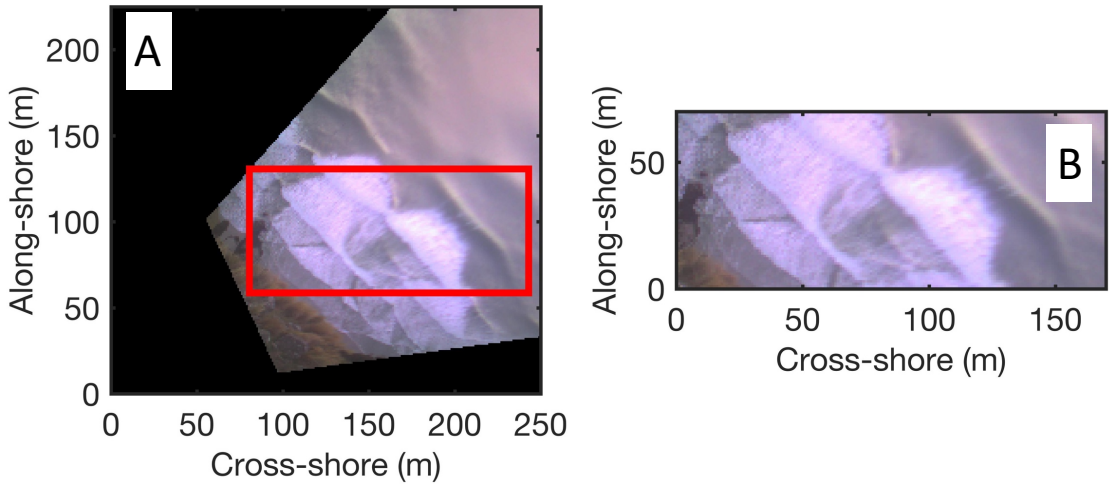

Figure 3-13 Indicates the original RSSI (A) for camera two and cropped RSSI area of interest (B) for camera two. The red box on the original RSSI is indicative of the cropped area of interest.

3.4.2 Peel Angle Detection

The RSSIs were then run through an algorithm called *'White_Water_Wave-_Crest_Detection'*, which was designed to obtain the white-water line length and orientation as well as the wave crest orientation of a breaking wave. These parameters were obtained by manually digitising the white-water and wave crest lines on the RSSIs. It is noted that user skill and interpretation on where the observed white-water and wave crest lines are located is a determining factor in creating this data. The white-water line length gives the 'length of ride', which is a targeted surfing parameter of interest, whereas the white-water line orientation and wave crest orientation are used to identify the peel angle of a breaking wave, which is also a targeted surfing parameter of interest. This is observed in Figure 3.15, which depicts the white-water line in orange and wave crest in blue. An algorithm called *'Angle_of_Two_Slopes'* was created to determine the peel angle of the breaking waves through basic trigonometry, similar to the method used by Atkin (2010) i.e. the angle between the orange and blue lines illustrated by the numbers one and two on Figure 3.15. The length of ride and peel angles of the both the ride-handers (number two), waves breaking left to right facing the shore, and left-handers (number one), waves breaking right to left facing the shore, can then be analysed against the observed orientation of the sand-bar segments within that particular area of interest. The comparison is to determine whether or not there are relationships between the observed geomorphic parameters and the surfing parameters.

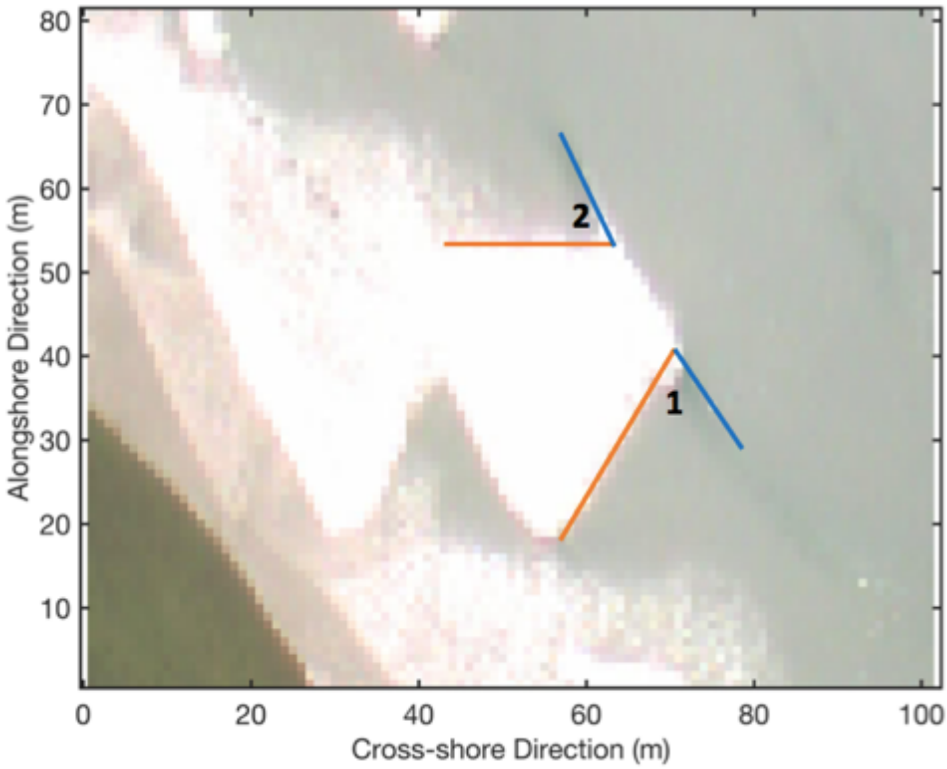

Figure 3-14 Depicts the cropped area as shown in Figure 3.13. Image shows a breaking wave within the desired area of interest. Note: The orange lines indicate the white-water lines and the blue lines represent the wave crest lines whereas the numbers indicate the peel angles of the breaking wave.

3.5 Chapter Summary

Two cameras were set up overlooking Aramoana Beach. Each camera snapped an image once every five minutes. NIWA supplied the time-averaged image. The *'Findpos_Stoyanov_jai'* script used information on the properties of lenses of each camera to correct the images for any distortions. Using GCPs, ICPs were ascertained and the discrepancies between the actual and calculated GCPs and ICPs were removed. Using T-Tide, tidal constituents were extracted, which allowed the images to be rectified to the correct vertical level. Each image was cross-referenced against a reference image with associated reference points for each camera. The reference points were used to correct for any camera position change and new camera position files were saved for images where the camera had moved. Using a script called *'Find_Low_Tide'*, images around the time of low tide and that were of a high enough calibre were saved.

The snap and time-averaged images were then batch rectified in a script called *'Rectify_all'.* Using a script called *'Barline_Finder',* sand-bars were detected in the RTAI by searching for local light intensity maxima associated with breaking waves. Only images with observed breaking waves were run through this script. The detected sand-bar position files were saved and then run through a script called *'Clean_Bar'*, which removed erroneous sand-bar positions. Long sand-bar segments were broken into shorter segments where identified changes in orientation were observed, which also occurred in the *'Clean_Bar'* script. The sand-bar orientations, lengths and mean positions were saved, as the geomorphic parameters of interest.

Areas of interest were identified for cameras one and two based on the most popular surfing locations at Aramoana Beach. The RSSIs were cropped to highlight these areas of interest. Using a script called *'White_Water_Wave_Crest_-Detection'*, the white-water line lengths and orientations, as well as the wave crest orientations of breaking waves, were digitised on the RSSIs and saved. The white-water line length indicates the length of ride surfing parameter, whereas the white-water line and wave crest orientations were used to calculate the peel angle surfing parameter of breaking waves in a script called *'Angle_of_Two_Slopes'*.

Chapter Four

Results

4.1 Introduction

This chapter presents the morphology and surfing parameter data for each year from camera one and camera two collected from Aramoana Beach. The raw image data, supplied by Port Otago Ltd, from camera one, was from September 2013 through to July 2017, whereas the data from camera two was only from April 2015 through to December 2016. The morphological and surfing parameter changes over time and space are extracted using methodology presented in Chapter 3 and analysed for seasonal and interannual patterns. The morphological data presented include the sand-bar orientation, length and location, whereas the surfing parameter data presented include the peel angle and length of ride. The changing nature and relationship between the morphological parameters and surfing parameters are also analysed. The main purpose of this chapter is to show how the morphology changes in the areas of interest and how this morphology influences the surfing parameters at these sites along Aramoana Beach.

The results presented are representative of the middle section of Aramoana Beach and not the entire beach. As discussed in Section 2.5.7, however, the middle section of Aramoana Beach is the most surfed location and in turn is the most relevant location for the purpose of this thesis. The bar orientation is given in degrees relative to north, whereas, the peel angle is given in degrees relative to the bar orientation angle.

The key findings of the results are summarised in Section 4.5.

4.2 Characterising the Annual Variations in the Morphological and Surfing Parameters at Aramoana Beach

4.2.1 Variations Observed at the Camera One Area of Interest

The annual bar orientation (BO) (degrees) mean (Figure 4.1A) increased from 2013 to 2014 (115° and 151°, respectively) and was of a similar value in 2015 (149°) after which the mean decreased in 2016 (118°) before it slightly decreased again in 2017 (117°). Likewise, the annual length of bar (LOB) (m) mean followed a similar pattern. The LOB annual mean decreased from 2013 to 2014 (72.8 to 58.0 m) before it slightly increased in 2015 (61.7 m) after which it increased in 2016 (69.9 m) before it slightly decreased in 2017 (68.40 m) (Figure 4.1B). There was an inverse correlation coefficient (CC) of -0.22 between BO and LOB (i.e. as the BO increased, the LOB decreased) which was statistically significant with a p-value of 0.03.

Both the left-hand peel angles (LHPA) and the right-hand peel angles (RHPA) (degrees) followed a similar pattern to each other with respect to the sample mean (Figure 4.1C and 4.1D, respectively). The RHPAs, however, had slightly higher sample means compared to the LHPAs across most years. For the LHPAs, from 2013 to 2014 the peel angle mean (PA) reduced from 47.6° to 44.9° before it increased to 49.0° in 2015 and 50.0° in 2016 after which the mean significantly reduced to 35.4° in 2017. For the RHPAs, from 2013 to 2015 the PA sample means increased from 46.1° to 49.7° and then to 55.4°, respectively, before reducing to 47.0° in 2016 before again reducing in 2017 to 39.3°. There was a correlation between the RHPA and the LHPA with a CC of 0.25; however, the correlation was not statistically significant (p-value of 0.14).

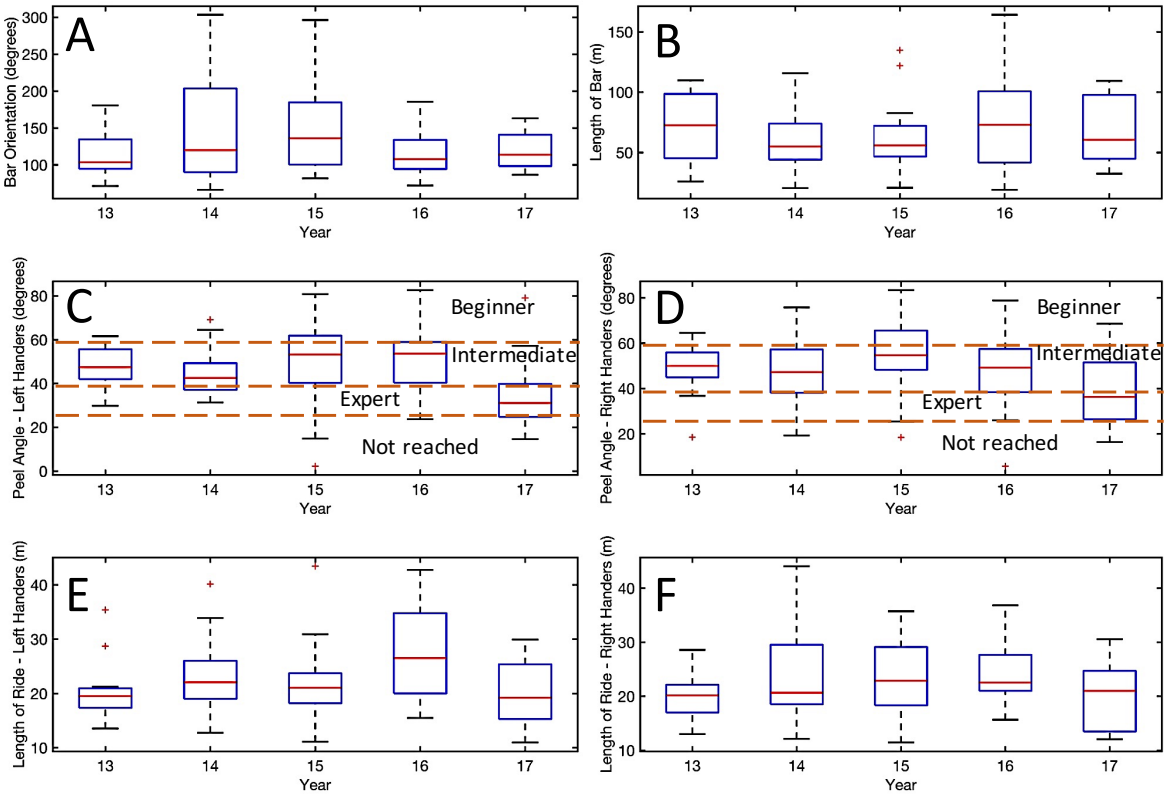

Figure 4-1 Box and whisker plots of camera one data indicating the bar orientation(degrees) plotted against time (years) (A), length of bar (m) plotted against time (years) (B), left hander peel angles (degrees) plotted against time (years) (C), right hander peel angles (degrees) plotted against time (years) (D), left hander length of ride (m) plotted against time (years) (E) and right hander length of ride (m) plotted against time (years) (F). Note the red lines in the box plots are the sample medians, the tops and bottoms of each box are the 75th and 25th percentiles of the samples, respectively, the whiskers extending above and below the boxes indicate the ends of the interquartile ranges and the red plus symbols indicate the outliers. The orange dashed lines indicate the surfer skill level required to ride peel angles within that range (refer to Table 2.1)

With respect to the left-hand length of ride (LHLOR) (m) and the right-hand length of ride (RHLOR) (m), means both seem to follow a similar pattern to each other (Figure 4.1E and F, respectively). From 2013 through to 2016 there was an overall increase in the sample mean length of ride (LOR) for both LHLORs (21.6, 21.8, 21.7 and 27.2 m) and RHLORs (20.8, 22.9, 23.4 and 24.4 m) before both decreased in 2017 (19.8 and 20.0 m, respectively). Interestingly, the LHLOR and the RHLOR were somewhat correlated with a CC of 0.42 and a statistically significant p-value of 0.01. These results are summarised in Tables 4.1 and 4.2.

There was a weak inverse CC between BO and the LHPA (Figure 4.3) of -0.13. The correlation, however, was not statistically significant with a p-value of 0.21. The correlation between BO and RHPAs also had a weak inverse correlation with a CC of -0.06 and there was no statistically significant relationship (p-value or 0.54).

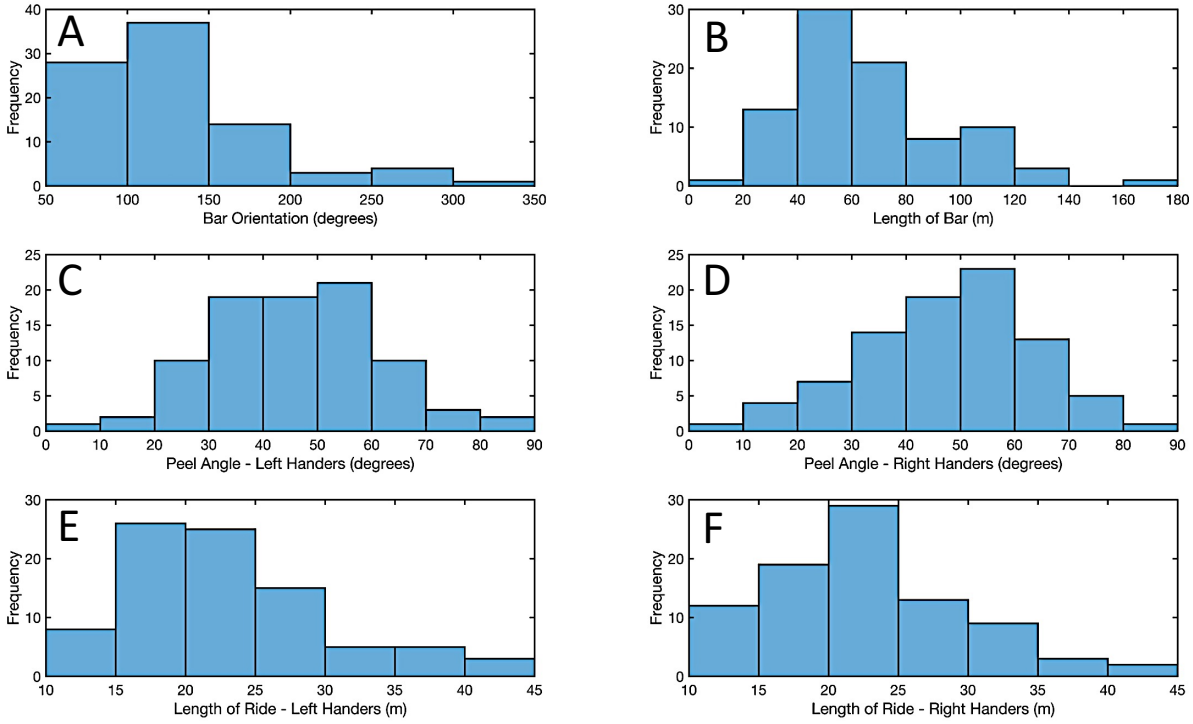

Figure 4-2 Histogram plots from camera one data of BO (degrees) (A), LOB (m) (B), LHPA (degrees) (C), RHPA (degrees) (D), LHLOR (m) (E) and RHLOR (m) (F). Note, histograms indicate frequency of variables.

There was a weak correlation with respect to the BO and LHLOR (Figure 4.4), as the BO increased, the LHLOR also increased, whereas the RHLOR only slightly decreased, as the BO increased. The CC for the BO and the LHLOR was 0.05, whereas the CC for the BO and the RHLOR was -0.018. There were no statistically significant relationships between either of the variables, however, with p-values of 0.86 and 0.59 for the RHLOR and BO and the LHLOR and BO, respectively.

When the RHPAs and LHPAs (degrees) were plotted against the RHLORs and LHLORs (m), respectively (Figure 4.5), there was a weak inverse correlation between RHPAs and RHLORs, which had a CC of -0.18 (i.e. as the RHPAs increased, the RHLORs decreased. In contrast, as the LHPAs increased, the LHLORs slightly

increased) which was indicated by an almost non-existent positive CC of 0.006. There was a weak statistically significant relationship between RHPAs and RHLORs with a p-value of 0.09, whereas there was no statistically significant relationship between the LHPA and the LHLOR with a p-value of 0.95.

The RHLOR and LHLOR (m) plotted against the LOB (m) (Figure 4.6) indicated a weak inverse correlation between the RHLOR and the LOB with a CC of -0.18, whereas there was no correlation between the LHLORs and LOB (CC of -0.008). As the LOB increased, the RHLORs decreased, whereas the LHLORs stayed a similar length or slightly decreased as the LOB increased. The associated p-values of 0.12 and 0.94 indicated no statistically significant relationship at all for the RHLORs with the LOB nor the LHLORs with the LOB, respectively. The RHPA and the LHPA (degrees), when plotted against the LOB (m) (Figure 4.7), indicated a very similar relationship to that of the RH and LH LOR with LOB. The RHPA had a very weak inverse correlation with the LOB with a CC of -0.02, whereas the LHPA had no correlation with the LOB (CC of 0.009). The p-values for both RHPA with LOB and the LHPA with LOB of 0.82 and 0.93, respectively, indicated no statistically significant relationship.

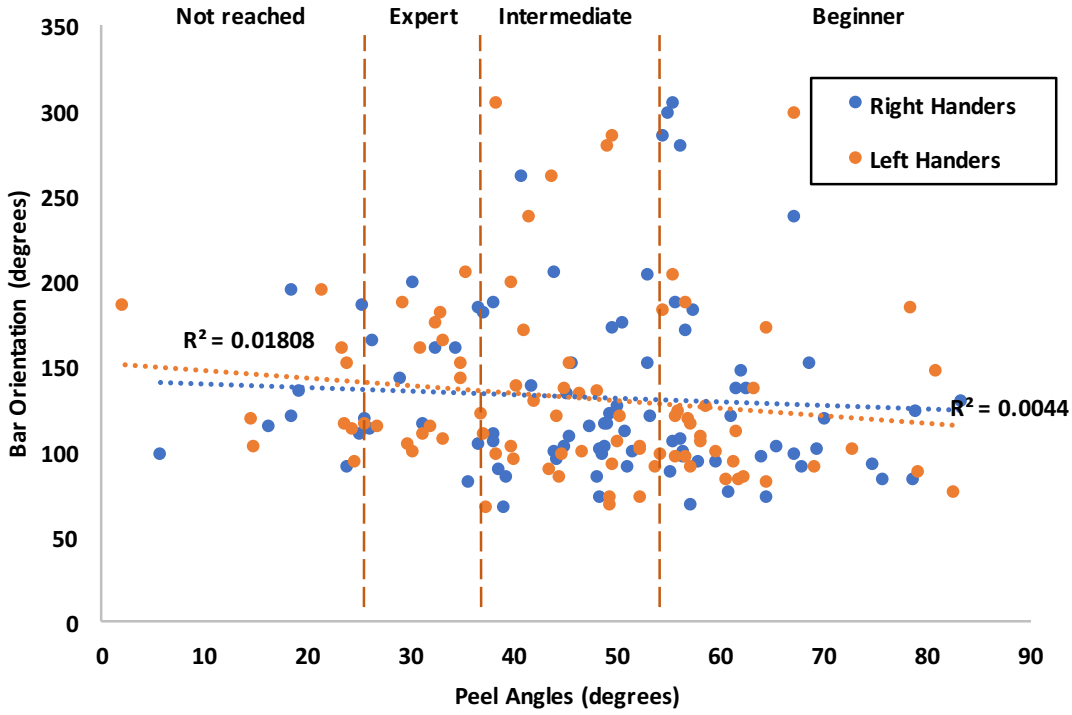

Figure 4-3 Scatter plot of bar orientation (degrees) plotted against the peel angles of both the right and left handers (degrees) for camera one all years. Note, the right and the left handers are by the represented by the colours blue and orange, respectively. The orange dashed lines indicate the surfer skill level required to ride peel angles within that range (refer to Table 2.1). There is a statistically significant relationship between the LHPAs with the BO (0.003), whereas there is none between the RHPAs with the BO (0.88).

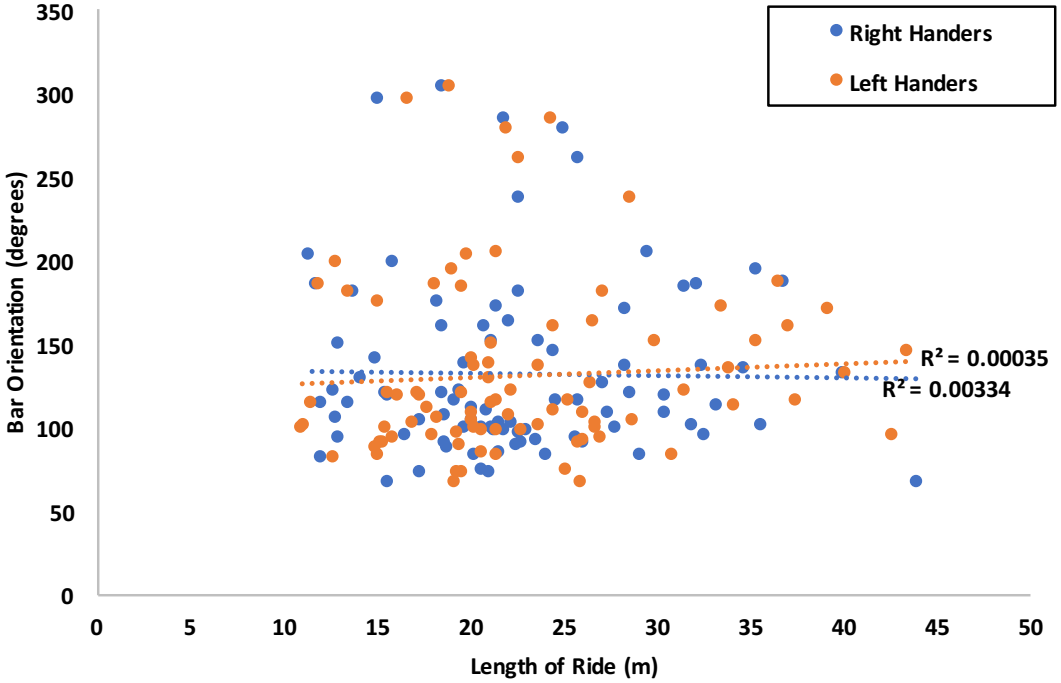

Figure 4-4 Scatter plot of bar orientation (degrees) plotted against the length of ride both the right and left handers (meters) for camera one all years. Note, the right and the left handers are by the represented by the colours blue and orange, respectively. There is no statistically significant relationship between LHLORs with the BO (0.20) nor the RHLORs with the BO (0.94).

The frequency of the BO (Figure 4.2) was highest among the 100 to the 150-degree range and was positively-skewed. The LOB frequency was highest between the 40 to 60 m range and also was positively skewed. The LHPA frequency was highest between the 50 to 60-degree range and a somewhat normal and negative skewed distribution was observed. In contrast, the RHPA frequency was also highest among the 50 to 60-degree range, however, a strong negative distribution was observed. With respect to the LHLOR, the frequency was highest between 10 to 15 m range and a positively skewed distribution was observed. In contrast, the RHLOR frequency was highest between the 20 to 25 m range and a positively skewed distribution was also observed.

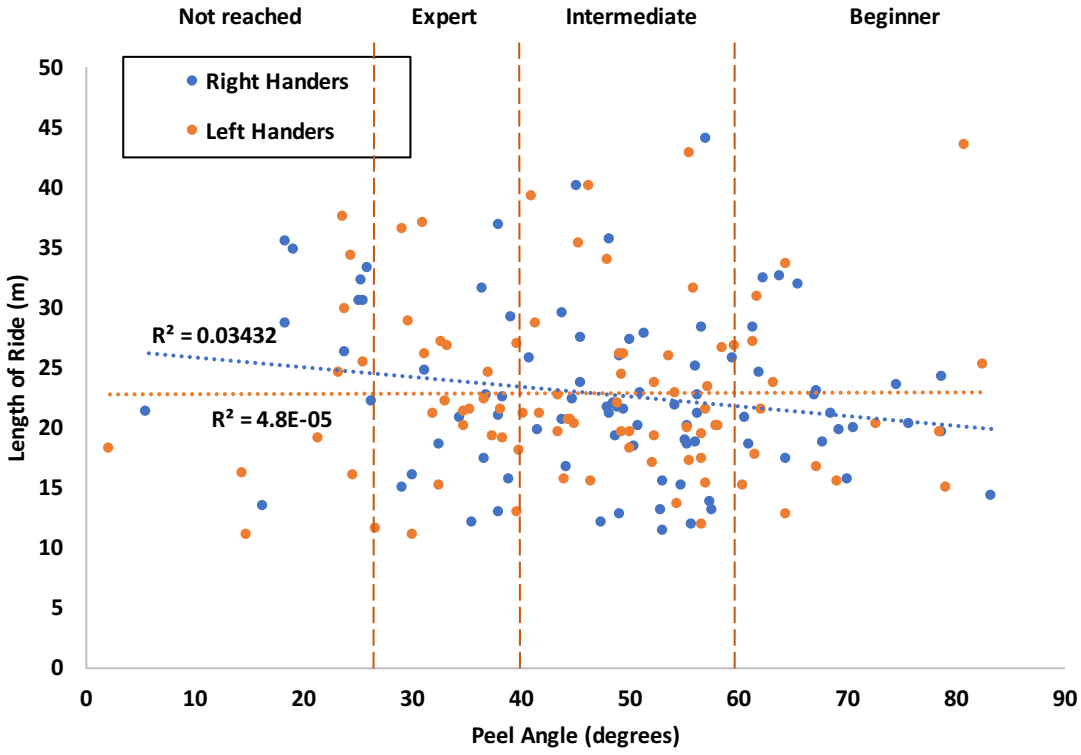

Figure 4-5 Scatter plot of peel angles both right and left handers (degrees) plotted against the length of ride both right and left handers (m) for camera one all years. Note, the right and the left handers are by the represented by the colours blue and orange, respectively. The orange dashed lines indicate the surfer skill level required to ride peel angles within that range (refer to Table 2.1). There is a weak statistically significant relationship between RHPA with the RHLORs (0.08), however, none between the LHPAs with the LHLORs (0.95).

From a surfing perspective, the LHPA average mean across all years was slightly more acute (46.2°) than the RHPAs (48.4°), which means that waves broke slightly faster 'going left' than 'going right' and thus required a slightly more experienced

surfer. The LHLOR average mean across all years, however, was almost identical to that of the RHLOR. In contrast, the RHPA average mean across all years broke at slightly less acute angles compared to the LHPA average mean across all years, which means less experience is required by a surfer to catch a wave and ride the different sections of a wave. As the LHLORs and RHLORs were very similar but the RHPAs were slightly greater than the LHPAs, surfers would have enjoyed a slower breaking wave 'going right' compared to 'going left' but the rides lengths would have been the same. Regardless, both PAs were within the same surfing skill range (intermediate surfing skill). These results are summarised in Tables 4.1 and 4.2.

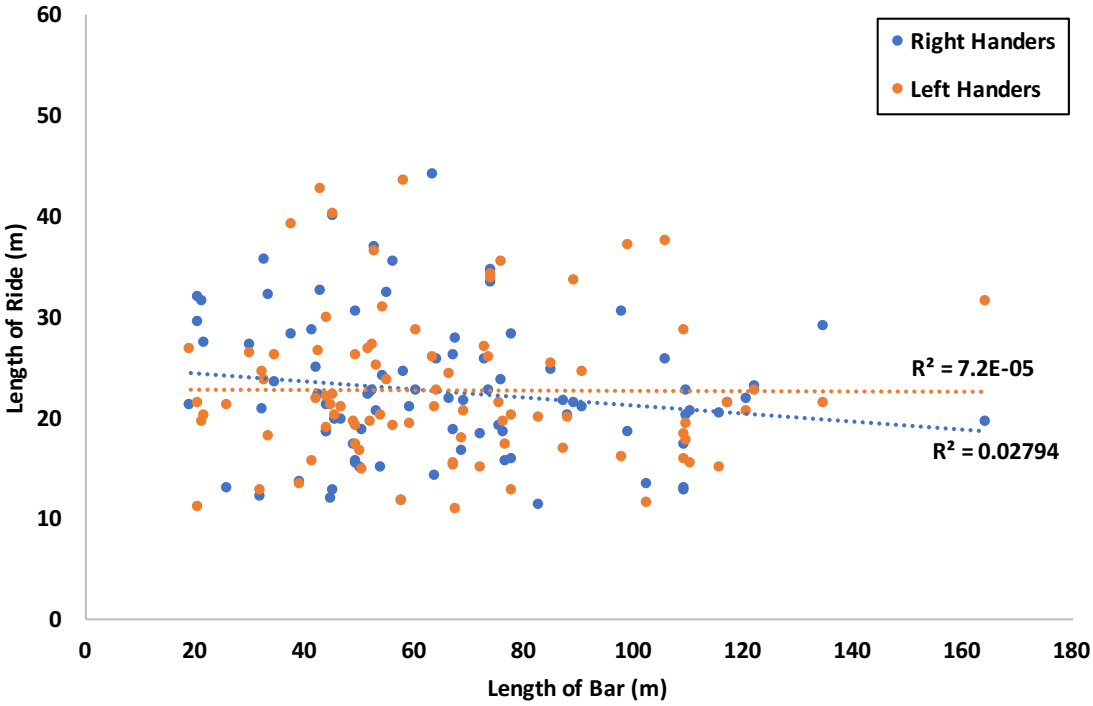

Figure 4-6 Scatter plot of length of ride (m) both right and left handers (m) plotted against the length of bar (m) for camera one all years. Note, the right and the left handers are by the represented by the colours blue and orange, respectively. There are no statistically significant relationships between LOB with the RHLORs nor the LOB with the LHLORs.

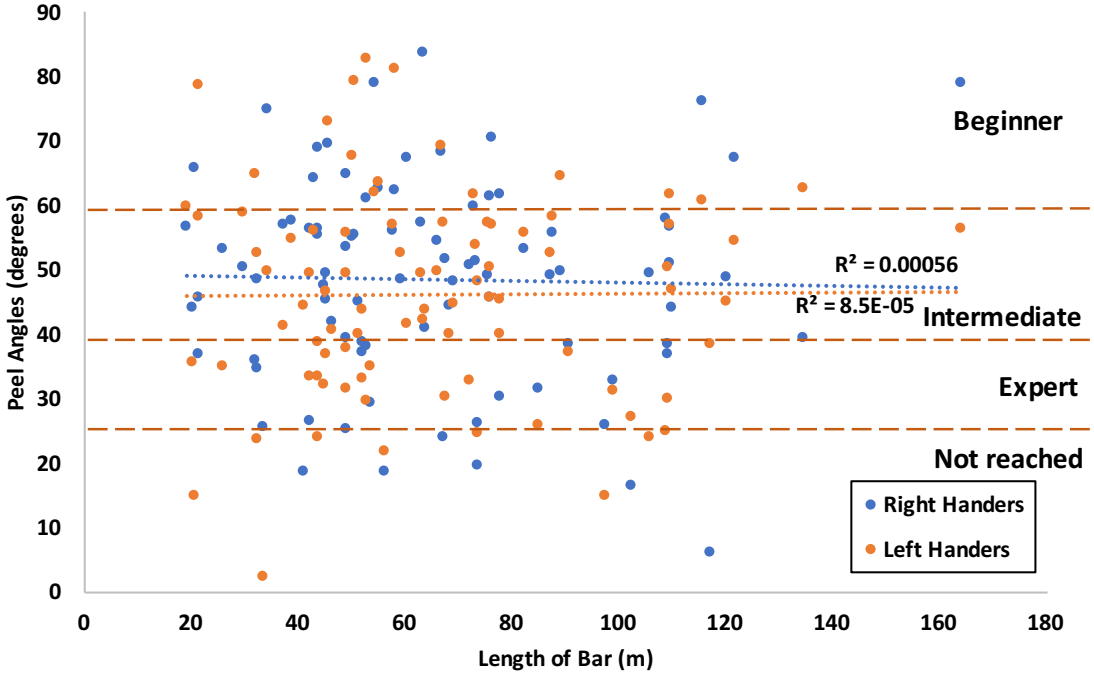

Figure 4-7 Scatter plot of peel angles both right and left handers (degrees) plotted against the length of bar (m) for camera one all years. Note, the right and the left handers are by the represented by the colours blue and orange, respectively. There is no statistically significant relationship between the LOB with the LHPAs (0.98) nor the LOB with the RHPAs (0.73). The orange dashed lines indicate the surfer skill level required to ride peel angles within that range (refer to Table 2.1).

4.2.2 Variations Observed at the Camera Two Area of Interest

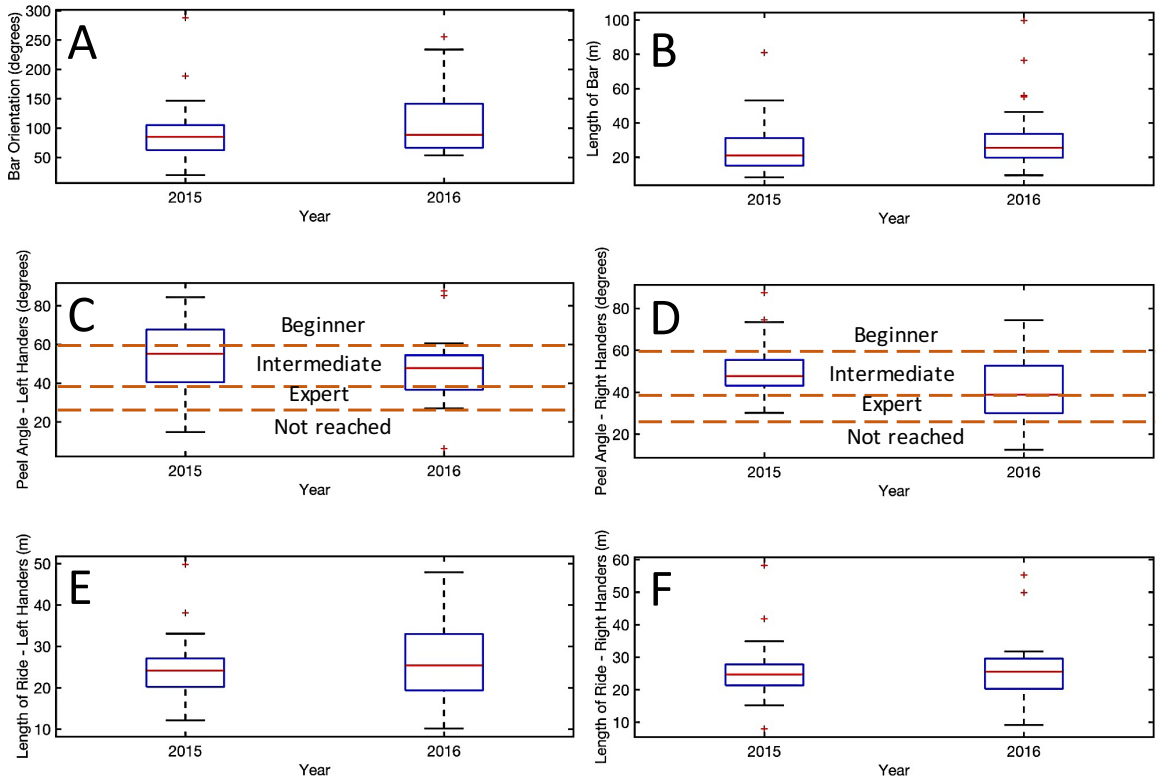

Figure 4-8 Box and whisker plots of camera two data indicating the bar orientation (degrees) plotted against time (years) (A), length of bar (m) plotted against time (years) (B), left hander peel angles (degrees) plotted against time (years) (C), right hander peel angles (degrees) plotted against time (years) (D), left hander length of ride (m) plotted against time (years) (E) and right hander length of ride (m) plotted against time (years) (F). Note the red lines in the box plots are the sample medians, the tops and bottoms of each box are the 75th and 25th percentiles of the samples, respectively, the whiskers extending above and below the boxes indicate the ends of the interquartile ranges and the red plus symbols indicate the outliers. The orange dashed lines indicate the surfer skill level required to ride peel angles within that range (refer to Table 2.1)

With respect to the results collated and analysed from the camera two area of interest, there were only two years of valid data (2015 through to 2016). The paucity of data limits the identification of trends and correlations between the morphological and surfing parameters of interest. In turn, it is hard to compare and contrast the camera one area of interest data with camera two area of interest data.

Both the BO and LOB means increased from 92° to 112° and 25.9 to 29.7 m, respectively, (observed in Figure 4.8A) from 2015 through to 2016. There was,

however, a weak inverse correlation between the BO (degrees) and the LOB (m), which had a CC of -0.21, i.e. as the BO increased, the LOB decreased. This correlation had a statistical significance with a p-value of 0.07.

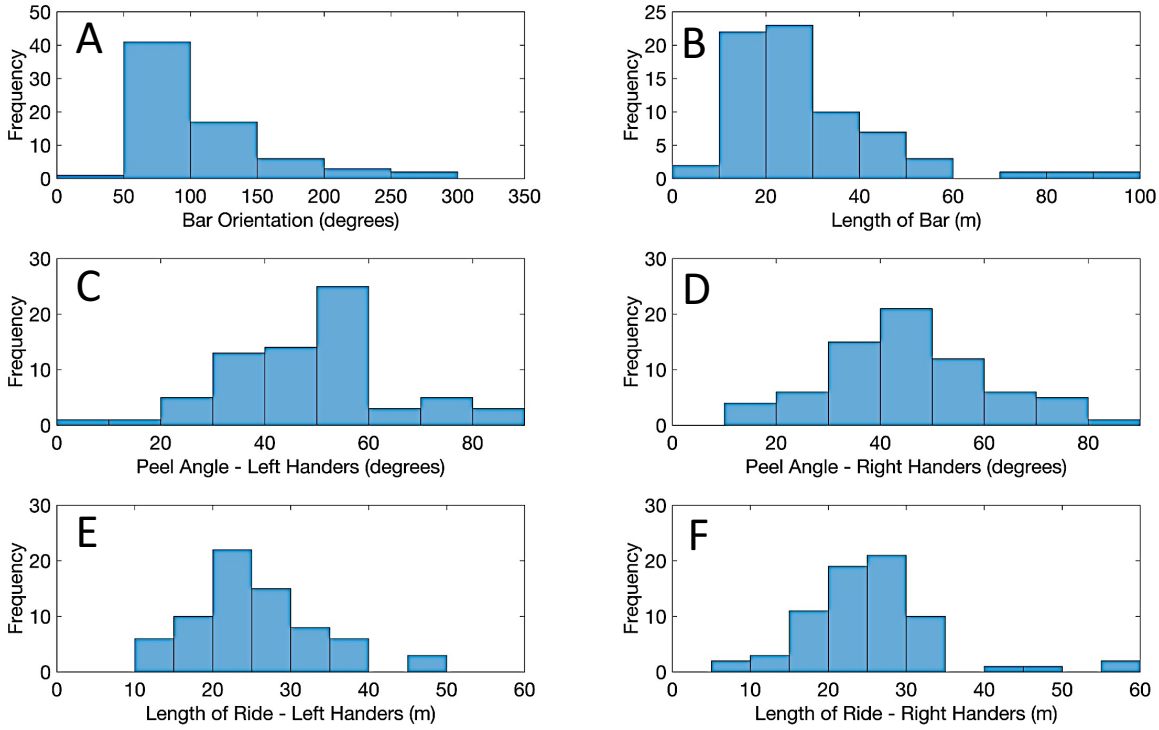

Figure 4-9 Histogram plots from camera two data of BO (degrees) (A), LOB (m) (B), LHPA (degrees) (C), RHPA (degrees) (D), LHLOR (m) (E) and RHLOR (m) (F). Not, histograms indicate frequency of variables.

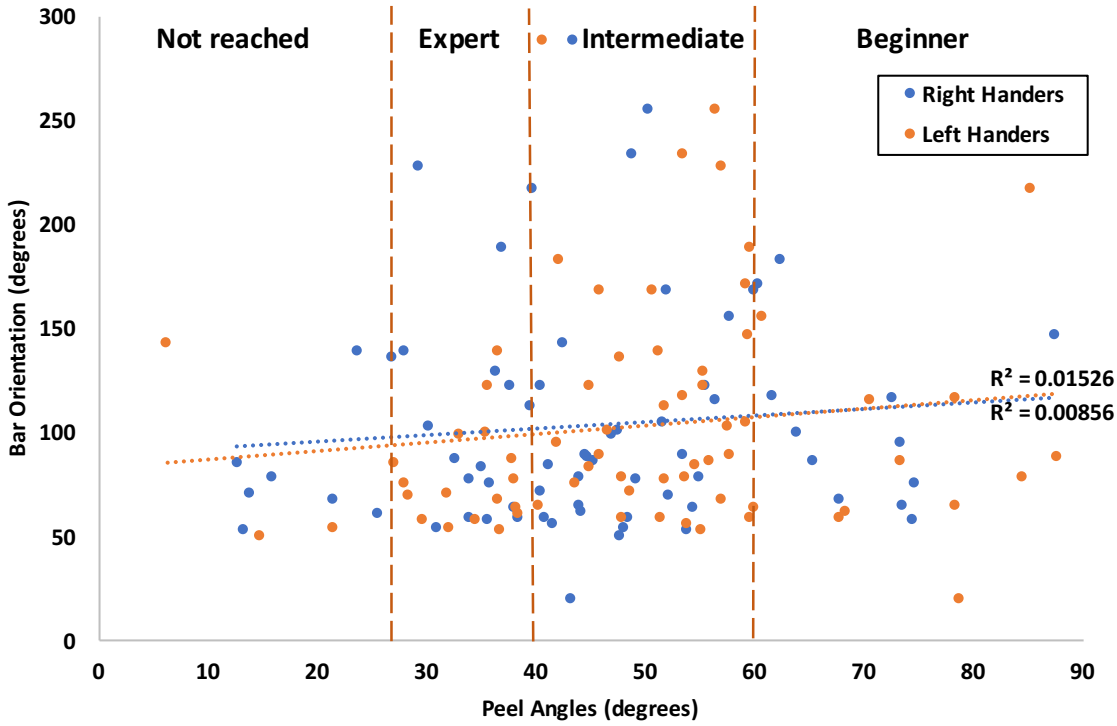

Figure 4-10 Scatter plot of bar orientation (degrees) plotted against the peel angles of both the right and left handers (degrees) for camera two all years. Note, the right and the left handers are by the represented by the colours blue and orange, respectively. The orange dashed lines indicate the surfer skill level required to ride peel angles within that range (refer to Table 2.1). There is a statistically significant relationship between the RHPAs with BO (0.05), whereas there is none between the RHPAs with the BO are not (0.12).

Both the LH and RH PAs means decreased (Figure 4.8C and D, respectively) from 53.0° to 46.9° and 51.1° to 40.8° from 2015 to 2016, respectively. While the LHLOR mean (Figure 4.8E) increased from 24.9 to 26.0 m, the RHLOR mean only slightly decreased (Figure 4.8F) from 25.9 to 25.4 m. These results are summarised in Tables 4.3 and 4.4. There was a weak inverse correlation between the BO and the LHPAs and also the BO and the RHPAs with CCs of -0.12 and -0.09 (Figure 4.10), respectively, i.e. as the BO increased, the LHPAs and the RHPAs decreased. There was, however, no statistically significant relationship between the RHPAs with BO and the LHPAs and BO with p-values of 0.44 and 0.30, respectively. With respect to the BO with the RHLOR, there was a weak inverse correlation with a CC of -0.29, which was supported by a statistically significant p-value of 0.01. In contrast, there was a very weak inverse correlation between BO with the LHLOR (Figure 4.11) with CC of -0.04, which was supported by a non-statistically significant p-value of 0.74 i.e. as the BO increased, the RHLOR and the LHLOR decreased.

When observing the LOB (m) with the LHLOR and RHLOR (m) (Figure 4.13) there was a weak inverse correlation between the LOB with the RHLOR with a CC of -0.11 and near nonexistent correlation between the LOB with the LHLOR with a CC of -0.005 i.e. as the LOB increased, the LHLOR and RHLOR decreased. As one might expect with such low CC values, there were no statistically significant relationships between the LOB with the RHLOR nor the LOB with the LHLOR with p-values of 0.35 and 0.96, respectively.

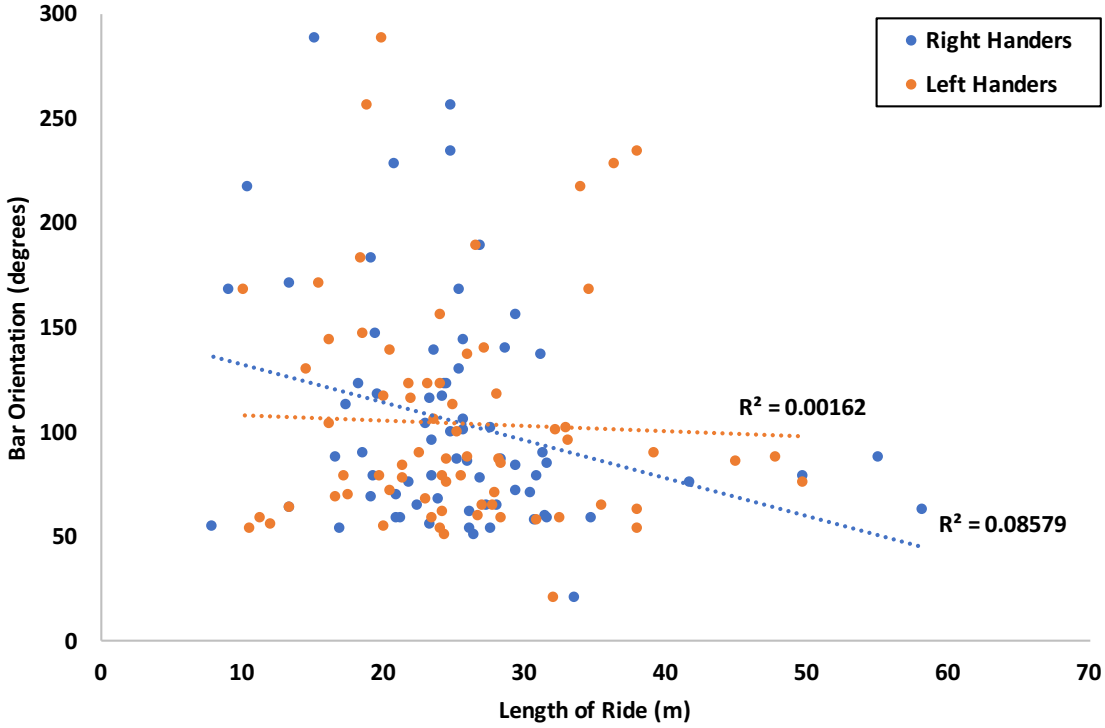

Figure 4-11 Scatter plot of bar orientation (degrees) plotted against the length of ride both the right and left handers (meters) for camera two all years. Note, the right and the left handers are by the represented by the colours blue and orange, respectively. There is no statistically significant relationship between LHLORs with the BO (0.56) nor the RHLORs with the BO (0.37).

There was a weak inverse correlation between the LOB (m) and both the RHPAs and LHPAs (Figure 4.14), with the CCs of 0.16 and 0.30, respectively. Only the LHPA and LOB, however, had a statistically significant relationship with a p-value of 0.009, whereas the RHPA and LOB had a p-value of 0.18.

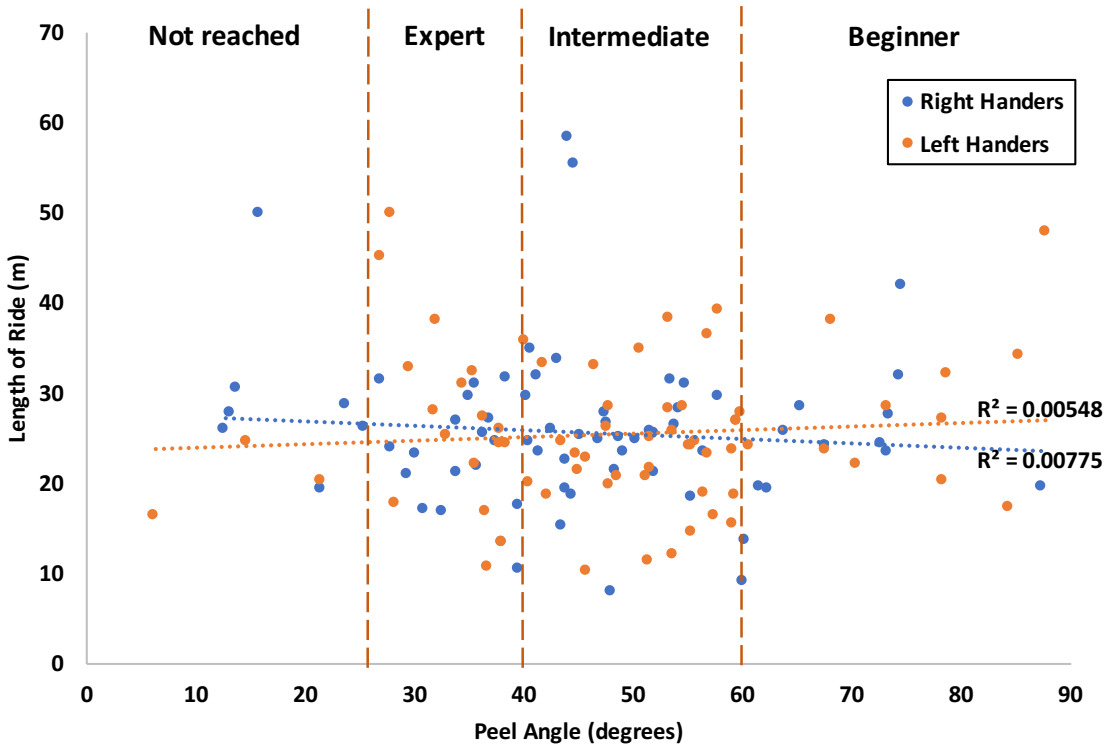

Figure 4-12 Scatter plot of peel angles both right and left handers (degrees) plotted against the length of ride both right and left handers (m) for camera two all years. Note, the right and the left handers are by the represented by the colours blue and orange, respectively. The orange dashed lines indicate the surfer skill level required to ride peel angles within that range (refer to Table 2.1). There is no statistically significant relationship between the RHPAs with the RHLORs (0.55) nor between the LHPAs with the LHLORs (0.60).

There was a very weak inverse correlation between the RHLORs with the RHPAs with CC of -0.08 and a very weak positive correlation between the LHLORs with LHPAs (Figure 4.12) with a CC of 0.07. There was, however, no statistically significant relationship between the RHPAs with the RHLORs (p-value of 0.46) nor the LHPAs with the LHLORs (p-value of 0.54). When looking at the RHPA with the LHPA and the RHLOR with the LHLOR, however, there were correlations present with a CC of 0.24 and 0.48, respectively, which were supported by statistically significant p-values of 0.04 and 0.00002, respectively.

The frequency of the BO was positively skewed, with the mode between the 50 and 100-degree range (Figure 4.9). The LOB frequency was highest between the 10 to 20 m range as well as the 20 to 30 m range. The LOB had a positively skewed distribution. The frequency of the LHPAs was highest between 50 and 60 degrees and had a negatively skewed distribution, whereas the frequency of the RHPAs

was highest between 40-50 degrees and had normal distribution. The frequency of LHLORs was highest between 20 and 25 m and had a positive distribution. In contrast, the highest frequency of RHLORs was between 25 and 30 m and had a positive distribution.

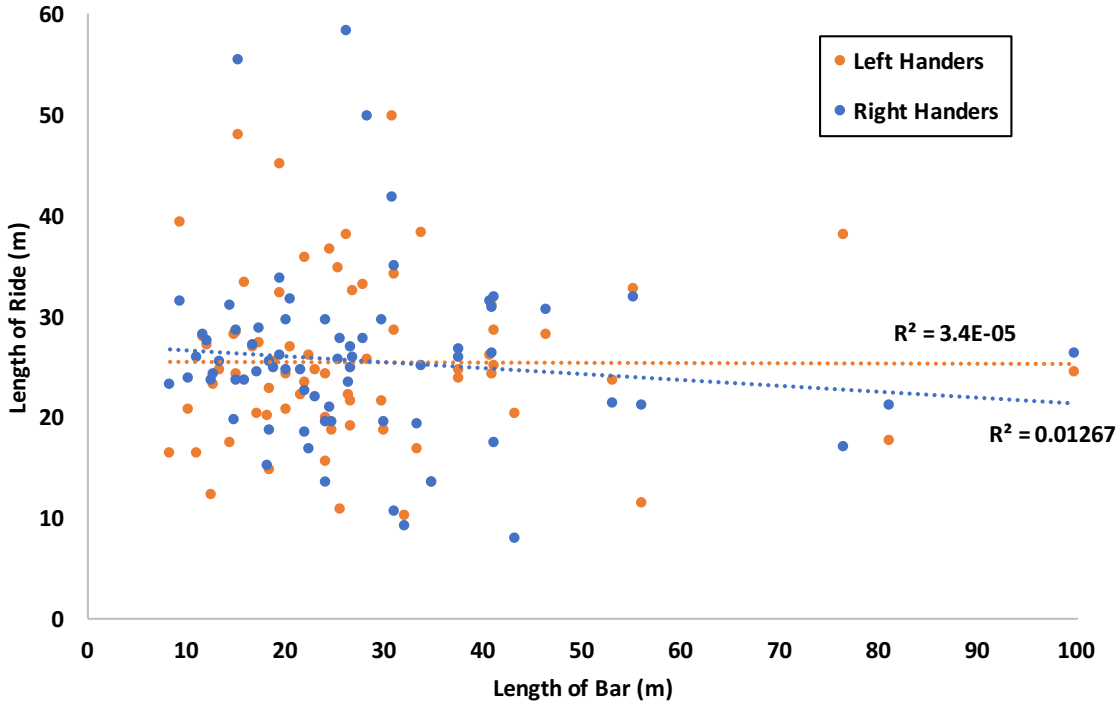

Figure 4-13 Scatter plot of length of ride (m) both right and left handers (m) plotted against the length of bar (m) for camera two all years. Note, the right and the left handers are by the represented by the colours blue and orange, respectively. There are no statistically significant relationships between LOB with the RHLORs (0.41) nor LOB with the LHLORs (0.95).

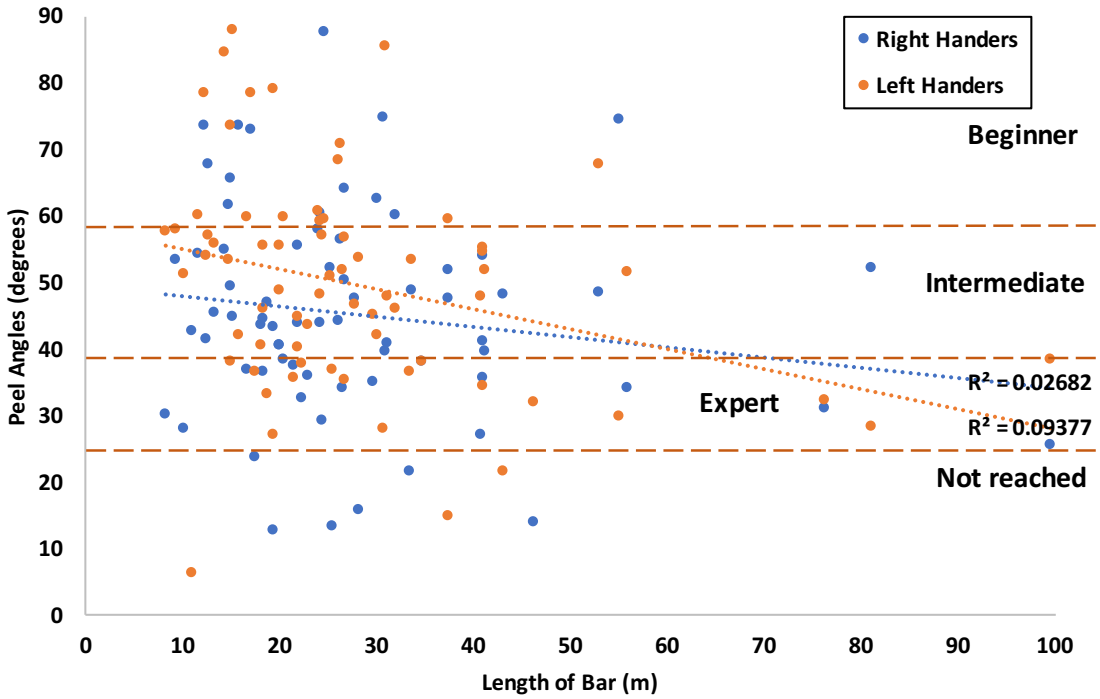

Figure 4-14 Scatter plot of peel angles both right and left handers (degrees) plotted against the length of bar (m) for camera two all years. Note, the right and the left handers are by the represented by the colours blue and orange, respectively. There is a statistically significant relationship between the LOB with the LHPAs (0.01), whereas there is none between the LOB with the RHPAs (0.17). The orange dashed lines indicate the surfer skill level required to ride peel angles within that range (refer to Table 2.1).

From a surfing perspective, at the camera two area of interest, the LHPA average mean across all years was higher than the RHPA average mean across all years, 49.5° and 45.2°, respectively, which means that waves broke faster ‘going right' than ‘going left' and thus ‘going right' required a surfer to have slightly more experience. Similar to the camera one area of interest data, the LHLOR and the RHLOR means across all years were near identical, 25.5 and 25.6 m, which suggests that even though a different level of skill is required to ‘go left and right' the ride lengths were the same on average. These results are summarised in Tables 4.3 and 4.4.

4.3 Characterising the Seasonal Variations in the Morphological and Surfing parameters at Aramoana Beach

4.3.1 Variations Observed at the Camera One Area of Interest

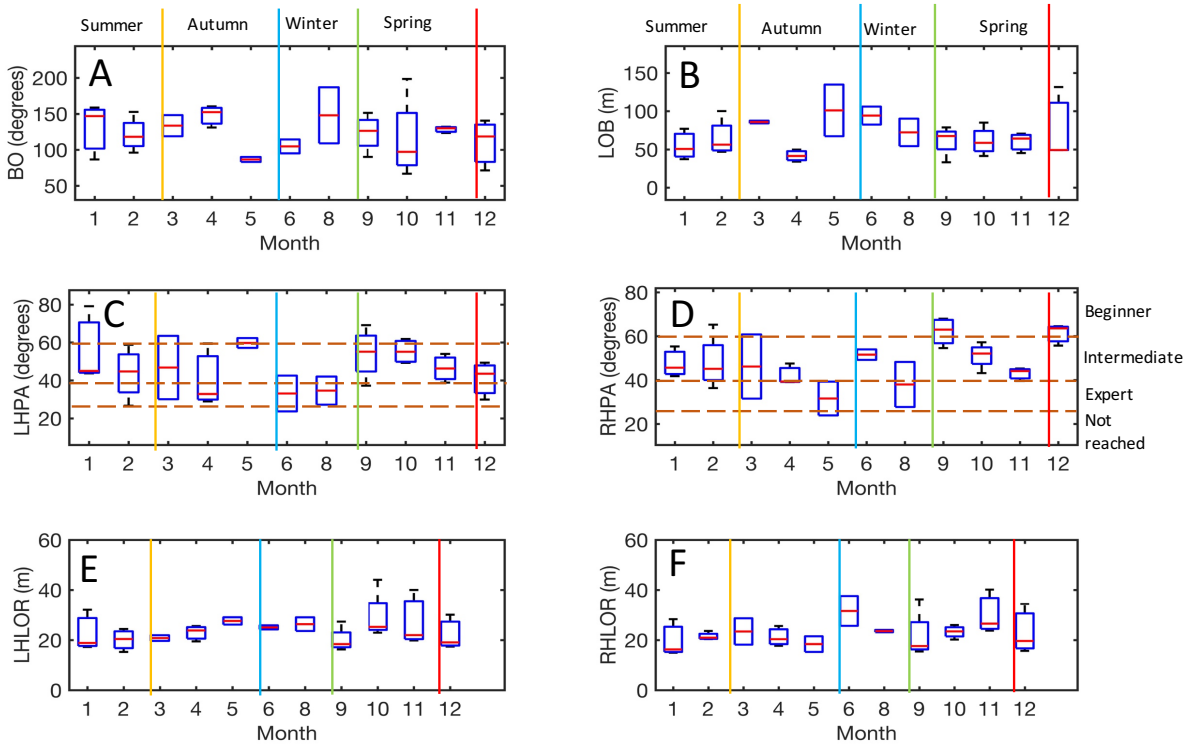

Figure 4-15 Box and whisker plots of camera one month averaged data indicating the bar orientation (degrees) plotted against time (months) (A), length of bar (m) plotted against time (months) (B), left hander peel angles (degrees) plotted against time (months) (C), right hander peel angles (degrees) plotted against time (months) (D), left hander length of ride (m) plotted against time (months) (E) and right hander length of ride (m) plotted against time (months) (F). Note the red lines are the sample medians, the tops and bottoms of each box are the 75th and 25th percentiles of the samples, respectively, the whiskers extending above and below the boxes indicate the ends of the interquartile ranges and the red plus symbols indicate the outliers. The orange dashed lines indicate the surfer skill level required to ride peel angles within that range (refer to Table 2.1). The summer months are illustrated between the red and orange lines, the autumn months between the orange and blue lines, the winter months between the blue and green lines and the spring months between the green and red lines.

When analyzing the seasonal variation between the morphological and surfing parameters at the camera one area of interest, there were some interesting trends. Summer had the lowest mean BO of 120° followed by spring with a mean BO of 122°. The BO mean increased in autumn to 133° and then further increased in winter to 196°. With respect to the LOB mean, summer and spring had the

lowest means with 60 and 65 m, respectively. Autumn and winter had the highest LOB with 76 and 69 m, respectively.

The RH and LH PA means were highest in spring and summer with means of 52° and 52° for the RHPAs, respectively, and 52° and 47° for the LHPAs, respectively. In autumn, the RHPA mean decreased to 41° whereas the LHPA increased to 50°. In winter, however, the opposite occurred, as the RHPA increased to 50° and the LHPA reduced to 36°. The RHLOR and LHLOR means were highest in spring with ride lengths of 25 and 25 m, respectively, which reduced to 22 and 22 meters in summer, respectively. In autumn, the RHLOR mean decreased to 21 m, whereas the LHLOR increased to 24 m. In contrast, in winter the RHLOR mean increased to 25 m, whereas the LHLOR decreased to 23 m. The PAs and LORs exhibited a considerable range between the seasons. Typically, both the RH and LH PAs exhibited a smaller range in summer and spring with ranges only extending between beginner and intermediate levels of surfing, whereas in autumn and winter the ranges extended further into the expert level of surfing. These results are summarised in Tables 4.1 and 4.2.

This indicated that surfing in autumn and winter was potentially better than surfing in spring and summer, as a higher level of surfing skill was required in autumn and winter compared to spring and summer at the camera one area of interest.

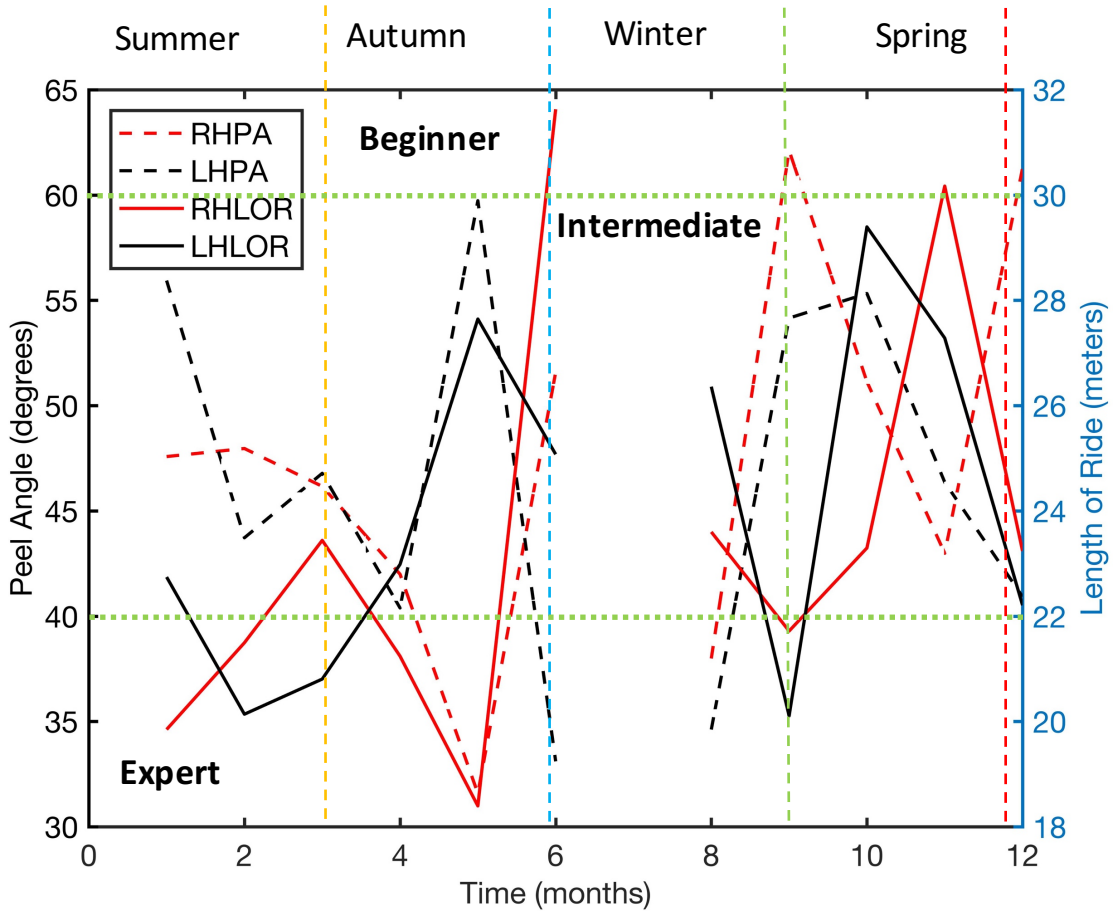

Figure 4-16 Illustrates the seasonal variation in mean data of the RH and LH PAs as well as the RH and LH LORs plotted over time (months) for camera one all years. The horizontal green dashed lines indicate the surfer skill level required to ride peel angles within that range (refer to Table 2.1). The summer months are illustrated between the red and orange lines, the autumn months between the orange and blue lines, the winter months between the blue and green lines and the spring months between the green and red lines. Note: July data has been removed due to an error.

4.3.2 Variations Observed at the Camera Two Area of Interest

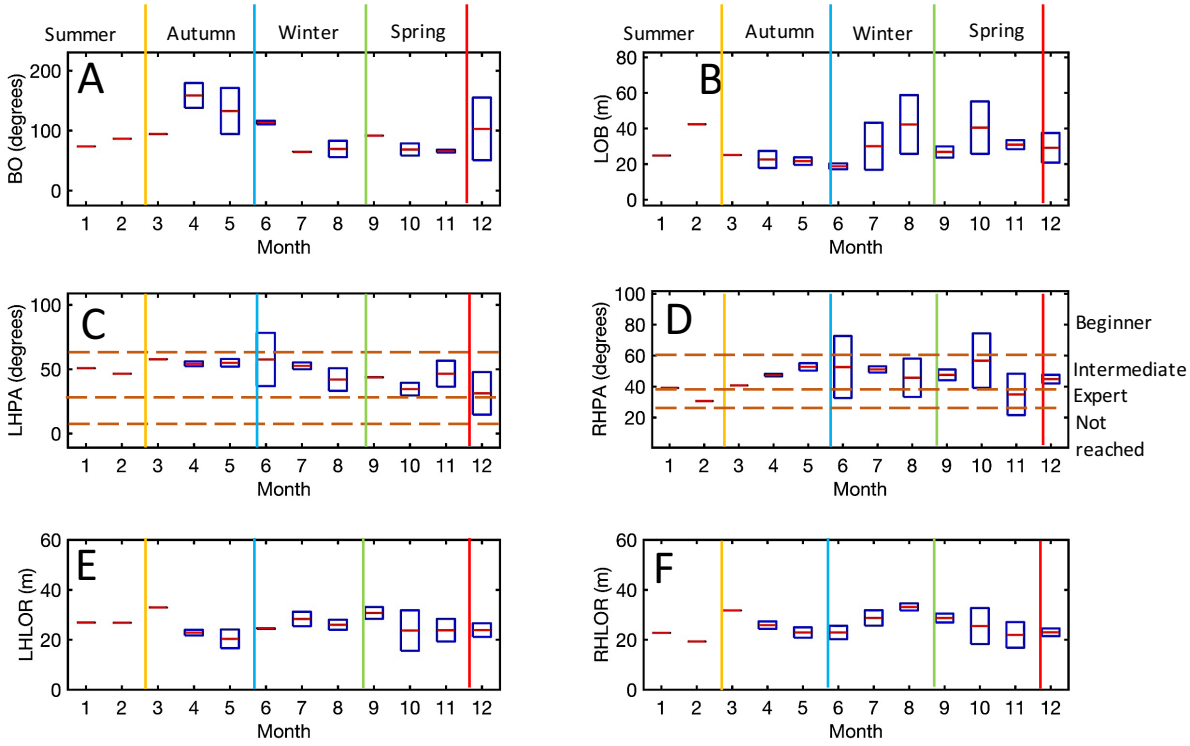

Figure 4-17 Box and whisker plots of camera two data indicating the bar orientation (degrees) plotted against time (months) (A), length of bar (m) plotted against time (months) (B), left hander peel angles (degrees) plotted against time (months) (C), right hander peel angles (degrees) plotted against time (months) (D), left hander length of ride (m) plotted against time (months) (E) and right hander length of ride (m) plotted against time (months) (F). Note the red lines are the sample medians, the tops and bottoms of each box are the 75th and 25th percentiles of the samples, respectively, the whiskers extending above and below the boxes indicate the ends of the interquartile ranges and the red plus symbols indicate the outliers. The orange dashed lines indicate the surfer skill level required to ride peel angles within that range (refer to Table 2.1). The summer months are illustrated between the 'vertical' red and orange lines, the autumn months between the orange and blue lines, the winter months between the blue and green lines and the spring months between the green and red lines.

The seasonal observations in Figures 4.17 and 4.18 may potentially be less accurate because of the paucity of data collected for the camera two area of interest. Furthermore, an El Niño phase occurred 2015, whereas from early 2016 a La Niña phase occurred (NIWA, 2017). In turn, the seasonal variation during the opposing El Niño and La Niña summers and autumns are likely to present different data with respect to the variables analysed.

The characteristics of the morphological and surfing parameters during the individual seasons indicated considerable variation and certain differences compared to the camera one area of interest. From spring to summer the BO mean increased from 75° to 87° before peaking in autumn at 135°, after which the mean decreased to 82° in winter. This is in contrast to the camera one area of interest, where the BO mean peaked in winter and was at its lowest in summer. The LOB mean was highest in spring and summer with sand-bars lengths at 32 and 32 m, respectively, whereas the LOB mean was lowest in autumn (inverse correlation to BO) at 25 m, before it increased to 30 m in winter.

The RHPA and the LHPA means indicated an interesting alternation between seasons. In spring and summer, the RHPA mean decreased from 46° to 38°, whereas the LHPA mean increased from 42° to 43°. Conversely, in autumn and winter the RHPA mean increased from 47° to 50°, whereas LHPA mean decreased from 55° to 51°. The RHLOR and the LHLOR show similar trends to the PAs. In spring and summer, the RHLOR decreased from 25 to 22 m, respectively, whereas the LHLOR stayed the same length at 26 m for both spring and summer. In autumn and winter, however, the RHLOR mean increased from 27 to 28 m, respectively, whereas the LHLOR mean increased from 25 to 26 m (not much of a change between months). These results are summarised in Tables 4.3 and 4.4.

From a surfing perspective, the PAs in summer and spring were lower than the autumn and winter PAs but the LORs were similar. In turn, the waves ‘going right and left’ in summer and spring broke faster but had similar ride lengths compared to autumn and winter. In turn, surfing condition and characteristics were more favourable during summer and spring at the camera two area of interest.

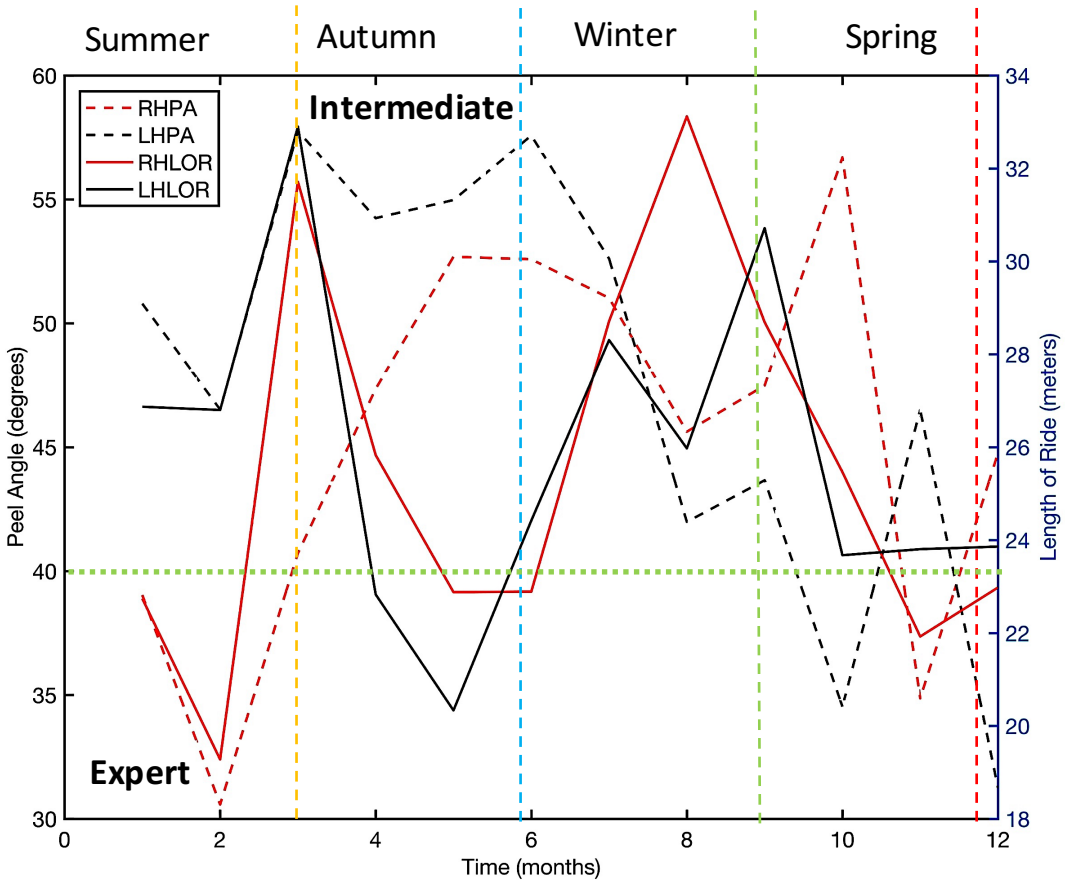

Figure 4-18 Illustrates the seasonal variation in mean data of the RH and LH PAs as well as the RH and LH LORs plotted over time (months) for camera one all years. The horizontal green dashed lines indicate the surfer skill level required to ride peel angles within that range (refer to Table 2.1). The summer months are illustrated between the red and orange lines, the autumn months between the orange and blue lines, the winter months between the blue and green lines and the spring months between the green and red lines.

4.4 Correlation with the Forcing Wave Climate

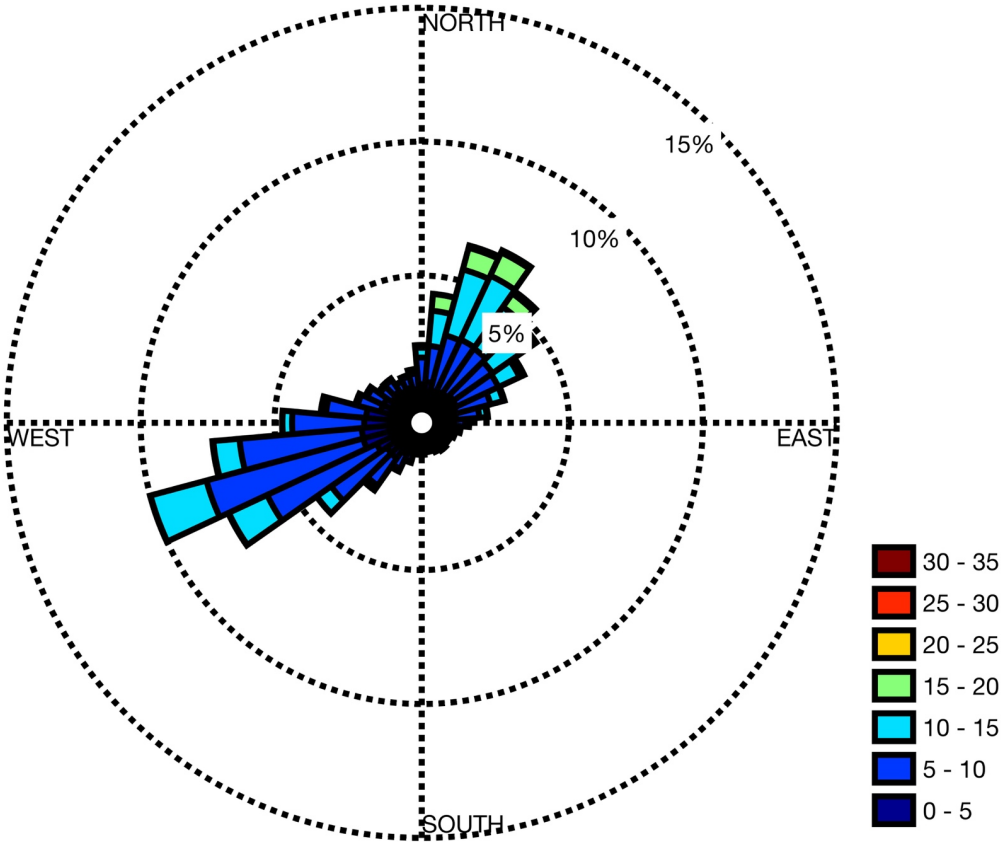

Figure 4-19 Wind rose indicating wind speed (m/s) and wind direction at Aramoana Beach. The colour bar indicates the wind speed in m/s and the bars from the center of the plot indicate the wind origin. The circles indicate the probability that a particular wind will occur from a particular direction. Data collected from NOAA and supplied by eCoast (NOAA, 2018). Hindcast wave model from 2013 to 2017.

The wind speed and more importantly the wind direction encountered at Aramoana and along the adjacent coastline directly influence the nature of the waves observed and experienced at the world-famous beach break. Ideal surfing conditions at Aramoana require an offshore wind, which pushes up wave faces, further steepening them and in the process promoting the creation of the ultimate form of a wave, known as a barrel or tube. According to the data collected by the National Oceanographic and Atmospheric Administration (NOAA) (2018), presented in Figure 4.19, the prevailing winds are predominantly from the south-west-west with secondary winds from the north-east. There is a higher probability that wind speeds of between 0 and 15 m/s would be from the south-west-west compared to any other direction. Higher wind speeds of between 15 and 20 m/s,

however, are only likely to have come from north-north-east or north-east, as observed in Figure 4.19. Since Aramoana Beach is situated adjacent to the north-east, the ideal offshore wind is from the south-west. Therefore, the probability of an offshore wind during the study period was quite high. When the winds were onshore, however, they were most likely quite strong between 15 and 20 m/s.

The 30 arc-minute global grid wind and wave rose hindcast data were pulled from the NOAA (2018). The data sets contained consist of wave hindcasts done using the WAVEWATCH 111 model and GFS analysis of winds. The hindcasts cover the entire globe and are carried out in monthly instalments. The multi-grid WW3 model is run as a mosaic of grids that are two way nested. The spectral parameters are computed on each of these grids and are stored in grib two format.

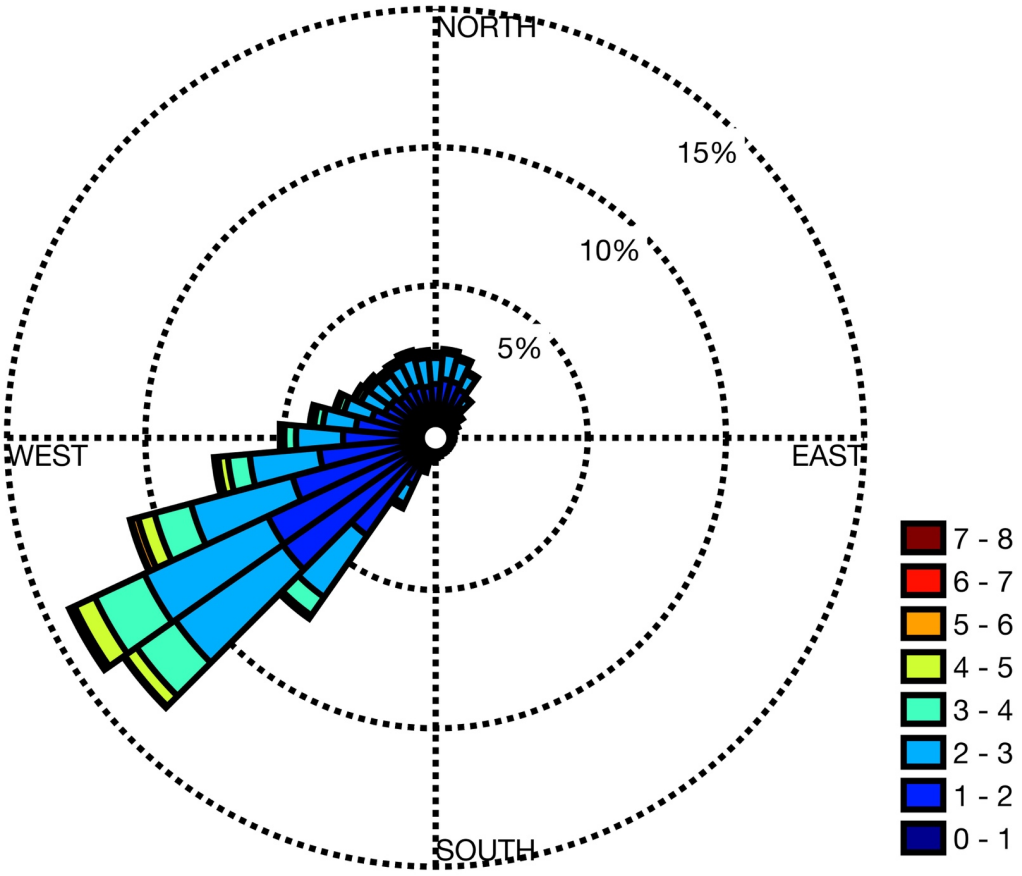

Figure 4-20 Wave rose indicating significant wave height (m) and peak wave direction at Aramoana Beach. The colour bar indicates the significant wave height (m) and the bars from the center of the plot indicate the wave direction (going to). The circles indicate the probability that a particular wave will head toward a particular direction. Data collected from NOAA and supplied by eCoast (NOAA, 2018). Hindcast wave model from 1979 to 2017.

Whilst wind direction and speed play an important role in creating the ideal atmospheric conditions for enhancing and promoting ideal surfing conditions, the peak wave direction and Hs (m) play the most important role in setting up the world-famous surfing waves observed at Aramoana Beach. The swell direction is important, as the initial direction of the swell determines whether or not the incoming swell waves line up with and more importantly interact with the preconditioning elements, the Otago Harbour ebb tidal delta (OHETD) and the Aramoana soil mound (ASM), which are essential to the converging, focusing and refraction of the wave orthogonal to align with the ideal surf contours at Aramoana Beach. The focusing and converging creates gradients in wave heights along the wave (i.e. increases the Hs along different sections of the wave) which promotes and initiates wave breaking when waves interact with local geomorphology (sand-bars) at the Aramoana Beach.

Research suggests that the ideal peak wave direction for creating the world-famous surfing waves at Aramoana are from the north-east around 70 degrees relative to true north (dominant swell) and from the south-east around 125 degrees relative to true north (secondary swell) (Sanford South Island Ltd, 2001). According to a 38-year hindcast extracted from the NOAA (2018) website, observed in Figure 4.20, the dominant swell approaching Aramoana Beach was from the north-east with a secondary swell approaching from the south-east. Waves with a Hs of between 1.0 and 2.0 m, 2.0 and 3.0 m, 3.0 and 4.0 m, 4.0 and 5.0 m, 5.0 and 6.0 m, and 6.0 to 7.0 had higher probabilities of propagating from the north-east than any other direction. There was, however, a small probability that the waves of the same magnitude could have propagated from the south-east. Hence, the primary swell was from the north-east and the secondary swell was from the south-east. This NOAA hindcast contradicts work by Oldman et al., (2008) who found that the mean peak swell direction was from 125 degrees (south-east) relative to true north.

From a surfing perspective, the swell waves from the north-east were more common but were typically smaller and had less energy than swell waves from the south-east (Single et al., 2010), thus surfing waves were likely to be smaller most of the time, except for when southerly swells propagated. Generally speaking, surfers desire bigger waves, and so the ideal swell direction would be from the south-east. Furthermore, the north-east swells would not efficiently interact with the OHETD, thus little to no preconditioning of the swell waves would occur, except for over the ASM, and the waves would remain smaller and less energetic.

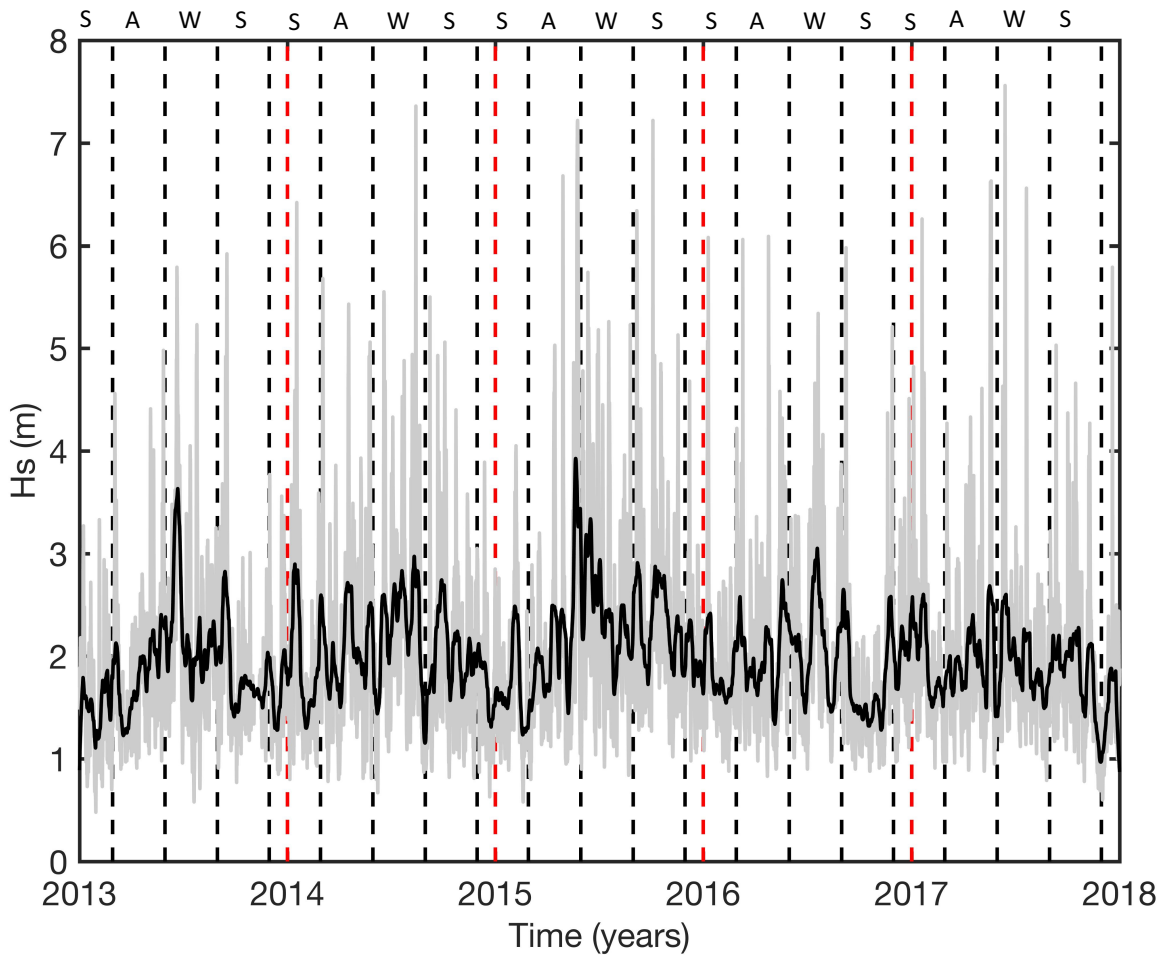

Figure 4-21 Illustrates the significant wave height (Hs) (m) plotted against time (years) for the wave forcing climate surrounding Aramoana. The grey line represents the raw Hs and the black line represents the running mean (100 to 1). The vertical dashed lines represent the seasonal separation (S, A, W, S = summer, autumn, winter and spring, respectively). Data collected from NOAA and supplied by eCoast (NOAA, 2018).

The mean significant wave height (Hs) (Figure 4.21) increased from 2013 through to 2015. After 2015 the mean Hs decreased through to 2017. This aligns with the

recorded ENSO phases (refer to Section 2.5.3 and Figure A4.1 in Appendix 4). During 2013, New Zealand experienced a La Niña phase (ENSO positive phase), which changed to an El Niño phase (ENSO negative phase) in early 2014. This El Niño phase became very strong and peaked in the summer of 2015 and 2016 before it started to weaken around March of 2016, after which time the a La Niña phase began (NIWA 2017). El Niño is associated with strong south-westerlies and in turn larger swell waves with large wave periods propagating from the south-west, which refract around the southern end of New Zealand (Gordon, 1986; Laing, 2000; Godoi et al., 2016). Hence, as El Niño peaked in the summer of 2015 and 2016 so too did the Hs. In contrast, La Niña is associated with north-easterlies and larger waves from the north-east but with smaller wave periods. These swell waves from the north-east are generally smaller than swell waves from the south-west, hence, the general reduction in Hs from the 2016 summer onwards (Gordon, 1986; Gorman et al., 2003; Godoi et al., 2016).

The winter of 2015 was characterised by a strong south-westerly flow anomaly, which produced higher than normal pressures over the North Island and lower than normal pressures over the South Island, which extended to the south and east of the South Island (El Niño, ENSO negative phase). Numerous storm systems were caused by this flow anomaly, during which time some of the coldest temperatures in 20 years were recorded as well as severe flooding in many places including Dunedin. The strong winter storms of 2015 during the El Niño phase correlate well with the peak Hs in the 2015 winter (Figure 4.21) (NIWA, 2015).

The Hs exhibits seasonal trends. Figure 4.21 indicates that the Hs was lower in summer and started to build through to autumn before it peaked in early winter, after which the Hs reduced in spring. This is consistent from 2013 right through to 2018. It is obvious, however, that winter Hs were considerably smaller through the 2017 period (La Niña phase). This correlates well with previous literature from Sanford South Island Ltd (2001), which used a 40-year hindcast model, which indicated the greatest swell waves typically occurred during the autumn and winter. Further, the same research indicated that the majority of these greater

swell waves in autumn and winter propagated from the south or south-east, which suggests that the greater swells in autumn and winter (Figure 4.21) most likely propagated from the south or south-east, as illustrated in Figure 4.20. Moreover, the Hs indicated the best season for surfing was during autumn and winter when the southerly and south-easterlies produced large waves with large wave periods, which become even larger and more desirable after preconditioning over the OHETD and ASM.

4.5 Chapter Summary

4.5.1 Camera One Key Findings

One of the key findings from the results was that the BO was much higher in 2014 and 2015 compared to 2013, 2016 and 2017. In contrast, the LOB was much higher in 2013, 2016 and 2017 compared to 2014 and 2015. There was an inverse correlation coefficient (CC) of -0.22 between BO and LOB (i.e. as the BO increased, LOB decreased), which was supported by a statistically significant p-value of 0.03. With respect to the BO seasonal mean, summer had the lowest mean of 120° followed by spring with a mean of 122°. The BO mean then increased in autumn to 133° and then further increased in winter to 196°. With respect to the LOB seasonal mean, summer and spring had the lowest means with 60 and 65 m, respectively. Autumn and winter had the highest LOB with 76 and 69 m, respectively. These results are summarised in Tables 4.1 and 4.2.

One might have expected to observe strong annual correlations between the LHPA and RHPA with the BO, respectively. The correlations, however, were weak and non-significant. Furthermore, the correlations between the LHLOR and the RHLOR with the BO, respectively, were also weak and non-significant. As the RHPA and the LHPA, as well as the RHLOR and the LHLOR, were very much a function of the BO characteristics, one might have expected to see stronger correlations. Interestingly, however, there was a weak inverse correlation (-0.18) between the RHPA and RHLOR, which was supported by a weak statistically significant p-value

of 0.09. In contrast, there was no correlation of any significance between the LHPA and the LHLOR.

Another key finding was that the LHLOR and the RHLOR with the LOB, respectively, also did not have strong correlations and were non-significant. One might have expected to observe that as the LOB increased the LOR would have increased, however, both relationships were of an inverse nature. Thus, as the LOB increased, the LOR decreased. The RHLOR and LOB, however, did have an inverse CC of -0.18 (p-value of 0.12), which was identical to the correlation between RHPA and the RHLOR, which was significant (p-value of 0.09). Furthermore, the RHPA and the LHPA also did not have strong correlations with the LOB, as one might have expected with no statistical significance.

The RH and LH PAs were within the same surfing range of ability of between 40° and 60° (intermediate level) except for 2017 where the PAs reduced to <40° requiring an expert surfing ability. Autumn and winter had more favourable surfing conditions than spring and summer.

Table 4-1 Illustrates the geomorphic parameter and surfing parameter annual means from the camera one area of interest. BO represents bar orientation (degrees relative to true north), LOB represents length of bar (m), LHLOR represents left hand length of ride (m), RHLOR represents right hand length of ride (m), LHPA represents left hand peel angle (degrees) and RHPA represents right hand peel angle (degrees).

	2013	2014	2015	2016	2017
BO (degrees)	115.00	150.50	149.20	118.00	117.00
LOB (m)	72.80	58.00	61.70	69.90	68.40
LHLOR (m)	21.60	21.80	21.70	27.20	19.80
RHLOR (m)	20.80	22.90	23.40	24.40	20.00
LHPA (degrees)	47.60	44.90	49.00	50.00	35.40
RHPA (degrees)	46.10	49.70	55.40	47.00	39.30

Table 4-2 Illustrates the geomorphic parameter and surfing parameter seasonal means from the camera one area of interest. BO represents bar orientation (degrees relative to true north), LOB represents length of bar (m), LHLOR represents left hand length of ride (m), RHLOR represents right hand length of ride (m), LHPA represents left hand peel angle (degrees) and RHPA represents right hand peel angle (degrees).

	BO (degrees)	LOB (m)	RHPA (degrees)	LHPA (degrees)	RHLOR (m)	LHLOR (m)
Spring	122.22	60.86	52.08	51.95	25.06	25.59
Summer	120.60	65.47	52.27	46.86	21.52	21.69
Autumn	133.45	76.23	41.09	49.70	21.08	23.98
Winter	196.40	69.02	50.08	36.27	24.98	23.11

4.5.2 Camera Two Key Findings

Of interest was the relationship between the BO and LOB, both the BO and LOB means increased from 92° to 112° and 25.9 to 29.7 m, respectively, from 2015 through to 2016. These results are summarised also in Tables 4.3 and 4.4 The increased BO was opposite to the camera one area of interest, which had a decreased BO from 2015 to 2016, although LOB values were the same. Further, an inverse correlation between BO and LOB was present, which was similar to the camera one area of interest. The PAs both RH and LH both decreased, whereas the RHLOR only slightly decreased and the LHLOR increased from 2015 to 2017. There was a weak inverse correlation between the BO and the LHPAs and also the BO and the RHPAs with CCs of -0.12 and -0.09, respectively, i.e. as the BO increased, the LHPAs and the RHPAs decreased but the correlations were non-significant.

Another key finding was the relationship between the BO and the RHLOR, as there was a weak inverse correlation with a CC of -0.29 and this was supported by a statistically significant p-value of 0.01. In contrast, BO with the LHLOR also had a weak inverse correlation with a CC of -0.04 (as the BO increased, the RHLOR and LHLOR decreased), which was non-significant.

A key finding of interest similar to the camera one area of interest was that there was no strong positive correlation nor statistical significance in the relationships between the LOB and LHLOR and RHLOR. In fact, as the LOB increased, the LHLOR and the RHLOR decreased, which is the complete opposite of what one might have

expected to observe. Oddly, the relationship between the LOB and the LHPA had a moderate correlation with a CC of 0.30 and a statistically significant p-value of 0.009, whereas the LOB and RHPA had a weak correlation and no statistical significance.

From a surfing perspective, annually the RH and LH PAs were within the same surfing range of ability of between 40° and 60° (intermediate level), however, the RHPAs broke faster than the LHPAs. From a seasonal surfing perspective, the PAs in summer and spring were lower than the autumn and winter PAs but the LORs were similar. In turn, the waves 'going right and left' in summer and spring broke faster but had similar ride lengths compared to autumn and winter. Therefore, surfing was better during summer and spring at the camera two area of interest.

Table 4-3 Illustrates the geomorphic parameter and surfing parameter annual means from the camera two area of interest. BO represents bar orientation (degrees to the vertical), LOB represents length of bar (m), LHLOR represents left hand length of ride (m), RHLOR represents right hand length of ride (m), LHPA represents left hand peel angle (degrees) and RHPA represents right hand peel angle (degrees).

	2015	2016
BO (degrees)	92.00	112.00
LOB (m)	25.90	29.70
LHLOR (m)	24.90	26.00
RHLOR (m)	25.90	25.40
LHPA (degrees)	53.00	46.90
RHPA (degrees)	51.10	40.80

Table 4-4 Illustrates the geomorphic parameter and surfing parameter seasonal means from the camera two area of interest. BO represents bar orientation (degrees to the vertical), LOB represents length of bar (m), LHLOR represents left hand length of ride (m), RHLOR represents right hand length of ride (m), LHPA represents left hand peel angle (degrees) and RHPA represents right hand peel angle (degrees).

	BO (degrees)	LOB (m)	RHPA (degrees)	LHPA (degrees)	RHLOR (m)	LHLOR (m)
Spring	75.27	32.70	46.35	41.57	25.36	26.06
Summer	87.61	32.11	38.12	42.85	21.67	25.84
Autumn	135.30	24.69	46.67	55.04	27.30	24.98
Winter	82.39	30.33	49.74	50.72	28.24	26.23

4.5.3 Forcing Wave Climate

The prevailing winds were predominantly from the south-west-west with secondary winds from the north-east. There was a higher probability that wind speeds of between 0 and 15 m/s were from the south-west-west compared to any other direction. Higher wind speeds of between 15 and 20 m/s, however, were only likely to have come from north-north-east or north-east. Annual and seasonal trends were observed. Autumn, winter and El Niño phases were associated with strong south-westerlies, whereas, spring, summer and La Niña phases were associated with strong north-easterlies.

The mean significant wave height (Hs) increased from 2013 through to 2015. After 2015 the mean Hs decreased through to 2017. This aligns with the recorded ENSO phases (refer to Section 2.5.3 and Figure A4.1 in Appendix 4). The strong winter storms of 2015 during the El Niño phase correlated well with the peak Hs in the 2015 winter. The Hs exhibited seasonal trends. The Hs was lower in summer and started to build through to autumn before it peaked in early winter, after which the Hs reduced in spring.

Chapter Five

General Discussion and Conclusions

5.1 Introduction

The objective of this chapter is to relate and explain the changes in the observed morphology at Aramoana Beach to the surfing parameters changes which occur over space and time. This discussion attempts to achieve this objective by exploring the four aims of this thesis, which are: (1) Can the morphological changes and changes to surfing parameters be successfully analysed from time-averaged video imagery of Aramoana Beach? (2) Are surfing parameters correlated with changes in morphology? (3) Are there predictable seasonal or interannual changes in morphology and surfing parameters? (4) Can seasonal and interannual changes be linked to changes in the wave climate around the Otago coast?

The camera one data stretches from September 2013 through to July 2017, whereas the data from camera two is only from April 2015 through to December 2016.

5.2 Beach State Variation at Aramoana

The annual variations in Hs at Aramoana Beach suggest that changes in beach state occur over time. Aramoana Beach changes from a beach state more reflective in nature, to a state more dissipative in nature and back again to a state more reflective in nature over the study period. During the years from 2013 to 2015 the ENSO phase shifted from La Niña (ENSO positive phase) in 2013 to El Niño (ENSO negative phase) in early 2014 (Figure 5.2B and A4.1). This shift in ENSO phase produced increased south-westerlies and increased swell waves propagating from the south-west, which refracted around the southern end of the South Island to become south and south-easterly swells (Gordon, 1986; Laing,

2000; Godoi et al., 2016). The El Niño phase also generated significant storm systems throughout the winter of 2015 (NIWA, 2015) just prior to the peak of El Niño in late 2015 and early 2016. This pattern of climatic weather produced an overall increase in Hs from 2013 through to 2015 (observed in Figure 4.21) (NIWA, 2015). The increase in storm systems and Hs (storm-weather profile concept (Sallenger, 2000)) suggests that Aramoana Beach was subject to a change in beach state from one more reflective in nature in 2013 to one more dissipative in nature in 2015. After the El Niño peak, the ENSO phase shifted back to a La Niña phase around March 2016, as observed in Figures 5.2B and A4.1 (NIWA 2017). The La Niña phase produced increased north-easterlies and smaller swell waves, comparatively, generated from the north-east (observed in Figure 4.21). Settled weather over New Zealand was also observed during the La Niña phase (Gordon, 1986; Gorman et al., 2003; Godoi et al.,2016). The more settled weather and smaller Hs suggests that Aramoana Beach likely shifted back to a more reflective state from early 2016 through to 2017 (fair-weather profile concept (Sallenger, 2000).

The seasonal variation in Hs indicates that Aramoana Beach likely underwent seasonal variations in beach states throughout the study period. As indicated by Figure 4.21, the Hs was greatest in autumn and winter and smallest in spring and summer, which suggests that during autumn and winter the beach was likely more dissipative in nature. In contrast, in spring and summer the beach was likely more reflective in nature. This aligns with Sallenger's (2000) fair-weather and storm profile concept illustrates the relationship of seaward movement of sand during high energy wave environments, such as during autumn and winter, and the shoreward movement of sand during low wave energy environments, such as during spring and summer. During autumn and winter as wave energy increases and sand moves seaward, the beach state becomes more dissipative, whereas, during spring and summer as wave energy decreases, the beach state becomes more reflective (refer to Section 2.3.2 for further detail).

5.3 Camera One Area of Interest

5.3.1 Morphological Parameters

The beach state changes discussed above, and their typical characteristics, however, do not well align with the BO and LOB features. Aramoana Beach exhibited somewhat opposite characteristics when comparing seasonal and annual observations throughout the study period. In autumn and winter, associated with greater Hs, the BO somewhat increased and was quite variable, whilst the LOB was consistent with typical beach state character and increased and was also variable. In comparison, during spring and summer, associated with smaller Hs, the BO decreased and became less variable, whilst the LOB was consistent with typical beach state character and decreased.

In contrast, the annual BO and LOB trends during the La Niña years (2013, 2016 and 2017) were associated with a lower BO (refer to Figure 5.1) and LOB was higher compared to the El Niño years (2014 and 2015) where the BO was higher and the LOB was lower. This relationship between the ENSO phases and the BO is illustrated in Figure 5.2A and B. Figure 5.2A clearly indicates an inverse correlation between the SOI and the BO, which have a correlation coefficient (CC) of -0.29 and is supported by a weak statistically significant p-value of 0.10. The variation in seasonal and annual observations may be a function of the smaller sample sizes collected during the winter periods (refer to Figure A3.1). The variation in seasonal and annual BO and LOB, however, it is more likely explained by the nature of the Hs and the swell direction relative to the angle of the beach.

5.3.1.1 Annual Variations

The BO decreased to face the north-north-east during La Niña phases because the dominant north-east swells were breaking at an angle to the beach. The beach angle at the camera one area of interest (C1AI) is approximately 162° relative to true north. The north-east swell waves do not break shore-normal because there is little preconditioning to align the wave orthogonal to the shore-normal (Kilpatrick, 2005; Scarfe et al., 2009a & b). Thus, the north and north-east swell waves break an angle to the beach angle. van de Lageweg et al. (2013) found that

the orientation of sand-bars is generally in phase with dominant wave energy flux. Therefore, as the dominant wave energy flux is from the north and north-east during La Niña phases, the BO decreased to about 117° relative to true north, which is north-north-east (observed in Figure 5.1).

In contrast, the increased BO during El Niño phases from more north-north-east facing toward more north-east facing is a result of the dominant south-east swells breaking at an angle to the beach. The south-east swell waves refract around Tairoa Head and then preconditon over the Otago Harbour ebb-tidal delta (OHETD) and Aramoana spoil mound (ASM) (refer to Section 2.5.6 for further detail). The preconditions aligns the wave crests more shore-normal, which is approximately 162° relative to true north (Kilpatrick, 2005; Scarfe et al., 2009a & b). As mentioned, van de Lageweg et al. (2013) found that the orientation of sand-bars is generally in phase with dominant wave energy flux. Therefore, as the dominant wave energy flux is function of the preconditioning of south-east swell waves, the BO increased to 150° during El Niño phases when waves broke more shore-normal (observed in Figure 5.1).

The decreased LOB during El Niño phases is hypothesised to be a result of the increased Hs breaking at an angle to the existing sand-bars resulting in topographicaly controlled rip currents. The south-east swell wave energy is increased during the El Niño phases (Gordon, 1986; Laing, 2000; Godoi et al., 2016) and the swell waves break in deeper water at an angle to the shoreline and existing sand-bars. It is thought that the angular breaking waves cut deep into the sand-bars and cause topographically controlled rip currents to develop. It is the cutting behaviour that breaks up the sand-bars, thus creating the decreased LOB segments, and the persistant topographically controlled rip currents, which keep the LOB reduced during the El Niño years (observed in Figure 4.15). Short (1985) and Elliot (1973) suggests that topographically controlled rip currents formed during high energy wave events, such as observed during El Niño phases, can persist as long as the wave conditions are constant. In one study, Gallop (2009) observed rip currents on Tairua Beach, Coromandel Peninsular to persist for up to 400 days.

The LOB increased during La Niña phases compared to El Niño phase, which was not expected. It is hypothesized that as the wave energy was decreased in the La Niña years compared to the El Niño years (Gordon, 1986; Gorman et al., 2003; Godoi et al.,2016), the decreased energy resulted in reduced dissipation of wave energy on the sand-bars. In turn, topographically controlled rip currents, associated with high energy periods (Short 1985; Eliot, 1973), such as created during El Niño phases, were less likely to occur and break up existing sand-bar segments during La Niña phases. Therefore, the sand-bars during La Niña phases were longer than the El Niño phase not because they grew longer but because they were not reduced in length by topographically controlled rip currents.

5.3.1.2 Seasonal Variations

Similar to the annual variations in BO associated with La Niña, the decreased BO during spring and summer to face more north-north-east is believed to be a result of the dominant north and north-east propagated swell waves. As mentioned, the camera one area of interest beach angle is approximately 162° relative to true north. As discussed, the orientation of the sand-bars is generally in phase with the dominant wave energy flux (van de Lageweg et al*.,* 2013). Therefore, as the north-east swell waves were dominant during spring and summer (Single et al., 2010) the BO decreased to 122° and 120° in spring and summer, respectively (as observed in Figure 4.15A and Table 4.2).

Similar to the annual variation in BO associated with El Niño, the BO increased relative to the true north to face north-east during autumn and winter. As stipulated, the beach face angle at the camera one area of interest is approximately 162° relative to true north. In autumn and winter, south-east swells propagate from the south and south-east (Oldman et al., 2008; cited by Single et al., 2010) and refract around Taiaroa Head, Otago Peninsular. As discussed, the south-east swell waves precondition over the OHETD and the ASM (refer to Section 2.5.6 - Kilpatrick, 2005; Scarfe et al., 2009a & b), which aligns the swell waves more shore-normal. van de Lageweg et al. (2013) found that the orientation of sand-bars is generally in phase with dominant wave energy flux. Therefore, as

the dominant wave energy flux is function of the preconditioning of south-east swell waves, the BO increased to 133° relative to true north during autumn and an extreme 196° relative to true north in winter (as observed in Figure 4.15A and Table 4.2).

The decreased LOB during spring and summer was likely a result of the fair-weather profile (Sallenger, 2000) typically observed spring and summer. In contrast, the increased LOB during autumn and winter was likely a result of the storm weather profile (Sallenger, 2000) typically observed autumn and winter (refer to Section 2.3.2 for further detail).

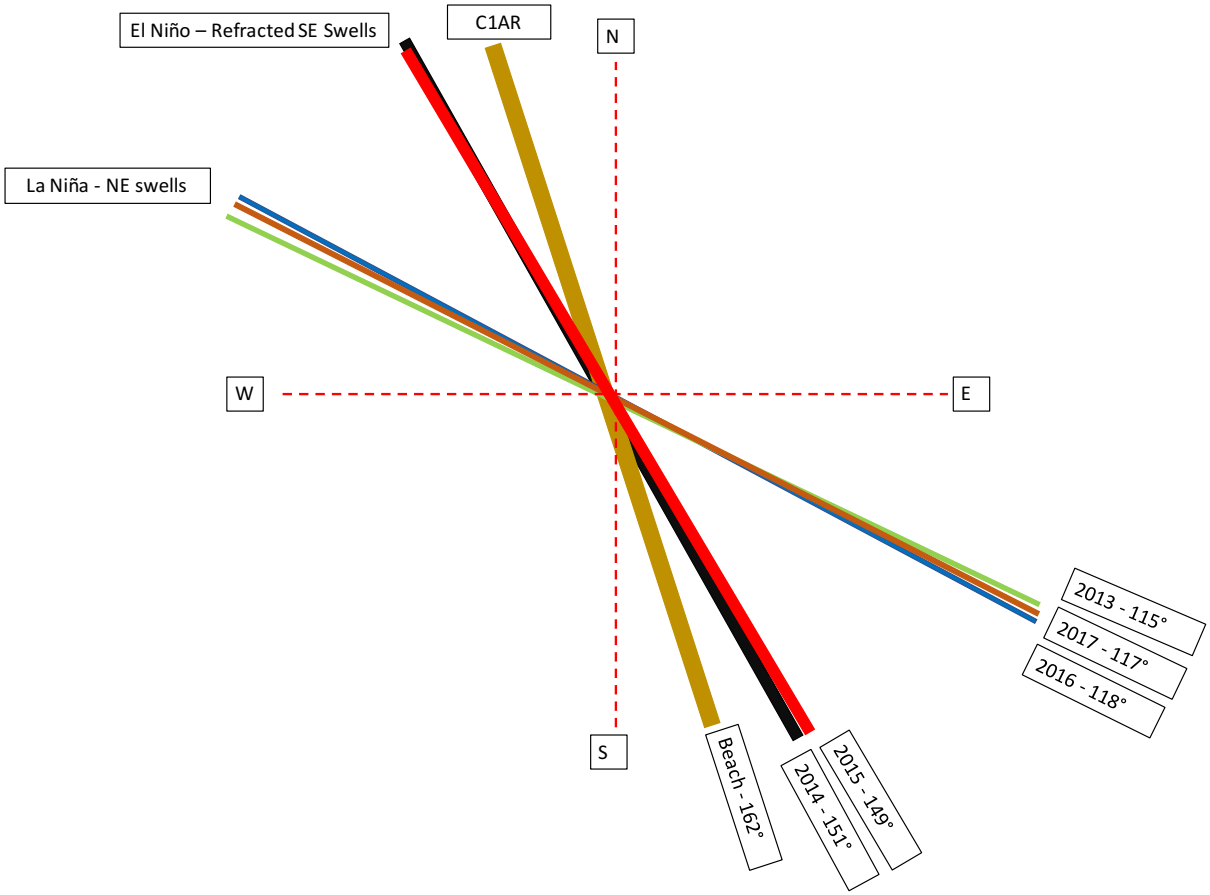

Figure 5-1 Diagram represents the sand-bar orientation (BO) from 2013 to 2017 and the BO correlation with the ENSO phases La Niña and El Niño with respect to the approximate beach angle at the camera one area of interest (C1AI). N, E, S, W, SE and NE are abbreviations for north, east, south, west, south-east and north-east, respectively.

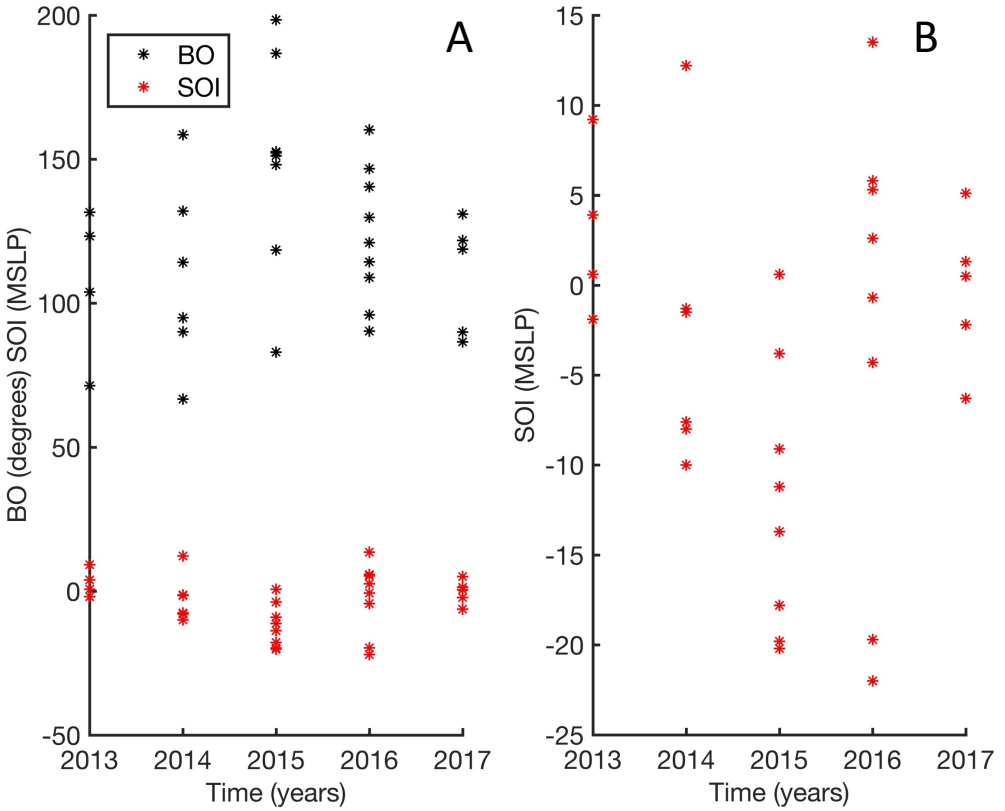

Figure 5-2 Illustrates the Southern Oscillation Index (SOI) monthly means (mean sea level pressure (MSLP)) and bar orientation monthly means (degrees) plotted against time (years) (A) and Southern Oscillation Index (SOI) monthly means (mean sea level pressure (MSLP)) plotted against time (years) (B). Note: sustained negative SOI values below -7 are indicative of El Niño phases and sustained positive SOI values higher than 7 are indicative of La Niña phases (AGBM, 2018). Note: the same data is plotted in A and B.

5.3.2 Surfing Parameters

The surfing parameters of interest are the peel angles (PA), both the left and right, referred to as the LHPA and the RHPA, respectively, and the length of ride (LOR), both 'going left' and 'going right', referred to as the LHLOR and the RHLOR, respectively. The peel angle of a breaking wave indicates the skill level at which a surfer 'must' possess to catch and then successfully ride a wave (refer to Table 2.1 for further detail). The length of ride, as the name suggests, indicates the distance over which it is possible to continue to surf the wave. The surfing parameters the PA and LOR are typically coupled with the morphological parameters BO and LOB and are thus a function of the same processes described earlier in Section 5.3.1.

According to the skill rating level created by Hutt et al. (2001), both the mean LHPA and RHPA at the camera one area of interest are within the same PA limit of between 40° and 50° relative to the BO. This is important, as the identical limit indicates that the same level of surfing experience (intermediate level of skill) is required to go both ‘left' and ‘right'. This intermediate level of surfing requires, at a minimum, that surfers be able to execute standard manoeuvres consistently on a single wave and, at a maximum, be able to execute advanced manoeuvres on occasion (refer to Table 2.1). Yet, the overall range of PAs indicates the waves often interchange between all surfer skill levels ranging from beginner through to expert. In turn, the camera one area of interest (C1AI) is suited to different surfing skill levels at various times of the year. Therefore, the skill level of surfing required at any particular time at the C1AI is a function of the wave forcing climate, which as discussed in Section 5.3.1, has observed seasonal and annual trends.

5.3.2.1 Annual Variations

The variation in both the LH and RH PAs throughout the study period indicates that there are annual shifts in orientation of the sand-bars (observed in Figure 4.1). The RHPA means increased from 2013 through to 2015, whereas the LHPAs initially decreased from 2013 to 2014 before increasing in 2015. As previously discussed, Aramoana Beach appears to have shifted from a more reflective state in 2013 and early 2014, associated with the observed La Niña phase, to a more dissipative state from early 2014 onwards to early 2016, associated with an El Niño phase. With this shift in ENSO phase and associated beach state change, more of a storm weather profile (Sallenger, 2000) occurred at Aramoana Beach (Gordon, 1986; Laing, 2000; Godoi et al., 2016).

One might have expected to observe that with the storm weather profile development, increased sand-bar lengths (LOB) and in turn greater LH and RH LORs (Figure 4.1) would have been observed annually. As previously discussed, however, it is hypothesised that the greater Hs, during El Niño phases, cut deep into the existing sand-bars, which creates topographically controlled rip currents and LOB lengths are reduced. In turn, the RH and LH PAs were reduced.

Furthermore, the winter storms of 2015, during the El Niño phase, may have intensified the breaking wave cutting energy effect on the sand-bars, thus further reducing the LOB and the RH and LH PAs.

The sand-bars rotated to face toward the north-east from 2013 to 2014. During this period, the LHPAs initially decreased, whereas the RHPAs increased over the same period. The BO increased from a north-north-east (117° relative to true north) orientation toward a more north-east (150° relative to true north) orientation, as the dominant north-easterly swells, associated with the La Niña phase in 2013 and early 2014, shifted to the dominant south-easterly swells associated with the El Niño phase, in early 2014. During the period where the BO was increasing, the RHPAs increased and the LHPAs decreased because of the breaking wave angle of incidence with the BO. Once the BO had more or less aligned to the dominant wave energy direction, however, which resulted in more shore normal sand-bars, (i.e. more north-east facing sand-bars from the south-east waves), both the RHPAs and LHPAs became more similar and the PAs of both increased.

In contrast, when Aramoana Beach started to shift back to a more reflective beach state in early 2016, which was associated with a shift from the El Niño phase back to a La Niña phase, both the LH and RH PAs decreased. From early 2016 to the end of the study period in 2017, both the RHPAs and LHPAs decreased with the reduction in 2017 being quite considerable. The La Niña phase produced dominant north-east waves and more settled weather over New Zealand (Gordon, 1986; Gorman et al., 2003; Godoi et al.,2016). The BO decreased back toward the north-north-east (117° relative to true north) orientation that was observed in the 2013 La Niña phase (observed in Figure 5.1), as the increased south-easterly swell component, associated with the El Niño phase, shifted back to the dominant north-easterly swell component, associated with the La Niña phase. During the transitional period, as the BO was decreasing from the north-east (150° relative to true north) toward to the north-north-east (117° relative to true north), the LHPAs were slightly greater than the RHPAs due to the depths of the breaking waves and BO incidence to the beach angle. Once the BO had more or less aligned with the

dominant north-north-east wave energy flux, however, which resulted in less shore-normal sand-bars, both the RHPA and LHPA means decreased drastically due to the considerably smaller Hs (Figure 4.21). The smaller Hs resulted in shallower breaking waves over the sand-bars (wave height to water depth ratio, Mead, 2003), which produced the smaller PAs.

The RHPA mean being slightly greater than the LHPA mean and vice versa is a function of the BO to the beach angle. For example, as mentioned, the beach angle at the C1AI is approximately 162° relative to true north and the BO during El Niño phases was 150° relative to true north. When the waves broke over the sand-bars, the waves 'going right' broke less acutely to the sand-bars compared to the waves 'going left'. In turn, the RHPA means were greater than the LHPA means. Therefore, because of the greater RHPA means and more favourable BO to breaking wave angle compared to the LHPA means and non-favourable BO, the RHLOR means were on average greater than the LHLOR means during El Niño phases.

5.3.2.2 Seasonal Variations

In spring and summer, LHPAs and the RHPAs, as well as the LHLORs and the RHLORs, have similar values, respectively (Figure 4.16), as the angle of incidence between the breaking waves and sand-bars was more less parallel. As discussed in the previous Section 5.2.1, during spring and summer the dominant swell is from the north and north-east, the swell waves of which carry less energy and are smaller than the south-east swell waves (Single et al., 2010). The north-east swells break less shore normal (120° to 122°) but more parallel to the spring and summer sand-bars. The smaller Hs and parallel breaking wave nature produces the smaller and similar LH and RH PAs as well as the smaller and similar RH and LH LORs.

In contrast, during autumn and winter, the south-east swell waves broke more shore-normal (autumn 133° and winter 196° relative to true north), which resulted in greater RHPAs and RHLORs and reduced LHPAs and LHLORs, as observed in Figures 4.15 and 4.16. As previously discussed, during autumn and winter, the

predominant swell is from the south-east, the swell waves of which carry more energy and are of a greater Hs compared to the north-east swell waves (Single et al., 2010). These south-east swell waves break more shore normal (autumn 133° and winter 196°) to the camera one area of interest beach angle (162°). As a result, less shore normal north-north-east orientated sand-bars, associated with spring and summer, are re-orientated to face more to the north-east in autumn and south-east in winter, as indicated by the greater BO (degrees) values in Figure 4.15.

As the south-east swell waves interact and shoal onto the more north-east facing sand-bars, the BO and breaking wave angle of incidence results in greater RHPAs and RHLORs values and smaller LHPAs and LHLORs values, as observed in Figures 4.15 and 4.16. This is because the waves 'going right' break at less acute angles compared to the waves 'going left', resulting in greater RHPAs compared to LHPAs. The waves 'going right' break in a direction that is becoming shallower, thus the unbroken part of the wave is able to shoal onto the sand-bar and continue breaking, in turn, creating the increased RHLORs. Whereas, the waves 'going left' break into deeper water, thus the unbroken part of the wave is unable to shoal onto the deeper sand-bar sections and break due to the wave height to water depth ratio not being exceeded (approximately 0.78 Mead, 2003). The shorter waves resulted in the decreased LHLORs. These seasonal trends can be better observed in Figure A3.1 (refer to Appendix 3). Data paucity in autumn and winter is noted.

Ultimately, from a surfing perspective, in spring and summer the PAs and LORs 'going right' and 'going left' were similar, thus requiring the same level of surfing skill. According to Hutt et al.'s (2001) surfing skill table (Table 2.1), the level of skill required to surf during spring and summer is between beginner and intermediate. In autumn and winter, the PAs and LORs 'going right' required a lower surfing skill level of beginner to intermediate and surfers would have enjoyed a longer wave 'going right' compared to 'going left'. The wave 'going left' would have required a greater surfing skill level of intermediate to expert.

During La Niña phases the PAs and LORs going ‘left’ and ‘right’ were likely to be similar as the Hs were reduced and breaking wave angle to sand-bar incidence was reduced. This resulted in the reduced PAs and also shorter LORs. In contrast, during the El Niño phase the PAs and LORs ‘going right’ were greater than of those ‘going left’ due to the favourable angle of incidence between the breaking waves and the sand-bar orientation. In general, the El Niño phase produced bigger waves with smaller north-east orientated sand-bars that resulted in longer waves to produce more surfing manoeuvres on ‘going right’ compared to ‘going left’. The La Niña phases produced smaller waves with longer north-north-east orientated sand-bars, which resulted in smaller PAs and more potential ‘close out’ wave sets from north-easterly swells. Generally speaking, El Niña years produced more favourable surfing characteristics and conditions than La Niña years.

5.4 Camera Two Area of Interest

As previously mentioned, the camera two area of interest only has data from April 2015 through to December 2016 whereas the camera one area of interest has data from September 2013 through to May 2017. Furthermore, the data collected and analysed for the camera two area of interest was recorded during the peak of the El Niño phase (ENSO negative phase) before shifting a La Niña phase in early 2016 (ENSO positive phase). The El Niño phase produced severe storms systems, which resulted in greater Hs (Figure 4.21). In contrast, when the El Niño phase shifted to La Niña the weather over New Zealand settled and the Hs reduced. The limited data and changes in atmospheric oscillations make analysis and interpretation of the camera two area of interest data problematic, as seasonal and yearly trends are not only difficult to identify but are also challenging to interpret and discuss. Furthermore, making comparisons between the camera one and camera two areas of interest becomes difficult, to say the least. The below, however, is an attempt at interpreting, discussing and comparing the ‘seasonal' and ‘annual' trends observed between the camera two area of interest with the camera one area of interest.

5.4.1 Morphological Parameters

The BO and LOB for the camera two area of interest (C2AI) increased over the 2015 and 2016 study period. In contrast, the BO and LOB for the camera one area of interest (C1AI) decreased and increased, respectively, over the same period. During the peak El Niño phase in 2015, the BO mean was 149° relative to true north (north-east facing) and the LOB mean was 62 m for the C1AI, whereas at the C2AI the BO mean was 92° relative to true north (north facing) and the LOB mean was 26 m. When the El Niño phase shifted to La Niña in early 2016, the BO mean for the C1AI decreased to 118° relative to true north (orientated more north-north-east) and the LOB mean increased to 70 m, whereas for the C2AI the BO mean increased to 112° relative to true north (orientated more north-north-east) and the LOB mean increased to 29 m. The increase and decrease in BO mean at the C2AI and the C1AI, respectively, during this shift in ENSO phase from El Nino to La Nina suggests that the C2AI location may respond differently to the distinctive phases of ENSO or maybe responding to other variables compared to the C1AI.

5.4.1.1 Annual Variations

The location of the C2AI potentially explains the observed geomorphology and surfing parameter differences at the C2AI compared to the C1AI. The C2AI lies approximately 300 m south of the C1AI and is characterised by sandy and rocky outcrop features. Initially, the rocky outcrop was thought to have had an influence on the BO as well as the LOB and in turn an influence on the surfing parameters. The location of the C2AI appears to be more in the lee of ‘the mole' compared to the C1AI with respect to the south-easterly swells. Thus, the south-easterly swells, which are preconditioned over the Otago Harbour ebb-tidal delta (OHETD) and again, but to a lesser extent, over the Aramoana spoil mound (ASM), may not feature to the same extent at the C2AI compared to the C1AI due to the refraction potential. In turn, it was thought that the C2AI was likely to be subject to or exposed to more north and north-east swells that influence the morphology in a different manner compared to the C1AI.

The C1AI beach angle, however, is approximately 162° relative to true north on a more north-north-west to a south-south-east axis, whereas the C2AI beach angle is approximately 142° relative to true north on a more north-west to south-east axis. As mentioned, El Niño results in greater Hs and wave periods propagating from the south and south-west (Gordon, 1986; Laing, 2000; Godoi et al., 2016), which when refracted around the southern end of New Zealand and eventually Taiaroa Head, Otago Peninsular, the waves interact with and precondition over OHETD and ASM (Kilpatrick, 2005; Scarfe et al., 2009a & b). This results in the waves breaking at an angle of approximately 150° relative to true north at C1AI. 'The mole', which is located at the entrance to the Otago Harbour, however, may have an increased shadow effect at the C2AI location, thus preventing a lot of the south-east wave energy.

During the 2015 El Niño year, however, the BO was lower than the 2016 La Niña year (refer to Figure 5.3), which was opposite to the C1AI. One suggestion as to why this may have occurred is that 'the mole' may have further refracted any south-east swell waves (refraction around 'the mole' observed in Figure 1.7 (McComb, 2016)) that interacted with the head of 'the mole' feature. It is thought that when the south-east swell waves interact with the head of the mole feature the waves sharply refract and when these waves reach the nearshore they break at greater angles (south) to the shore-normal (142° relative to true north). In turn, as the BO is a function of the dominant wave energy flux (van de Lageweg et al., 2013) it is believed that this is why the BO was shifted toward facing north at 92° relative to true north.

In contrast, at the C2AI, during the 2016 La Niña phase, the BO mean was 112° relative to true north and is thought to be a result of the dominant north and north-east swell waves breaking at an angle to the C2AI beach angle. The C2AI beach angle is approximately 142° relative to true north. The BO means at C1AI and C2AI during the 2016 La Niña phase were quite similar, and this suggests that the north-east swell waves orientate the BO in a similar manner at both beach locations. As mentioned, van de Lageweg et al. (2013) found that the orientation

of sand-bars is generally in phase with dominant wave energy flux. Therefore, as the dominant wave energy flux is from the north and north-east, the BO increased to 112° relative to true north to face north-north-east during the 2016 La Niña phase, as waves broke at an angle to the shore-normal (observed in Figure 5.1).

The LOB increases from 2015 to 2016 and it is believed that the LOB was lower in 2015 compared to 2016 because of the greater breaking wave angle of incidence (92° relative to true north) with respect to the beach angle (142° relative to true north) during the 2015/2016 El Niño period compared to the 2016 La Niña period (112° relative to true north). As suggested, the high energy, south-east swell waves, associated with El Niño, sharply refract around the head of 'the mole' feature and this results in the waves breaking at greater angles of incidence to the beach angle, which reduces the BO and LOB (refer to Section 5.3.1 for further detail). In contrast, the LOB is higher in the 2016 period. As mentioned, the lower energy, north-east swell waves, associated with La Niña, break with less energy and do not create topographically controlled rip currents. Thus, the lack of these persistent rip currents meant that the LOB was longer compared to 2015 El Niño sand-bars, which were subject to reduction in length due to the topographically controlled rip currents.

5.4.1.2 Seasonal Variations

The seasonal variations in the BO and LOB observed at the C2AI were somewhat similar and also very different to those observed at the C1AI. The BO was lowest in spring (75° relative to true north) and summer (87° relative to true north) and greatest in autumn (135° relative to true north), which is similar to the C1AI, whereas winter had a low BO of 82° relative to true north, which is very different to the C1AI. As previously discussed, during spring and summer the north and north-east swells are dominant, whereas in autumn and winter the south-east swells dominant (Single et al., 2010). The winter BO of 82° relative to true north aligns with the above suggestion that the south-east swell waves interact with and refract sharply around the head of 'the mole' feature, which may produce the reduced BO observed. The summer and spring BO of 87° and 75° relative to true

north, respectively, however, are very similar to the winter BO, which suggests that the waves interacting with the shoreline may have propagated from the south-east and not from the north or north-east. Moreover, the autumn BO (135°) aligns with the north-east swell wave direction, which suggests that the data from autumn is more in phase with La Niña rather than El Niño swell characteristics.

Interestingly, over the 2015 and 2016 study period, the SOI was greatest in summer and second highest in winter (observed in Figure 5.3), as the only summer data recorded was during the 2015/2016 El Niño phase when El Niño was at its peak, whereas the data recorded in autumn was recorded during both El Niño and La Niña phases. Furthermore, the data collected during spring was recorded during the 2015/2016 El Niño phase peak and a weak La Niña phase. Hence, summer, spring and winter BOs may be similar because of the dominant El Niño south-east swell waves refracting around the head of 'the mole' feature. The winter storms of 2015 (NIWA, 2015) may have further exacerbated the effect on the BO. Whereas the autumn data may have been more influenced by the dominant north-east swells during the La Niña phase, hence the BO is increased (135° relative to true north) toward the shore normal (142° relative to true north) during autumn. The notion that the BO is correlated with the SOI during the El Niña phase at the C2AI can be observed in Figure 5.3.

The seasonal LOB mean is highest in spring and summer and lowest in autumn and then winter and is thought to be because of same reasons discussed for the C1AI. In summer and spring, the dominant swell is from the north-east, whereas in the autumn and winter the dominant swell is from the south-east (Single et al., 2010). The north-east swell waves, despite breaking at an angle to the shore-normal, broke with less energy over the sand-bars and topographically controlled rip currents were not produced and this resulted in the increased LOB during spring and summer. In contrast, the south-east swell waves in autumn and winter also broke at an angle to the shore-normal but broke, however, with greater energy than the north-east swell waves. In turn, LOB decreased because of the increased wave energy acting on the sand-bars, which may have produced topographically controlled rip currents. As mentioned, the potential formation of these persistent

rip currents may have reduced the lengths of the LOB during autumn and winter (refer to Section 5.3.1 for further detail).

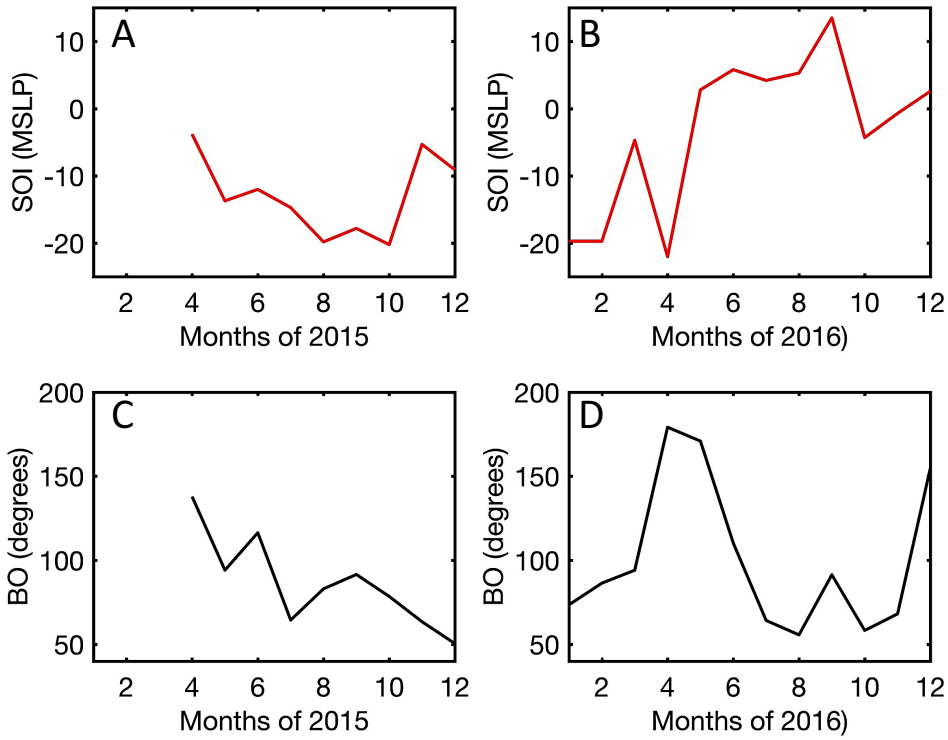

Figure 5.3 Illustrates the Southern Oscillation Index (SOI) monthly means (mean sea level pressure (MSLP)) plotted against the 2015 months (A), SOI monthly means (mean sea level pressure (MSLP)) plotted against the 2016 months (B), the BO (degrees) plotted against the 2015 months (C) and the BO (degrees) plotted against the 2016 months (D). Note, sustained negative SOI values below -7 are indicative of El Niño phases and sustained positive SOI values higher than 7 are indicative of La Niña phases (AGBM, 2018).

5.4.2 Surfing Parameters

According to the surfer skill level rating produced by Hutt et al. (2001) the level of surfing skill required to surf at the camera two area of interest (C2AI) is the same as the camera one area of interest (C1AI). The RH and LH PA means over the study period of 46° and 50° relative to the BO, respectively, indicated that an intermediate level of surfing skill is required both 'going left' and 'going right' as the PAs are within the same range of ability. This intermediate level of surfing requires, at a minimum, that surfers be able to execute standard manoeuvres consistently on a single wave and, at maximum, be able to execute advanced manoeuvres on occasion (refer to Table 2.1). The overall range of PAs, however, indicated that the waves were observed to interchange between all surfer skill

levels ranging from beginner through to expert. In turn, the C2AI is suited to different surfing skill levels at various times of the year. Thus, the skill level of surfing required at any particular time is a function of the wave forcing climate, which is observed to have seasonal and annual trends (refer to Section 5.3.1 for further detail).

5.4.2.1 Annual Variations

The variation in the RHPA and the LHPA means as well as the RHLOR and the LHLOR means over the 2015 and 2016 study period indicated that there are annual shifts in the BO and LOB means (observed in Figure 4.8). As a result of the BO shifting from north-north-east facing at the start of 2015 through to north facing toward the end of 2015, both the RHPA and the LHPA means decreased over the 2015 period, as the waves started to break more parallel with the BO over time.

When the BO became more or less aligned with the dominant wave energy flux, however, the RHPAs increased and the LHPAs decreased. This inverse relationship is a result of the breaking wave angle of incidence with the BO. As the waves interacted with the sand-bars and broke, the waves 'going right' broke toward the beach at slightly less acute angles compared to waves 'going left' and were able to continue peeling or breaking because of the wave height to water depth wave breaking ratio of approximately 0.78 (Mead, 2003). In contrast, the waves 'going left' were peeling or breaking into deeper water and eventually stopped breaking and probably reformed due to the wave height to water depth wave breaking ratio not being exceeded (Mead, 2003). Hence, the RHPAs and RHLORs were greater than the LHPAs and the LHLORs at the C2AI during 2015.

In contrast, during the 2016 period, the BO increased and shifted from north facing (92° relative to true north) to north-north-east facing (112° relative to true north). As mentioned, the north-east swell waves broke more shore normal at the C2AI. In turn, the BO was increased to 112° relative to true north. During the BO shifting phase from north to north-north-east facing, the RHPAs decreased, whereas the LHPAs increased. Once the BO had more or less aligned with the dominant wave

flux (van de Lageweg et al., 2013) to the north-north-east, however, the LHPAs increased and became greater than the RHPAs. This may be due to more northerly swell waves breaking over the sand-bars. In turn, the when the northerly swell waves broke over the sand-bars, the waves 'going left' broke at less acute angles to waves 'going right', thus the LHPAs were greater than the RHPAs. Further, the waves 'going left' broke for longer due to the breaking wave angle of incidence with the BO, which resulted in the greater LHLORs compared to the RHLORs, as discussed earlier.

5.4.2.2 Seasonal Variations

From a seasonal perspective, the mean BO in spring, summer, autumn and winter were 75°, 87°, 135° and 82° relative to true north, respectively. Note, the summer data recorded was only from the 2015/2016 El Niño phase whereas, the spring, autumn and winter data was recorded during a strong El Niño phase in 2015 and early 2016 and weak La Niña phase during 2016. In turn, the data was highly variable due to the ENSO phases.

Despite the above statement regarding data collection, the BO was lowest in spring at 75° relative to true north and it is thought to be a result of the north swell waves decreasing the BO toward north-north-west facing due to the breaking wave angle of incidence with the BO. This resulted in the greater RHPAs compared LHPAs in spring. Interestingly, the LHLORs and RHLORs were not dissimilar. In summer, the BO increased to 87° relative to true north, as a result of the El Niño south-east swell waves refracting around the mole and increasing BO toward north facing from north-north-west. This resulted in increased LHPAs and LHLORs and decreased RHPAs and RHLORs.

In autumn, the BO mean increased to 135° relative to true north and was a result of the La Niña dominant north and north-east swell waves re-orientating and increasing BO toward the north-east. The north and north-east swell waves breaking over the north-east facing sand-bars resulted in reduced RHPAs and increased LHPAs, due to the breaking wave angle of incidence with the BO. The

RHLORs, however, were greater than the LHLORs. The suggested reason is that the waves ‘going right' broke toward shallower depths and could continue breaking, whereas the waves ‘going left' broke toward deeper depths and eventually stopped breaking due to the wave height to water depth breaking wave ratio of approximately 0.78 (Mead, 2003) not being exceeded.

In winter, it appears that the strong El Niño phase dominated the weak La Niña phase. In turn, the strong south-east swells, once refracted around the head of ‘the mole' feature, decreased the BO toward the north and north-north-west. Once the BO had more or less aligned with the dominant wave flux (van de Lageweg et al*.,* 2013) this resulted in near equal RHPA and LHPA means as the breaking wave angle of incidence with the BO became near parallel. Further, just as the RHLOR means were greater than the LHLOR means during autumn, the winter RHLOR means were also greater than the LHLOR means, which is most likely a result of the same processes, as discussed for autumn.

Ultimately, the variation in data recorded between 2015 and 2016 at the C2AI is considerable. In turn, annual and seasonal trends are not only difficult to identify but are challenging to discuss and make sense of. From a surfing perspective, the months during the 2015 El Niño period produced lower BOs compared the C1AI, and lower PAs ‘going left and right’ compared to the months during the 2016 La Niña period that produced greater BOs and higher PAs ‘going left and right’. With respect to surfing, the El Niño months produced smaller LOBs compared to La Niña months and the LORs were typically longer in the La Niña months due to the more favourable breaking wave angle of incidence with the BO. The Seasonal trends were almost impossible to identify because of the influence of the ENSO phase shifts and because the data paucity over two years. Yet, the surfing conditions were more favourable in spring, summer and winter compared to autumn.

5.5 Chapter Summary

The C1AI results indicated a distinct relationship with the ENSO phases and in turn the associated forcing wave climate. A La Niña phase was present from 2013 to early 2014, after which an El Niño phase occurred until early 2016 before ENSO shifted back to La Niña in early 2016. The La Niña phase was present to the end of the study period. During the La Niña years, the weather over New Zealand was quite settled and it is believed that the state of Aramoana Beach became more reflective during this time. La Niña produced north to north-east swells and winds. The resulting north-east swells decreased the BO to face north-north-east, whilst the LOB increased.

In contrast, during the El Niño years, the weather over New Zealand became very unsettled (winter storms of 2015). It is believed that the state of Aramoana Beach became more dissipative during this period. El Niño produced strong south-westerly winds and large waves, which when refracted around the southern end of the South Island of New Zealand became strong south-east swells. The south-east swell waves preconditioned over the Otago Harbour Ebb Tidal Delta (OHETD) and again over the Aramoana spoil mound (ASM). The preconditioning resulted in the waves aligning more shore-normal than the north-east swell waves, which resulted in the BO increasing to face toward the north-east, whilst the LOB decreased due to topographically controlled rip currents.

In general, surfing conditions at the C1AI were better during El Niño years compared to La Niña years. During La Niña years, the PAs and LORs going ‘left’ and ‘right’ were similar, as the Hs and breaking wave angle to sand-bar incidence was reduced. This resulted in reduced PAs and also shorter LORs. In contrast, during the El Niño years the PAs and LORs ‘going right’ were greater than of those ‘going left’ due to the favourable angle of incidence between the breaking waves and the sand-bar orientation. Generally speaking, El Niño years produced greater Hs with shorter, north-east orientated sand-bars, which resulted in longer waves to ‘work’ on ‘going right’ compared to ‘going left’. In contrast, La Niña years produced smaller Hs with longer north-north-east orientated sand-bars, which resulted in smaller PAs and more potential ‘close out’ wave sets from north-easterly swells.

El Niño years produced more favourable surfing characteristics and conditions than La Niña years.

Seasonal variation also produced some interesting trends. During spring and summer, north and north-east swell waves dominated. Like La Niña years, the BO decreased to face toward to the north-north-east, whilst the LOB increased. In contrast, during autumn and winter, the south-east swell waves dominated. Like the El Niño years, the BO increased to face toward the north-east, whilst the LOB decreased. In general, the surfing conditions in spring and summer produced PAs and LORs 'going right' and 'going left', which were similar and required the same level of surfing skill (beginner to intermediate). The similar PAs, however, indicated more potential 'close out' wave sets from the smaller Hs from north-east swell waves. In contrast, autumn and winter produced PAs and LORs 'going right', which required a lower surfing skill level (beginner to intermediate) compared to 'going left' (intermediate to expert) but produced longer LORs 'going right' compared to 'going left'. Generally speaking, autumn and winter provided more favourable surfing characteristics and conditions compared to spring and summer.

The C2AI results also indicated a similar relationship with the ENSO phases. It is noted, however, that the data collected and analysed from the C2AI does not represent two full years of data and in turn, the accuracy of the annual and seasonal trends observed may not be precise. That data collected during the 2015 and early 2016 period was during an El Niño phase, whereas the data collected after early 2016 was during a La Niña phase.

In contrast to the C1AI, the BO decreased toward the north in the El Niño phase, whilst the LOB also decreased. It is believed the strong south-east swell waves sharply refracted around the head of 'the mole' feature, which increased the angle of wave breaking and sand-bar incidence as well as the breaking wave to beach angle incidence. This resulted in the BO decreasing toward north facing. The greater Hs and wave energy breaking at an angle to the BO created topographically controlled rip currents and the LOB was decreased. Furthermore, contrary to the C1AI, the BO increased in the La Niña phase toward the north-

north-east, whilst the LOB also increased. The north and north-east swells of the La Niña phase increased the BO, whereas, the reduction in Hs meant topographically controlled rip currents were not produced and the sand-bars did not break up as much and stayed longer compared to the El Niño phase sand-bars.

In general, the surfing conditions at the C2AI were not nearly as good as compared to the C1AI. The morphological and surfing parameters of interest were more favourable with respect to surfing at the C1AI compared to the C2AI. At the C2AI, the El Niño phase produced greater PAs compared to the La Niña phase, which meant a higher level of surfing skill was required to surf during the La Niña phase compared to the El Niño phase. The LORs, however, were similar between the respected ENSO phases. Although the Hs were greater during the El Niño phase, from a surfing perspective, the morphological and surfing parameters were better during the La Niña phase than the El Niño phase, which is the complete opposite to the C1AI. In short, the La Niña phase at the C2AI produced better surfing characteristics and conditions compared to the El Niño phase.

Seasonal trends identified at the C2AI are likely to be inaccurate because of the paucity of data and contradicting influences of El Niño and La Niña. Thus, the identified trends should be treated with caution. During summer, spring and winter BO decreased toward north facing, whilst the BO in autumn increased toward north-north-east facing. The LOB during summer, spring and winter was greater than the LOB during autumn. From a surfing perspective, the surfing conditions and characteristics were more favourable in summer, spring and winter compared to autumn. It must be stressed, however, the variation in the seasonal data is considerable and highly influenced by the paucity of data and ENSO phase shifts.

Chapter Six

Conclusions

6.1 Introduction

This chapter summarises the thesis and its findings, identifies the limitations of the study and discusses the implications for future research and for the application of the New Zealand Coastal Policy Statement (2010).

6.2 Thesis Summary

Aramoana Beach has had a very colourful history, from the early dredging projects of the early 1900s to the construction of the 'the mole' in the late 1900s, right the way through to the dredging projects of the 21st century. Aramoana or "pathway to the sea" is a singular site of great importance to local Māori, as the area has provided a great source of Kai, a highway, sheltering for human settlement, a burial ground and is a symbol of ancestral, spiritual and religious practices of the people of Kai Tahu.

Aramoana Beach is a well-known surfing beach and is recognised by the NZCPS (2010) as a surf break of national significance. Until recently, little baseline data had been collected on the surf break. The objective of this thesis was to understand how the morphological and surfing parameters interact within and between each other and with the forcing wave climate at Aramoana Beach. Using remote camera imagery analysis, analysis of the forcing wave climate, and detailed information collected by the Port of Otago on the use of the break, baseline data was collected, and the results of this work will help inform and support the NZCPS (2010) in protecting Aramoana Beach and other surf breaks around New Zealand and will advance future research in this field.

Two cameras were set up overlooking Aramoana Beach to monitor and capture images for the purpose of analysis. Camera one was set up, in 2013, to look toward

the north end of the beach, whereas camera two was set up, in 2015, overlooking an area near the middle of the beach. The data used in this work was from September 2013 to July 2017 for camera one and April 2015 to December 2016 for camera two. A snapshot image was captured every five minutes from each camera. These images were then time-averaged to provide a time-lapsed view of the beach processes. Selected low tide snapshot and time average images were then rectified to allow for analysis. The most highly surfed area at Aramoana Beach is in the middle. Two focus areas of interest were identified at this middle beach location. The rectified snapshot images were cropped to better represent the identified areas of interest. These were known as the camera one area of interest (C1AI) and the camera two area of interest (C2AI).

The time-averaged images were run through a suite of computer algorithms to determine the location of the sand-bars as well as the sand-bar orientation and length, whilst the cropped rectified snapshot images were run through a different suite of computer algorithms to determine the peel angle (PA) and the length of ride (LOR) of the broken waves over the sand-bars. The morphological parameters of interest were the location, bar orientation (BO) and the length of the sand-bars (LOB), whereas the surfing parameters of interest were the right and left-hand peel angles (RHPA and LHPA, respectively) and the right and left-hand length of rides (RHLOR and LHLOR, respectively).

The state of Aramoana Beach, as well as the morphological and surfing parameters, are subject to annual and seasonal trends, which are dictated by the forcing wave climate associated with the ENSO phase shifts as well as seasonal shifts. At the C1AI, El Niño phases as well as the forcing wave climate associated with autumn and winter increased the BO and decreased the LOB, whilst the state of Aramoana Beach became more dissipative in nature. In contrast, La Niña phases as well as the forcing wave climate associated with summer and spring decreased the BO and increased the LOB, whilst the state of Aramoana Beach became more reflective in nature. Surfing conditions were more favourable in El Niño years and during autumn and winter compared to during La Niña years and during spring and summer. At the C2AI, the El Niño phase resulted in decreased BO and LOB,

whilst the La Niña phase increased the BO and LOB. The seasonal trends at the C2AI were likely inaccurate because of the paucity of data. Surfing conditions at the C2AI were more favourable during La Niña phases compared to El Niño phases.

6.3 Research Questions

Specifically, the thesis examined the following questions and the major findings are as follows:

(1) *Can the morphological changes and changes to surfing parameters be successfully analysed from time-averaged video imagery of Aramoana Beach?*

The morphological changes **can be** successfully analysed from time-averaged video imagery of the beach, whereas the surfing parameters required still video imagery. The bar orientations (BO) and the length of the sand-bars (LOB) were detected and then analysed via Lippmann & Holman's (1989) sand-bar detection technique, which works by detecting local light intensity maxima created by the bubbles and foam that result from breaking waves over shallow sand-bars. It is assumed that the bands of white in the time-averaged images, associated with the foam and bubbles of breaking waves, give the approximate position of submerged sand-bars.

In contrast, the peel angles and length of rides **cannot** be successfully analysed from time-averaged video imagery of Aramoana Beach. This is because individual wave crests and white-water lines, the information of which is required to determine the right and left-hand peel angles (RHPA and LHPA, respectively) as well as the right and left-hand length of ride (RHLOR and LHLOR, respectively), cannot be physically observed in time-averaged video imagery. The wave crests and white-water lines, however, **can be** observed and analysed in snapshot video imagery. The snapshots provide, as the name suggests, an instantaneous moment in time, which allows the wave crest and white-water lines to be located and in turn the associated surfing parameters to be determined.

(2) Are surfing parameters correlated with changes to morphology?

The results definitively indicate that surfing parameters **are** correlated with changes in morphology, although the correlation coefficients were not strong and only some of the p-values indicated statistical significance between the morphological parameters and surfing parameters. The results at both the camera areas of interest indicated that as the morphological parameters change, the surfing parameters change to align with the changed morphology.

(3) Are there predictable seasonal or interannual changes to morphology and surfing parameters?

(4) Can seasonal and interannual changes be linked to changes in the wave climate around the Otago coast?

Questions three and four are interlinked. For both questions, the results indicate that there **are** predictable seasonal and interannual changes in morphology and surfing parameters and that seasonal and interannual changes can be linked to changes in the wave climate around the Otago Coast. The following presents a summary of the findings for each of the cameras related to questions three and four.

Camera One Area of Interest

There **are** predictable seasonal and interannual changes to the morphology and surfing parameters and these **can be** linked to changes in the wave climate around not only the Otago Coast but wider New Zealand. ENSO phase shifts between La Niña and El Niño resulted in the interannual changes to the morphology at Aramoana Beach. During El Niño phases, south-westerly winds dominate, and large Hs propagate from the south-west, which become south-east swells as they refract around the south end of the South Island of New Zealand. Further, weather over New Zealand becomes unsettled. The BO during El Niño phases increased relative to true north to face north-east, whilst the LOB decreased. In contrast, during La Niña phases, north-easterly winds dominate, large Hs (smaller than El Niño phases) propagate from the north-east and weather over New Zealand

becomes more settled. The BO during La Niña phases decreased relative to true north to face more north-north-east, whilst the LOB increased.

El Niño years produced more favourable surfing characteristics and conditions than La Niña years. The surfing parameters are correlated with the morphology, therefore, as the morphology shifts due to the interannual ENSO phase shifts so too do the surfing parameters. The El Niño phases produced greater Hs with shorter, north-east orientated sand-bars, which resulted in in greater peel angles and ride lengths (longer more open wave faces to 'work' on) 'going right' compared to 'going left'. In contrast, the La Niña years produced smaller Hs with longer north-north-east orientated sand-bars, which resulted in smaller peel angles and ride lengths 'going left and right'. This means more potential 'close out' wave sets from north-easterly swells.

There are distinct seasonal changes to the morphology at Aramoana Beach. In autumn and winter, south-east swells were dominant. Similar to El Niño phases, the south-east swell waves of autumn and winter increased the BO relative to true north to face north-east, whilst the LOB also increased. The BO increased to align with the dominant wave energy flux. The LOB increased as a result of the stormier weather experienced during autumn and winter. In contrast, during spring and summer, north-east swells were dominant. Similar to La Niña phases, the north-east swell waves of spring and summer decreased the BO relative to true north to face more north-north-east, whilst the LOB decreased. The BO decreased to align with the dominant wave energy flux. The LOB decreased as a result of the fairer weather experienced during spring and summer.

As there are distinct seasonal changes to the morphology at Aramoana Beach, there are in turn distinct seasonal changes to the surfing parameters. Autumn and winter provided more favourable surfing characteristics and conditions compared to spring and summer. The surfing conditions in spring and summer produced peel angles and ride lengths 'going right' and 'going left', which were similar and required the same level of surfing skill (beginner to intermediate). The similar peel angles, however, indicate more potential 'close out' wave sets from the smaller

Hs from north-east propagated swell waves. In contrast, autumn and winter produced peel angles and ride lengths which required a lower surfing skill level ‘going right’ (beginner to intermediate) compared to ‘going left’ (intermediate to expert) and produced longer ride lengths ‘going right’ compared to ‘going left’.

Camera Two Area of Interest

There **are** predictable interannual changes to the morphology and surfing parameters, which **can be** linked to the wave climate around the Otago Coast and wider New Zealand, however, the seasonal changes to the morphology and surfing parameters are unclear due to the paucity of data recorded from the camera two area of interest. Similar to the camera one area of interest (C1AI) ENSO phase shifts between La Niña and El Niño result in the interannual changes to the morphology at Aramoana Beach. In contrast to the C1AI, the BO decreased relative to true north to face north in the El Niño phase, whilst the LOB also decreased. It is believed the strong south-east swell waves sharply refracted around the head of ‘the mole' feature, which increased the angle of wave breaking and sand-bar incidence as well as the breaking wave to beach angle incidence. This resulted in the BO decreasing relative to the true north toward north facing. Furthermore, contrary to the C1AI, the BO increased relative to true north in the La Niña phase toward the north-north-east, whilst the LOB also increased.

There are predictable interannual changes of the surfing parameters at the C2AI, which are linked to the phases of ENSO, however, the seasonal changes are unclear due to the paucity of data. The La Niña phases at the C2AI produced better surfing characteristics and conditions compared to the El Niño phase. The El Niño phase produced greater peel angles compared to the La Niña phase, which means a higher level of surfing skill is required to surf during the La Niña phase compared to the El Niño phase. The ride lengths, however, were similar between the respected ENSO phases. Although the Hs were greater during the El Niño phases, from a surfing perspective, the morphological and surfing parameters were better during the La Niña phases, which is the complete opposite to the C1AI. The surfing conditions at the C2AI are not nearly as good as compared to the C1AI.

Predictable seasonal surfing parameters are unclear at the C2AI due to the paucity of data. Thus, the identified trends should be treated with caution. During summer, spring and winter BO decreased relative to the true north toward north facing, whilst the BO in autumn increased toward north-north-east facing. The LOB during summer, spring and winter was greater than the LOB during autumn. From a surfing perspective, the surfing conditions and characteristics were more favourable in summer, spring and winter compared to autumn. It must be stressed, the variation in the seasonal data is considerable and highly influenced by the paucity of data.

6.4 Limitations

The following limitations have been identified.

6.4.1 Forcing Wave Climate

The study relies on images, which capture breaking waves over shallow sand-bar features. If there are no breaking waves, however, such as during periods of low wave energy, then there is little to no data for that period recorded. In contrast, during high wave energy events and in particular during storm events, the nearshore wave environment can be very messy and individual swell waves are difficult to identify and analyse.

Many of the images with breaking waves that were recorded during autumn and winter were not of a high quality necessary for the computer algorithms to work. The low-quality images, that were distorted or not able to be used in the analysis, resulted from rainy days, low cloud and or fog, smudges or drops on the camera lens, sun glare reflecting off the ocean surface, stormy conditions creating messy wave environments and multiple swell directions interrupting wave identification processes. These factors were outside the researcher's control. The effect was a paucity of data for periods during autumn and winter (refer to Chapter four). One possible solution to address low cloud and fog would be to have multiple cameras at various elevations to reduce the impact of the above effects, however, it is likely that lower elevations would reduce the overall view of the beach and capture less data.

6.4.2 Camera set-up

The likelihood of a full wave segment being captured from the very start of a breaking wave to the very end of a breaking wave was not high. The length of rides and peel angles obtained in the analysis of the data was a direct function of the timing of the cameras. An image was recorded once every five minutes. In turn, if a peel angle was to change half way through a wave but the image was recorded prior to the peel angle change, there would be no way of knowing this. For future studies, it is beneficial to set up cameras to record an image every second for a period of time either side of the predicted low tide or a camera set up that records periodic videos, as Atkin (2010) accomplished. Not only would this ensure that only valuable data of interest is being recorded at the appropriate times but also that the data would contain full wave segments from the start to the finish. Further, potential peel angle changes could be identified with complete wave identification. The cameras were set up independently from this study. The researcher was not involved in the camera set-up, as camera one was set up in 2013 and camera two in 2015 for resource consent purposes. Subsequently, there was a delay the receipt of data by the researcher culminating in a reduced time frame to complete a comprehensive analysis of the entire beach. Thus, the researcher made a decision to focus on two key areas of interest, which were located in the middle section of Aramoana Beach.

6.4.3 Data

The data received for camera two was very limited. The data covered the period from April 2015 to December 2016. In turn, the data did not represent two full years and seasonal differences between years could not be identified. The timing of the data is important, as a strong El Niño phase was present during 2015 to early 2016 and a weak La Niña phase present from early 2016 to the end of data recording in December 2016. In turn, the different ENSO phases are associated with different climatic conditions, which implicate the forcing wave climate, in turn, producing different seasonal data.

6.4.4 Shoreline Detection

The shoreline was not visible in the images from either camera. The camera angles did not present a full view of the beach within the images. Subsequently, the shoreline detection algorithms were not successful and the change in shoreline position over time could not be detected. The shoreline position is important because the shoreline orientation is linked to the sand-bar orientation, which is a function of the wave energy flux (van de Lageweg et al., 2013). If the shoreline position is known as well as the sand-bar orientation, then these variables can be correlated to further strengthen geomorphic and surfing parameter relationships within the nearshore environment, both seasonally and annually. Shoreline detection could have been achieved by placing a camera on the cliff overlooking Aramoana Beach.

6.4.5 Areas of Interest

Two areas of interest were analysed in this study. These two areas do not represent the entire beach. The results indicate a clear difference between the camera one area of interest and the camera two area of interest. This suggests that other locations on Aramoana Beach might respond differently to the observed forcing wave climate on a seasonal and annual basis. Therefore, observations and generalisations cannot be made about Aramoana Beach as a whole. The limitation could be addressed in a larger research project with a greater time frame than allowed for in this study.

6.5 Future Directions

This study is a part of a wider project, which is aimed at gathering baseline data on surf breaks of regional and national significance within New Zealand. The data will be used to help inform and support the New Zealand Coastal Policy Statement in protecting the recognised surf breaks of regional and national significance. Whilst valuable information has been gathered from this study, there were many limitations, which hampered the efforts to record and gather data. The following are recommendations for further research following on from this thesis:

(1) Cameras in future studies should be set up to record as videos during the periods of interest to ensure that complete waves are identified for the purpose of analysis. Firstly, this will ensure significantly more data is recorded and secondly, more accurate observations can be made from the analysed data.

(2) With the recorded videos, the computer algorithms could be further refined to detect changes in peel angles as breaking waves shoal and break further shoreward. If complete waves can be detected more accurate ride lengths can be identified.

(3) The computer algorithms could be set up to automate the data analysis. This would save thousands of person-hours, as the detection and error removal of sand-bars would not have to be completed manually. Further, if the computer algorithms, which are used to manually detect the white-water and wave crest lines through digitisation are automated, this will also save thousands of person-hours. In the future, it is not hard to imagine that data will be recorded and sent to a cloud database where researchers will have set up algorithms to automatically pull this data as it arrives, which will run through a series of algorithms to extract the relevant information.

(4) Longer data sets are required to make more accurate observations about the seasonal and annual differences between changing morphology and surfing parameters. Seasonal and annual differences were observed during this study. The accuracy of the seasonal data, however, is questionable at the camera two area of interest because of the paucity of the data. Further, as ENSO phases influence the morphology and in turn the surfing parameters via the associated forcing wave climates, it makes sense to have longer datasets which encompass multiple ENSO phases. The longer

datasets will allow more accurate observations on the changing morphology and surfing parameters during ENSO phase shifts.

(5) The findings of this study add weight to the importance of protecting the swell corridor that contains the pre-conditioning features that are essential to producing the world-class waves observed at Aramoana Beach.

References

Aarninkhof, S. (2003). Nearshore Bathymetry Derived from Video Imagery. Delft, The Netherlands: Delft University of Technology. thesis, Doctoral thesis, 155p.

Aarninkhof, S., & Roelvink, J. (1999) Argus-based monitoring of intertidal beach morphodynamics. In Coastal Sediments: (pp. 2429-2444): ASCE.

Aarninkhof, S. G., Caljouw, M., & Stive, M. J. (2001). Video-based, quantitative assessment of intertidal beach variability. In Coastal Engineering 2000 (pp. 3291-3304).

Aarninkhof, S. G., Turner, I. L., Dronkers, T. D., Caljouw, M., & Nipius, L. (2003). A video-based technique for mapping intertidal beach bathymetry. *Coastal Engineering*, 49(4), 275-289.

Anders, F. J., & Byrnes, M. R. (1991). Accuracy of shoreline change rates as determined from maps and aerial photographs. *Shore and Beach*, 59(1), 17-26.

Andrews, P. B. (1973). Late quaternary continental shelf sediments off Otago Peninsula, New Zealand. *New Zealand Journal of Geology and Geophysics*, 16(4), 793-830.

Andrews, P. B. (1976). Sediment transport on the continental shelf, east of Otago-a reinterpretation of so-called relict features: Comment. *New Zealand Journal of Geology and Geophysics*, 19(4), 527-532.

Atkin, E. (2010). The Impact of an Artificial Surfing Reef on Breaking Wave Conditions at Boscombe, UK. Master of Oceanography Dissertation, University of Southampton.

Australian Government Bureau of Meteorology (AGBM). (2018). Southern Oscillation Index (SOI) since 1876. Retrieved from http://www.bom.gov.au/climate/current/soihtm1.shtml.

Bardsley, W. E. (1977). Dispersal of some Heavy Minerals along the Otago-Eastern Southland Coast. New Zealand Geographer, 33(2), 76-79.

Battalio, B. (1994). Estimating breaking wave height at Ocean Beach, San Francisco. Shore and Beach, 62(4), 33-36.

Beamsley, B., & Black, K. (2003) The effect of offshore reefs on inshore surfing conditions. In Proceedings of the 3rd International Surfing Reef Conference. ISBN 0-473-09801-6.

Bell, R., Oldman, J., Beamsley, B., Green, M., Pritchard, M., Johnson, D., McComb, P., Hancock, N., Grant, D., & Zyngfogel, R. (2009). Port of Otago dredging project: Harbour and offshore modelling. NIWA client report HAM2008-179 prepared for Port Otago Ltd.

Bellomo, D., Pajak, M. J., & Sparks, J. (1999). Coastal flood hazards and the national flood insurance program. *Journal of Coastal Research*, 21-26.

Black, K. P., Hutt, J. A., & Mead, S. T. (1998). Narrowneck reef report 2: Surfing aspects. University of Waikato, prepared for Gold Coast City Council.

Boak, E. H., & Turner, I. L. (2005). Shoreline definition and detection: a review. *Journal of coastal research*, 688-703.

Buckley, R. (2002). Surf tourism and sustainable development in Indo-Pacific Islands. I. The industry and the islands. *Journal of sustainable tourism*, 10(5), 405-424.

Bunting, K., Single, M., & Kirk, R. (2003). Sediment transport pathways around Otago Harbour and north to Karitane Peninsula. Report for Port Otago Ltd. Land and Water International Ltd. 75p.

Button, M. (1991). Laboratory study of artificial surfing reefs. University of Western Australia.

Byrnes, M. R., McBride, R. A., & Hiland, M. W. (1991) Accuracy standards and development of a national shoreline change data base. In Coastal Sediments: (pp. 1027-1042): ASCE.

Cai, F., Su, X.Z., & Xia, D.X. (2004). Study on the difference between storm effects of beaches on two sides of the tropical cyclone track. *Advances in Marine Science*, 22(4), 436-445.

Caljouw, M. (2000). Video-based monitoring of the Egmond beach and shoreface nourishments. Rijkswaterstaat Z2773 RIKZ.

Carter, L. (1986). A budget for modern-Holocene sediment on the South Otago continental shelf. *New Zealand Journal of Marine and Freshwater Research*, 20(4), 665-676.

Chen, Z. S. (1995). The response of beaches in arc-shaped coasts to storm waves. Chinese Science Bulletin 40(23), 2168–2170.

Couriel, S., Horton, P., & Cox, D. (1998). Supplementary 2d physical modelling of breaking wave characteristics. Technical Report. Water Research Laboratory, TR98-14.

Dean, R. G. (1973). Heuristic models of sand transport in the surf zone. In First Australian Conference on Coastal Engineering, 1973: Engineering Dynamics of the Coastal Zone (p. 215). Institution of Engineers, Australia.

Dean, R. G. (1991). Equilibrium beach profiles: Characteristics and applications. *Journal of Coastal Research*, 7(1), 53–84.

Dronkers, T. (2001). Intertidal morphodynamics at Narrowneck Reef.

Elliot, E. L. (1958) Sandspits of the Otago Coast. New Zealand Geography 14 (J): 65-71.

Elliot, I. (1973). The persistence of rip current patterns on sandy beaches. In First Australian Conference on Coastal Engineering, 1973: Engineering Dynamics of the Coastal Zone (p. 29). Institution of Engineers, Australia.

Gallop, S. L. (2009). Rip current dynamics on an embayed beach. Thesis, The University of Waikato.

Gibbs, R. J., Matthews, M. D., & Link, D. A. (1971). The relationship between sphere size and settling velocity. *Journal of Sedimentary Research*, 41(1), 7-18.

Godoi, V. A., Bryan, K. R., & Gorman, R. M. (2016). Regional influence of climate patterns on the wave climate of the southwestern Pacific: The New Zealand region, Journal Geophysical Research Oceans, 121, 4056–4076, doi:10.1002/2015JC011572.

Gordon, N. D. (1986). The Southern Oscillation and New Zealand weather. Monthly Weather Review. 14, 371–387. doi:10.1175/1520-0493(1986)114<0371:TSOANZ>2.0.CO;2.

Gorman, R. M., Bryan, K. R. & Laing, A. K. (2003). Wave hindcast for the New Zealand region: Deep-water wave climate. *New Zealand Journal of Marine and Freshwater Research*, 37(3), 589–612, doi:10.1080/00288330.2003.9517191.

Gourlay, M. R., & Meulen, T. (1968). Beach and dune erosion tests (I). Deltares (WL).

Griggs, G. B. (1987). Littoral cells and harbor dredging along the California coast. *Environmental Geology and Water Sciences*, 10(1), 7-20. http://dx.org/10.1007/BF02588001.

Guza, R. T., & Inman, D. L. (1975). Edge waves and beach cusps. *Journal of Geophysical Research*, 80(21), 2997-3012.

Hanson, H., Gravens, M. B., & Kraus, N. C. (1989). Prototype applications of a generalized shoreline change numerical model. In Coastal Engineering 1988 (pp. 1265-1279).

Heath, R. (1972). The southland current. *New Zealand Journal of Marine and Freshwater Research*, 6(4), 497-533.

Hicks, D. M. (1985). Sand Dispersion from an Ephemeral Delta on a Wave-Dominated Coast. Santa Cruz, California: University of California, Santa Cruz (Doctoral dissertation, Ph. D. thesis, 210p).

Holman, R. A., Sallenger, A., Lippmann, T. C., & Haines, J. W. (1993). The application of video image processing to the study of nearshore processes. *Oceanography*, 6(3), 78-85.

Hutt, J. A. (1997). Bathymetry and wave parameters defining the surfing quality of five adjacent reefs (Doctoral dissertation, University of Waikato).

Hutt, J. A., Black, K. P., & Mead, S. T. (2001). Classification of surf breaks in relation to surfing skill. *Journal of Coastal Research*, 66-81.

Jackson, D. W. T., Cooper, J. A. G., & Del Rio, L. (2005). Geological control of beach morphodynamic state. *Marine Geology*, 216(4), 297-314.

Kilpatrick, D. (2005). Determining Surfing Break Components at Aramoana Beach, Dunedin. Dunedin, New Zealand: University of Otago, postgraduate diss., 68p.

Komar, P. D. (1998). Beach processes and sedimentation.

Laing, A. K. (2000). New Zealand wave climate from satellite observations. New Zealand. *Journal of Marine and Freshwater Research*, 34(4), 727–744, doi:10.1080/ 00288330.2000.9516973.

Leatherman, S. P. (1983) Historical and projected shoreline mapping. In Coastal Zone'83: (pp. 2902-2910): ASCE.

Leatherman, S. P., & Anders, F. J. (1999). Mapping and managing coastal erosion hazards in New York. *Journal of Coastal Research*, 34-42.

Lippmann, T. C., & Holman, R. A. (1989). Quantification of sand bar morphology: A video technique based on wave dissipation. *Journal of Geophysical Research: Oceans*, 94(C1), 995-1011.

Lusseau, D. (1999). A Review of Dredging Activities in Otago Harbour and Their Relocation, 1899-1998. University of Otago.

Masselink, G., & Hughes, M. G. (2003). Introduction to Coastal Geomorphology and Processes.

Masselink, G., & Short, A. D. (1993). The effect of tide range on beach morphodynamics and morphology: a conceptual beach model. *Journal of Coastal Research*, 785-800.

McComb, P. (2016). Deposition of dredged material at Heyward Point, Aramoana and Shelly Beach. Statement of evidence of Peter John McComb on behalf of Port Otago Ltd - Resource consent application RM16.175.

McCurdy, P. (1950). Coastal delineation from aerial photographs. Photogrammetric Engineering, 16(4), 550-555.

McKenzie, L. (2015). Summary report of surf surveys. Retrieved from https://www.portotago.co.nz/assets/Uploads/InshoreDredgingConsultation/Surf-Survey-Summary-Report-2-September-14-May-2015.pdf.

McNinch, J. E. (2004). Geologic control in the nearshore: shore-oblique sandbars and shoreline erosional hotspots, Mid-Atlantic Bight, USA. *Marine Geology*, 211(1), 121-141.

Mead, S. (2003). Keynote address—surfing science. Artificial Surfing Reefs, 1-36.

Mead, S., & Black, K. (2001a). Predicting the breaking intensity of surfing waves. *Journal of Coastal Research*, 51-65.

Mead, S., & Black, K. (2001b). Field Studies Leading to the Bathymetric Classification of World-Class Surfing Breaks. *Journal of Coastal Research*, 5-20.

Mead, S., & Black, K. (2001c). Functional component combinations controlling surfing wave quality at world-class surfing breaks. *Journal of Coastal Research*, 21-32.

Mead, S. T., Black, K., Blenkinsopp, C., & McComb, P. (2003). Lyall Bay Surfing Reef: Reef Design and Physical Processes. Prepared for the Lyall Bay Reef Charitable Trust, March 2003.

Mead, S., Black, K., Scarfe, B., Frazerhurst, J., Black, K., & Mead, S. (2003). The effect of wave focusing on surfing site selection and design at scales of intercontinental shelf to sub-tidal reef. Artificial Surfing Reefs, 115-137.

Mil-Homens, J. (2016). Longshore sediment transport: Bulk formulas and process based models (Doctoral dissertation, TU Delft, Delft University of Technology).

Moore, L. J., Benumof, B. T., & Griggs, G. B. (1999). Coastal erosion hazards in Santa Cruz and San Diego Counties, California. *Journal of Coastal Research*, 121-139.

National Institute of Water and Atmospheric Research (NIWA). (2015). Global setting: December 2017. Retrieved from https://www.niwa.co.nz/climate/summaries/monthly/climate-summary-for-june-2015.

National Institute of Water and Atmospheric Research (NIWA). (2017). Global setting: December 2017. Retrieved from https://www.niwa.co.nz/climate/nzcu/new-zealand-climate-update-199-january-2016/global-setting-december-2017.

Nelsen, C., Pendleton, L., & Vaughn, R. (2007). A socioeconomic study of surfers at Trestles Beach. *Shore and Beach*, 75(4), 32.

Nicholson, D. C. (1979). Sand Beaches in southern Blueskin Bay. Christchurch, New Zealand: Canterbury University, Master's thesis, 185.

Orams, M. (1999). Marine tourism: development, impacts and management. Psychology Press.

Otago Regional Council. (2017). Port Otago Limited Application - RM10.193. Retrieved from https://www.orc.govt.nz/consents/current-notified-applications/archived-applications/port-otago-limited-application-rm10193.

Peregrine, D. H. (1983). Breaking waves on beaches. Annual Review of Fluid Mechanics, 15(1), 149-178.

Peryman, P. B. (2011). Identification of surf breaks of national significance.

Port Otago Limited. (2013). Dredge disposal records summary and graphs from 1985 to 2013. Retrieved from Otago Regional Council website.

Port Otago Ltd. (2018). Map of disposal sites. Retrieved from https://www.portotago.co.nz/assets/Uploads/InshoreDredgingConsultation/DredgingDisposalApplicationAndAEE/Appendix-A-Location-of-disposal-sites.pdf.

Potiki, T. (2011). Statement of Evidence of Tahu Potiki on behalf of Te Runanga o Ōtākou. In the matter of an application for resource consents for Project Next Generation by Port Otago Limited. Retrieved from http://www.orc.govt.nz/Documents/Content/Information%20Services/Resource%20Consent/Port%20Otago/Evidence/Submission%20-%20Evidence%20of%20Tahu%20Potiki%20-%2012%20Apr%2011.pdf .

Potiki, M. (2016). The Otago Peninsular, a unique identity. *Shima: The International Journal of Research into Island Cultures*, 10(1).

Priest, G. R. (1999). Coastal shoreline change study northern and central Lincoln County, Oregon. *Journal of Coastal Research*, 140-157.

Qi, H., Cai, F., Lei, G., Cao, H., & Shi, F. (2010). The response of three main beach types to tropical storms in South China. *Marine Geology*, 275(1–4), 244-254.

Ranasinghe, R., Symonds, G., Black, K., & Holman, R. (2004). Morphodynamics of intermediate beaches: a video imaging and numerical modelling study. *Coastal Engineering*, 51(7), 629-655.

Raybould, M., & Mules, T. (1998). Northern Gold Coast beach protection strategy: A benefit-cost analysis. Report prepared for the Gold Coast City Council.

Renwick, J., & Thompson, D. W. J. (2006). The Southern Annular Mode and New Zealand climate, *Water Atmosphere*. 14, (24–25).

Sallenger, A. H. (2000). Storm impact scale for barrier islands. *Journal of Coastal Research,* 16(3), 890–895.

Salmon, S. A. (2008). A New Technique for Measuring Runup Variation Using Sub-Aerial Video Imagery. thesis, The University of Waikato.

Sanford South Island Ltd. (2001). Brinns Point Marine Farm - Resource consent application and assessment of environmental effects. Unpublished report.

Sayce, A. (1997). Transformation of surfing waves over steep and complex reefs. Unpublished Thesis, University of Waikato, New Zealand.

Scarfe, B. E., Healy, T. R., Rennie, H. G., & Mead, S. T. (2009a). Sustainable management of surfing breaks–An overview. *Reef Journal*, 1(1), 44-73.

Scarfe, B. E., Healy, T. R., Rennie, H. G., & Mead, S. T. (2009b). Sustainable management of surfing breaks: case studies and recommendations. *Journal of Coastal Research*, 684-703.

Single, M., Bell, R., & McComb, M. (2010). Physical costal environment of Otago Harbour and offshore: assessment of effects of proposed dredging by Port Otago Ltd.

Single, M., & Benn, J. (2007). Port Otago project next generation summary of existing physical coastal environment information and scoping for further studies. Port Otago Ltd, Dunedin.

Smith, A., & Jackson, L. (1992). The variability in width of the visible beach. *Shore and Beach*, 60(2), 7-14.

Smith, R., & Bryan, K. (2007). Monitoring beach face volume with a combination of intermittent profiling and video imagery. *Journal of Coastal Research*, 892-898.

Sport New Zealand. (2015). Sport and active recreation in the lives of New Zealand adults. 2013/2014 active New Zealand survey results. Wellington: Sport New Zealand.

Stafford, D., & Langfelder, J. (1971). Air photo survey of coastal erosion. Photogrammetric Engineering.

Stockdonf, H. F., Sallenger Jr, A. H., List, J. H., & Holman, R. A. (2002). Estimation of shoreline position and change using airborne topographic lidar data. *Journal of Coastal Research*, 502-513.

Toutin, T. (2004). Review article: Geometric processing of remote sensing images: models, algorithms and methods. *International journal of remote sensing*, 25(10), 1893-1924.

Trenberth, K. E., & Hurrell, J. W. (1994). Decadal atmosphere-ocean variations in the Pacific. *Climate Dynamics,* 9(6), 303–319, doi:10.1007/ BF00204745.

van de Lageweg, W. I., Bryan, K. R., Coco, G., & Ruessink, B. G. (2013). Observations of shoreline–sandbar coupling on an embayed beach. *Marine Geology*, 344, 101-114.

van Enckevort, I. M. J., & Ruessink, B. G. (2003). Video observations of nearshore bar behaviour. Part 1: alongshore uniform variability. *Continental Shelf Research*, 23(5), 501-512.

van Enckevort, I. M. J., & Ruessink, B. G. (2003b). Video observations of nearshore bar behaviour. Part 2: alongshore non-uniform variability. *Continental Shelf Research*, 23(5), 513-532.

van Enckevort, I. M. J., Ruessink, B. G., Coco, G., Suzuki, K., Turner, I. L., Plant, N. G., & Holman, R. A. (2004). Observations of nearshore crescentic sandbars. *Journal of Geophysical Research: Oceans*, 109(C6).

Walker, J. R. (1974a). Recreational surfing parameters. LOOK Laboratory TR-30, University of Hawaii, Department of Ocean Engineering, Honolulu, Hawaii.

Walker, J. R. (1974b). Wave transformations over a sloping bottom and over a three-dimensional shoal. University of Hawaii, James KK Look Laboratory of Oceanographic Engineering.

Weppe, S., & McComb, P. (2016). Proposed plans for dumping at Heyward Point and Aramoana Beach ground during the third quarter of 2016. Technical report prepared for Port Otago Limited. MetOcean Solutions Limited. Technical Report 0140-05h prepared for Port Otago Limited.

Weppe, S., McComb, P., & Coe, L. (2015) Numerical Model Studies to Support the Sustainable Management of Dredge Spoil Deposition in a Complex Nearshore Environment. In Proceedings of the Coastal Sediment.

Williams, J. J. (1979). Quaternary sedimentation of the north Taieri Bight, Otago continental shelf. University of Otago.

Wright, L. D., & Short, A. D. (1984). Morphodynamic variability of surf zones and beaches: a synthesis. *Marine Geology*, 56(1-4), 93-118.

Wright, L. D., Short, A. D., & Green, M. O. (1985). Short-term changes in the morphodynamic states of beaches and surf zones: an empirical predictive model. *Marine Geology*, 62(3-4), 339-364.

Zhang, K., Huang, W., Douglas, B. C., & Leatherman, S. (2002). Shoreline position variability and long-term trend analysis. *Shore and Beach*, 70(2), 31-35.

Zhang, Y., Wallace, J. M., & Battisti, D. S. (1997). ENSO-like interdecadal variability: 1900–93. *Journal of climate*, 10(5), 1004-1020.

Appendices

Appendix 1: Computer Algorithm Structure

Figure A1.1 illustrates a brief flow diagram and a small description of the suite of computer algorithms used to find and rectify images as well as the detection and the cleaning up of sand-bars for the RTAIs. The flow diagram also illustrates the suite of algorithms used to detect the length of ride and peel angles of breaking waves in the RSSIs.

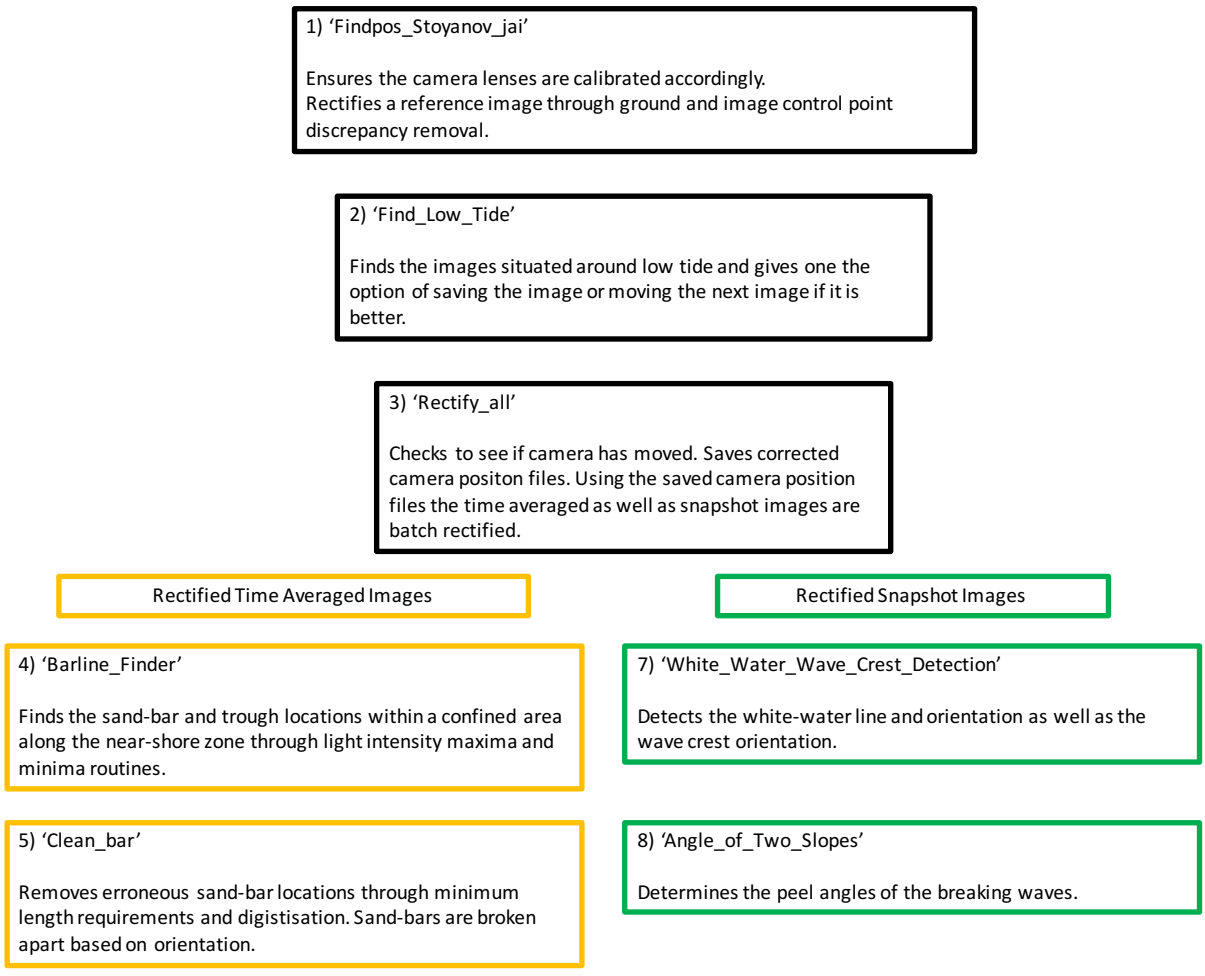

Figure A1- 1 Flow diagram of computer algorithms used to find and rectify images as well as the detection of the geomorphic and surfing parameters of interest.

Appendix 2: Whareakeake Methodology

A2.1 Extrinsic Calibration

A2.1.1 Remote Imagery Acquisition

A remote camera was installed above Whareakeake Surf Break by Port Otago Limited (POL) to monitor for the change in surf quality over time during periods were dredge spoil was being disposed of. The camera was positioned on farmland overlooking the break. The position of this camera is indicated on the Figure A2.1. Camera three is located at 45 45' 30.39''S 170 40' 00.67''E. This camera was also programmed to record a snapshot of the surf break every five minutes. Snapshot images have been recorded since 1 September 2015 and will continue into the future. An example of the image recorded at Whareakeake is illustrated in the Figure A2.1B. Images were and are stored on a hard drive at the camera location. POL regularly downloads these images and stores them in their database. These images have been made available by POL to the University of Waikato and eCoast for surf break analysis.

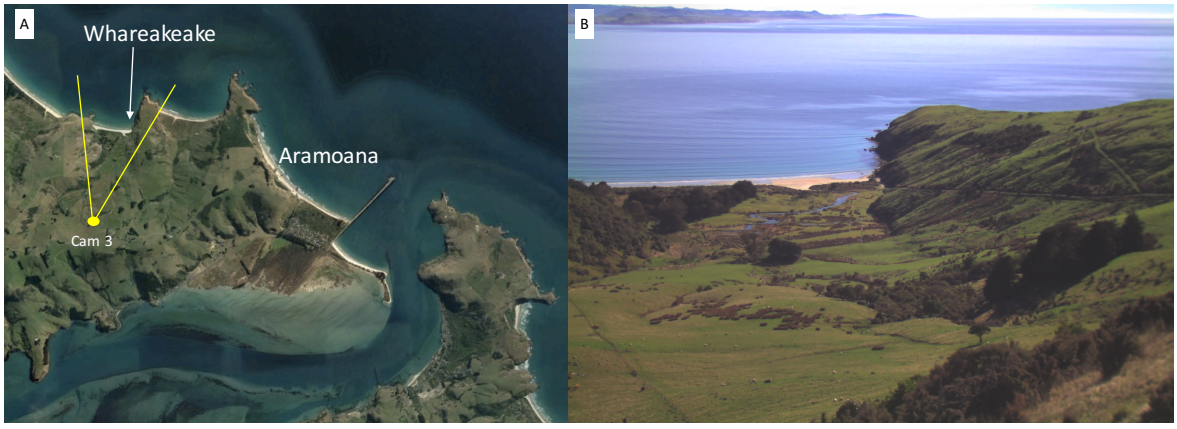

Figure A2- 1 Indicates the Whareakeake Surf Break location as well as the camera location and angle (A) (Google Earth, 2017). Note Cam 3 represents Camera 3. B) depicts an image from the camera.

A2.1.2 Rectification of Images

Once the images were received from POL, the process of rectifying the images could begin. Image rectification is the process of converting images to a standard map coordinate system. This is typically achieved by matching ground control points (GCPs) in the mapping system to points or coordinates from the images

(Ranasinghe et al., 2004; Toutin, 2004). The GCPs were collected by staff from POL and eCoast. A survey jet ski was navigated up and down Whareakeake surf break and was stationed at various non-specific locations, which covered a wide range of proximities to the Whareakeake coastline. Once stationed at these sites, a Global Positioning System (GPS), which was positioned on the back on the jet ski (near the motor), was turned on, and recorded the exact time (UTC), date, easting and northing coordinates of the respective GCPs and the water level relative to ellipsoid (m). These non-specific sites were also given a location name. As the camera was programmed to take a snapshot at five-minute intervals, it was essential that the jet ski was stationed at the sites during the times the images were periodically taken. Examples of the GCP collecting process can be observed in Figure A2.2. GCPs were also taken on land. Dean Sandwell walked across the topography and rocks along the waters edge within the frame of the camera. Dean would place a large checkered black and orange panel off the ground. This panel was also used gather ICPs and help rectify the images. The ICPs collected from land can be observed in Figure A2.3, letters A, B and C indicates ICPs collected on land.

Figure A2- 2 Image depicts GCPs being collected on a jet ski at Whareakeake break on the 18th January 2017 by Ed Atkin, eCoast. Note: the red box indicates the position of the survey jet ski.

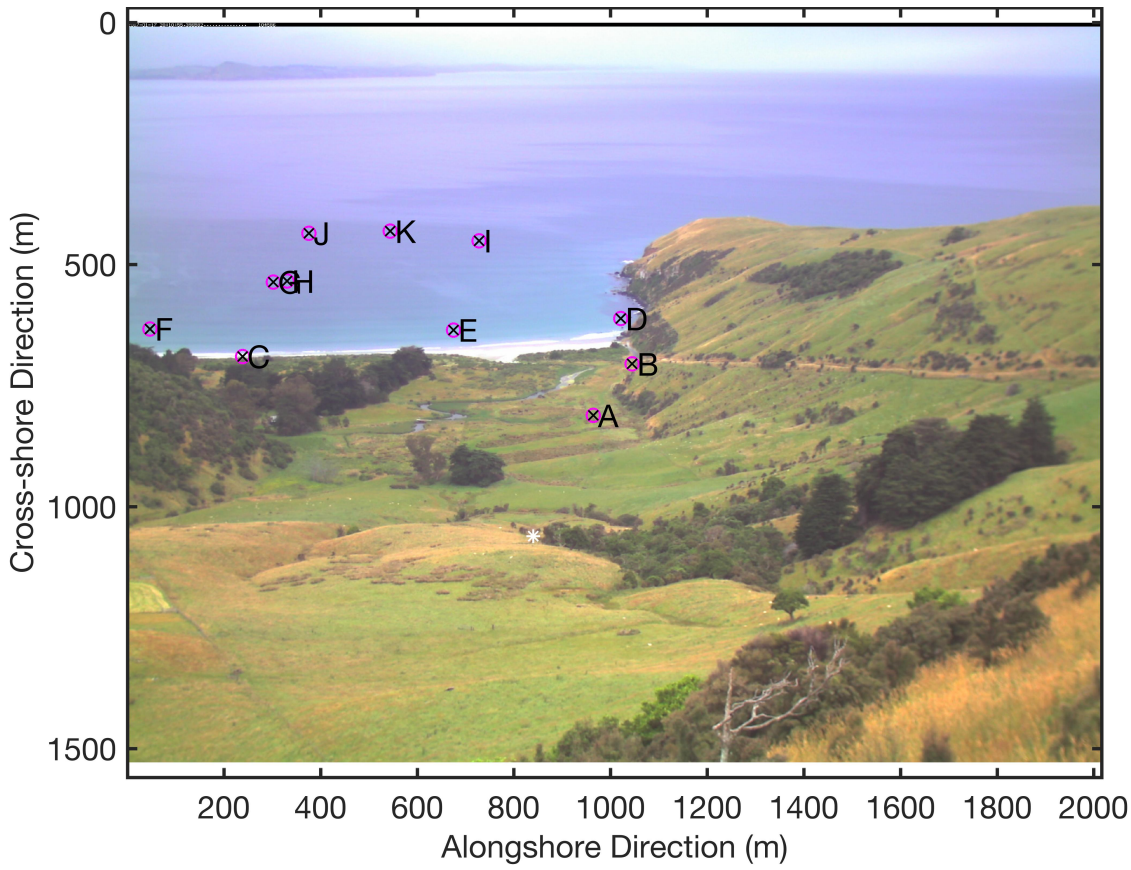

Figure A2- 3 Depicts the easting and northing (m) image coordinates of the GCPs from Camera 3 at Whareakeake. Each letter corresponds to a GCP. This image was taken on the 17th January 2017 at 6.05.20am.

The time-stamped GCP data were then synchronised with the time-stamped images to create a chronological match. The images were then loaded into Matlab to an algorithm called *'Findpos_Stoyanov_jai'*. This script used information on the properties of lenses of each camera to correct the images for any distortions. The properties of the lenses were measured in the laboratory by the National Institute for Water and Atmospheric Research, by taking images of black and white grids from a number of different positions. These were used by a computer algorithm to find the optimum values of the focal length, image centre, aspect ratio and radial and tangential distortion coefficients (the intrinsic parameters of the camera). The ICPs ascertained from the GCPs along Aramoana and Whareakeake can be observed in Figure A2.3. The saved GCP and ICP data was then reloaded back into the '*Findpos_Stoyanov_Jai'* script and so that the discrepancies between the actual and calculated GCPs and ICPs could be compared. Through error identification, the discrepancies between the actual and calculated GCPs and ICPs,

within the plots (Figures A2.4. B and C) were removed, which produced a rectified image (birds-eye-view) from the camera (Figure A2.4. A)

Tidal data from 1st January 2014 through to 14th January 2017 of the Otago Harbour Entrance was extracted from the Land Information New Zealand (LINZ) website to represent the tidal heights at both Aramoana and Whareakeake surf breaks. This tidal data was loaded into T-Tide and subsequently into the *'Findpos_Stoyanov_jai'* script, which removed errors associated with the tidal displacement associated with the difference between the GCPs and the ICPs.

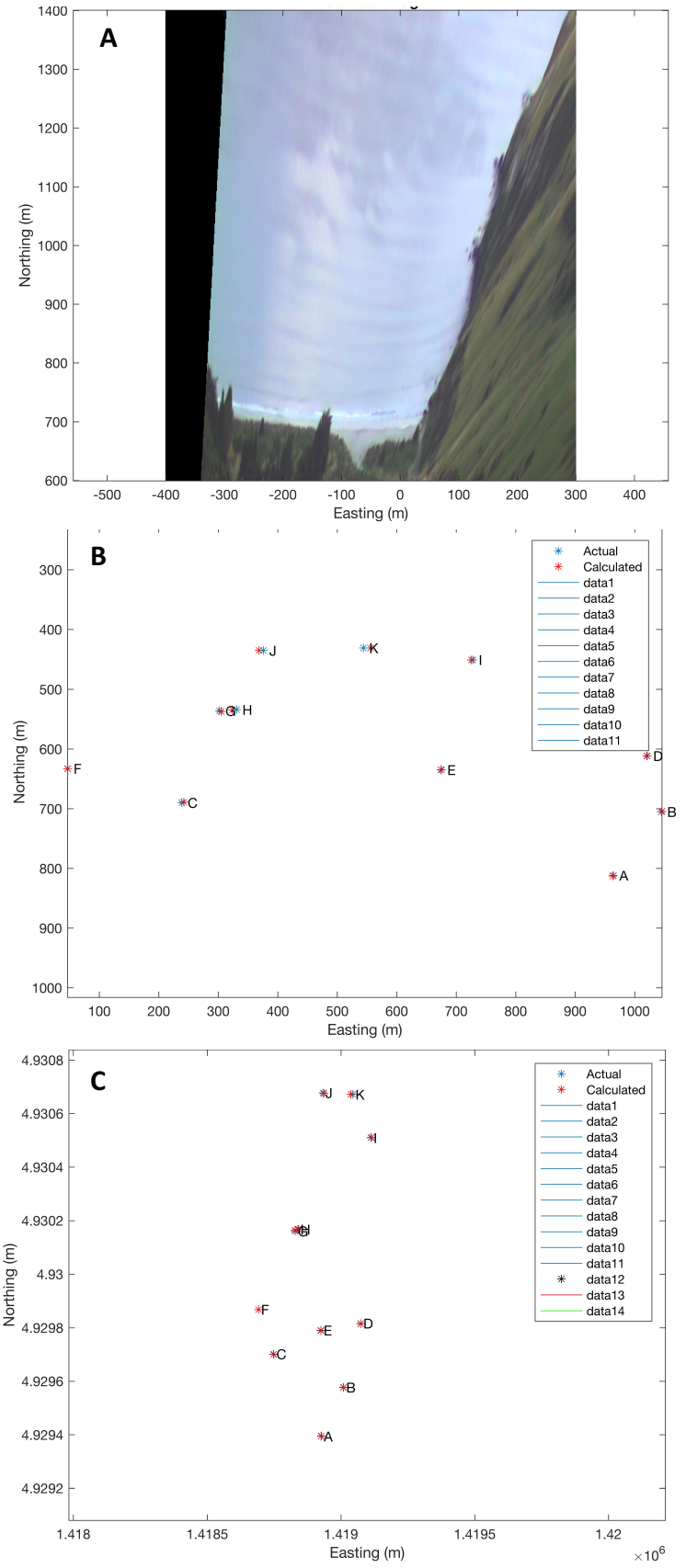

Figure A2- 4 Depicts the rectified image for the Whareakeake Camera (A), the actual ICPs plotted against calculated ICPs (B) and the actual GCPs plotted against the calculated (C). Note: the axes vary in length (m). The GCPs are a function of GPS coordinates (easting and northing (m)) and the ICPs are a function of image coordinate triangulation (easting and northing (m)).

The reference image was then digitized in the *'Rectify_all'* script to provided reference points and in turn, a means to check if the any of the cameras had moved over time. Each image was individually cross-referenced against the reference image reference points to see if the cameras had moved. If an image had moved the reference points were used to correct the change in camera position, at which point a new camera position file for that particular image was saved. An example of this can be observed below in Figure A2.5.

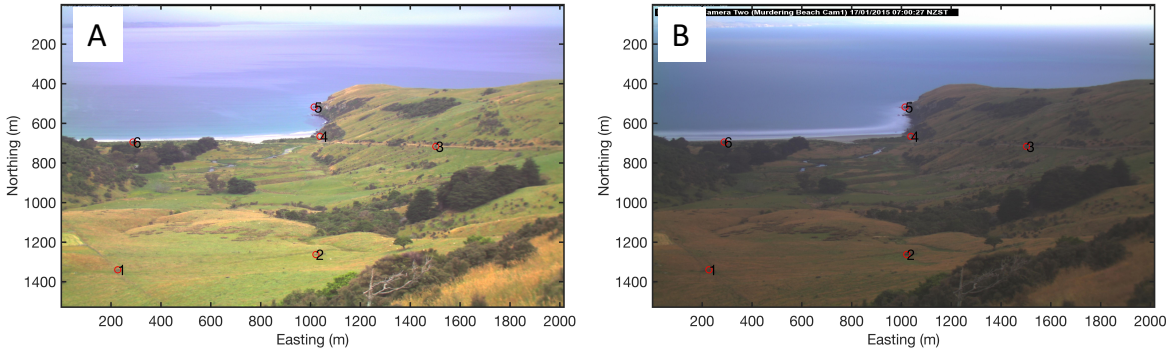

Figure A2- 5 Depicts the reference image (A) and associated reference points one to six (represented by small red circles and numbers) and the time-averaged image (B). The x-axis represents the easting (m) and the y-axis represents the northing (m).

With the saved image position files (camera position files), it was then possible to batch run the rectification process in the *'Rectify_all' script,* which provided rectified images of all time-averaged images, which were provided by NIWA, and the associated individual snapshot images from the period during the time-average duration. Not all images were rectified, however. To prevent the unnecessary and time-consuming analyses of thousands of images, only images situated around low tide were rectified and even then, there was a selection process. A script called *'Find_low_Tide'* was created, which as the name suggests, found the low tide for each day using T-Tide, mentioned above, and found the associated images situated around these low tide times for each day. From here, the images around the low tide times were individually checked to see if the images were of a high enough calibre. Only images of a high enough quality were saved to a final image folder. With respect to the snapshot images, however, only images identified as having a high enough calibre and having breaking waves were

desired and saved. These saved images were then batch rectified in the *'Rectify_all' script.*

Identifying images of a high enough calibre and with breaking waves was not as simple as it seemed. Many of the images during autumn and winter with breaking waves were not quality images, as these images were in one way or another distorted or ruined. Low-quality images resulted from rainy days, low cloud and or fog, smudges or drops on the camera lens, sun glare reflecting off the ocean surface, stormy conditions creating messy wave environments and multiple swell directions interrupting wave identification processes. Thus, the paucity of data collated during autumn and winter (refer to Chapter Four).

Appendix 3: Surfing Parameter Monthly Means

Figure A3.1 contains the monthly surfing parameter means for the RHPAs and LHPAs (degrees) as well as the RHLORs and LHLORs (m) plotted against time (months) for the years 2013 (A), 2014 (B), 2015 (C), 2016 (D) and 2017 (E) for the camera one area of interest. The RHPAs and LHPAs are represented by red and black solid lines, respectively, whilst the RHLOR and LHLOR are represented by red and black dashed lines, respectively. Where the lines are incomplete, there was no data for those particular months.

Figure A3.2 contains the monthly surfing parameter means for the RHPAs and LHPAs (degrees) as well as the RHLORs and LHLORs (m) plotted against time (months) for the years 2015 (A) and 2016 (B) for the camera two area of interest. The RHPAs and LHPAs are represented by red and black solid lines, respectively, whilst the RHLORs and LHLORs are represented by red and black dashed lines, respectively.

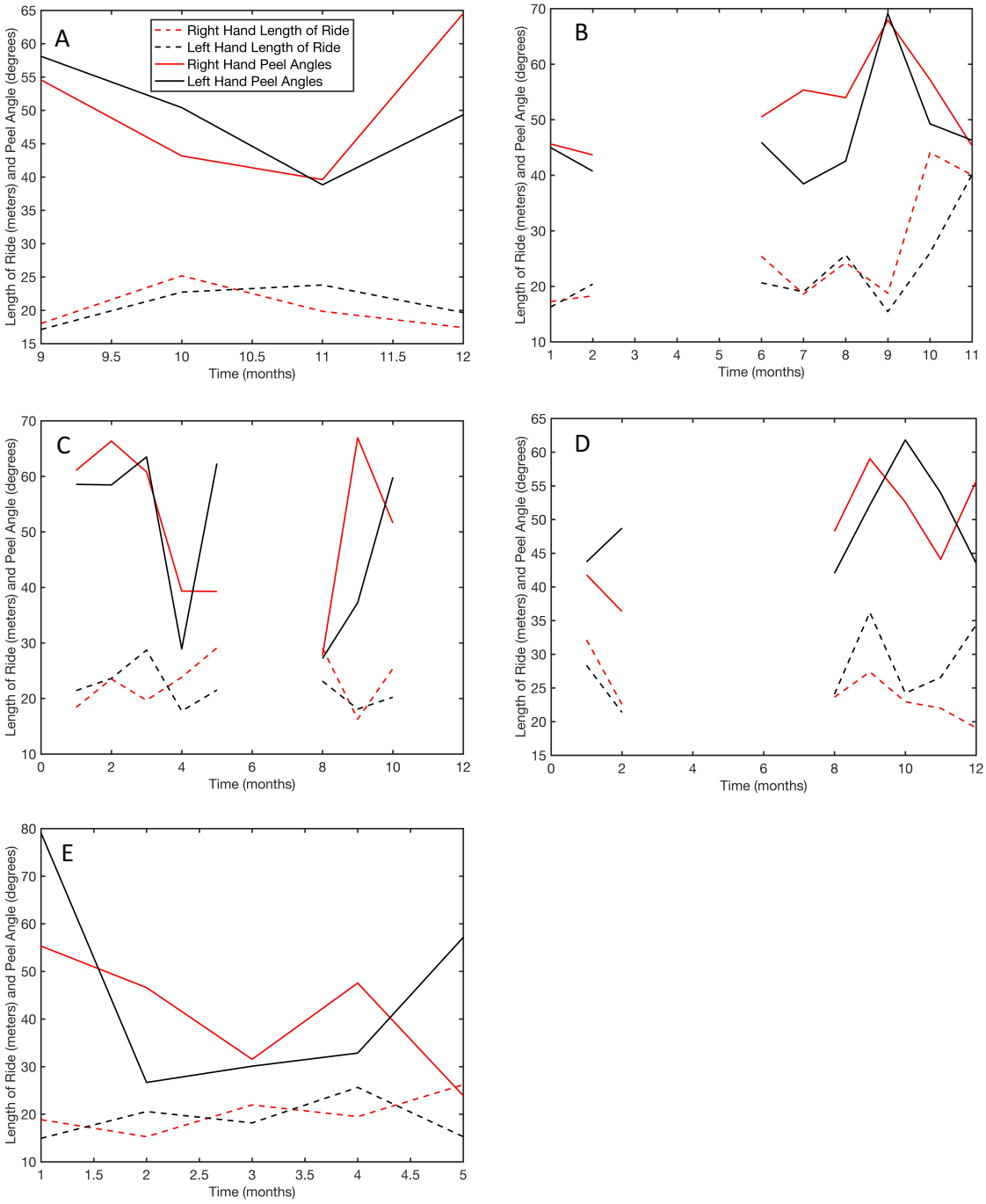

Figure A3- 1 Illustrates the monthly surfing parameter means for the RHPAs and LHPAs (degrees) as well as the RHLORs and LHLORs (m) plotted against time (months) for the years 2013 (A), 2014 (B), 2015 (C), 2016 (D) and 2017 (E) for the camera one area of interest. Note the RHPAs and LHPAs are represented by red and black solid lines, respectively, whilst the RHLOR and LHLOR are represented by red and black dashed lines, respectively. Note where the lines are incomplete, there was no data for those particular months.

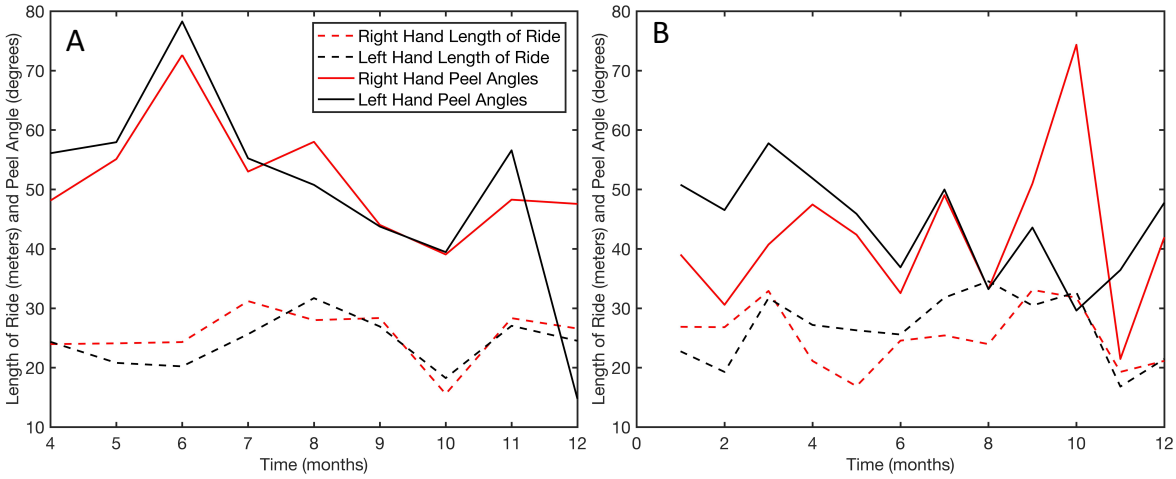

Figure A3- 2 Illustrates the monthly surfing parameter means for the RHPAs and LHPAs (degrees) as well as the RHLORs and LHLORs (m) plotted against time (months) for the years 2015 (A) and 2016 (B) for the camera two area of interest. Note the RHPAs and LHPAs are represented by red and black solid lines, respectively, whilst the RHLORs and LHLORs are represented by red and black dashed lines, respectively.

Appendix 4: Monthly Values of the Southern Oscillation Index

Figure A4.1 indicates the ENSO phases from January 2007 through to December 2017.

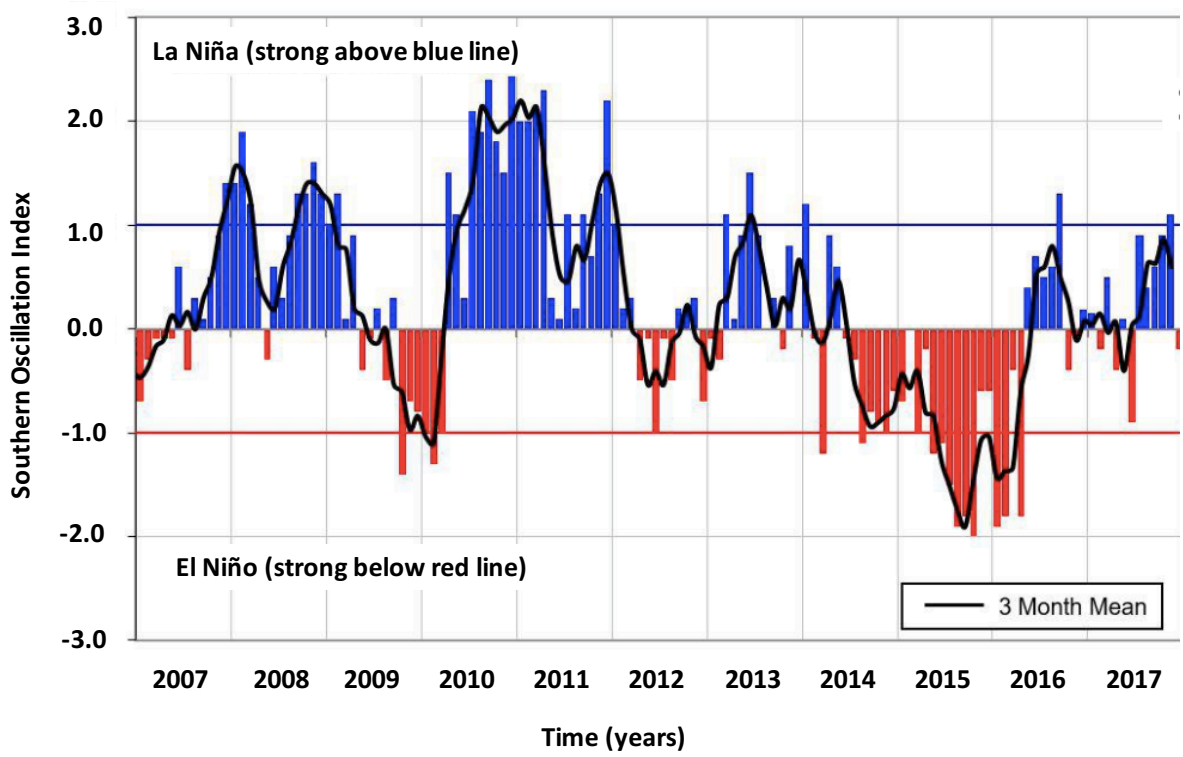

Figure A4- 1 Illustrates the monthly values of the Southern Annual Index (SOI), a measure of changes in the atmospheric pressures across the Pacific and the 3-month mean, which is represented by the blackline through months January 2007 through to December 2017. Note, months recorded as La Niña and El Niño are represented by the colours blue and red, respectively. The figure was extracted from NIWA (2017).

Appendix 5: Acronyms and their Respective Meanings

Table A5- 1 Presents the acronyms and their respective meanings in order of appearance.

Acronyms	Meanings	Acronyms	Meanings
NZCPS	New Zealand Coastal Policy Statement	SLIM	Shoreline Intensity Model
POL	Port Otago Ltd	RGB	Red, Green and Blue
SAM	Southern Annual Mode	HSV	Hue Saturation Value
ENSO	El Niño Southern Oscillation	GCP	Ground Control Point
SOI	Southern Oscillation Index	GPS	Global Positioning System
VC	Victoria Channel	UTC	Universal Time Coordinate
LHC	Lower Harbour Channel	ICP	Image Control Point
ASG	Aramoana Spoil Ground	LINZ	Land Information New Zealand
OHETD	Otago Harbour Ebb Tidal Delta	RTAI	Rectified Time Averaged Images
ASM	Aramoana Spoil Mound	RSSI	Rectified Snapshot Images
HPSM	Heyward Point Spoil Mound	BO	Sand-bar Orientation
ASR	Artificial Surf Reef	LOB	Length of Sand-Bar
Hb	Breaking Wave Height	m	meters
Ws	Sediment Falling Velocity	CC	Correlation Coefficient
T	Wave Period	LHPA	Left Hand Peel Angle
RTR	Relative Tidal Range	RHPA	Right Hand Peel Angle
TR	Tidal Range	PA	Peel Angle
MPC	Mean Profile Change	LHLOR	Left Hand Length of Ride
HWL	High Water Line	RHLOR	Right Hand Length of Ride
DIG	Digital Image Analysis	LOR	Length of Ride
PIC	Pixel Intensity Clustering	°	Degrees
H	Hue	NOAA	National Oceanographic and Atmospheric
S	Saturation	Hs	Significant Wave Height
V	Value	C1AI	Camera One Area of Interest
ANN	Artificial Neural Network	C2AI	Camera Two Area of Interest